



AMERICAN UNIVERSITY OF BEIRUT

ROLE OF HYOID BONE POSITION IN UPPER  
AIRWAY PATENCY AND TISSUE MECHANICS:  
A COMPUTATIONAL FINITE ELEMENT  
MODELING APPROACH

by  
DIANE NABIL SALMAN

A thesis  
submitted in partial fulfillment of the requirements  
for the degree of Master of Science  
to the Department of Biomedical Engineering  
of the Maroun Semaan Faculty of Engineering and Architecture  
at the American University of Beirut

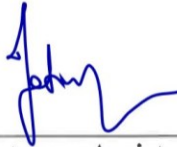
Beirut, Lebanon  
July 2021

AMERICAN UNIVERSITY OF BEIRUT

ROLE OF HYOID BONE POSITION IN UPPER AIRWAY  
PATENCY AND TISSUE MECHANICS:  
A COMPUTATIONAL FINITE ELEMENT  
MODELING APPROACH

by  
DIANE NABIL SALMAN


Approved by:



---

Dr. Jason Amatory, Assistant Professor  
Biomedical Engineering Program  
AUB, Beirut, Lebanon

Advisor



---

Dr. Joseph Ghafari, Professor and Head of Division  
Otorhinolaryngology and Head and Neck Surgery,  
Orthodontics, AUBMC, Beirut, Lebanon

Co-Advisor



Digitally signed by Rami  
Mhanna  
DN: cn=Rami Mhanna, o,  
ou, email=rm136@aub.  
edu.lb, c=US  
Date: 2021.08.05 11:03:49  
+03'00'

---

Dr. Rami Mhanna, Assistant Professor  
Biomedical Engineering Program  
AUB. Beirut. Lebanon

Member of Committee



---

Dr. Samir Mustapha, Associate Professor  
Department of Mechanical Engineering  
AUB, Beirut, Lebanon

Member of Committee



---

Dr. Lynne Bilston,  
Senior Principal Research Scientist, NeuRA, and  
Conjoint Professor, University of New South Wales,  
Sydney, Australia

Member of Committee

Date of thesis defense: July 14, 2021

# AMERICAN UNIVERSITY OF BEIRUT

## THESIS RELEASE FORM

Student Name: Salman Diane Nabil  
Last First Middle

I authorize the American University of Beirut, to: (a) reproduce hard or electronic copies of my thesis; (b) include such copies in the archives and digital repositories of the University; and (c) make freely available such copies to third parties for research or educational purposes:

- As of the date of submission
- One year from the date of submission of my thesis.
- Two years from the date of submission of my thesis.
- Three years from the date of submission of my thesis.



18/08/2021

Signature

Date

(This form is signed & dated when submitting the thesis to the University Libraries ScholarWorks)



## ACKNOWLEDGEMENTS

First and foremost, I am extremely grateful to my advisor, Dr. Jason Amatory, for his unparalleled support and relentless encouragement throughout these difficult times. His vast knowledge and experience have guided me during my academic research and daily life. I am fortunate to have had the opportunity to work with an exceptional mentor that continuously believed in me and pushed me to sharpen my work.

I would also like to extend my gratitude to the members of my thesis committee, Dr. Joseph Ghafari, Dr. Samir Mustapha, Dr. Rami Mhanna and Dr. Lynne Bilston for their insightful feedback and valuable advice.

Special thanks to my colleagues from the SUARG team, Dr. Corine Samaha and Dr. Hiba Tannous, for their friendship and for the help they provided me in the medical aspect of the study.

I gratefully acknowledge the funding received towards this project from the University Research Board. I would also like to recognize the assistance of the MSFEA IT unit at AUB that provided me with the necessary technical support to complete this research.

Finally, I must express my deepest appreciation to my family and friends that granted me their love, comfort and support through it all.

# ABSTRACT OF THE THESIS OF

Diane Nabil Salman

for

Master of Science

Major: Biomedical Engineering

Title: Role of Hyoid Bone Position in Upper Airway Patency and Tissue Mechanics:  
A Computational Finite Element Modeling Approach

**Background:** The hyoid is a mobile bone and central structure of the upper airway, serving as an anchor to several upper airway dilator muscles. As such, the hyoid is believed to play an important role in keeping the upper airway open (patent) during sleep and breathing. In cases where upper airway patency is compromised during sleep, repeated narrowing or complete collapse of the airway can occur. These events are characteristic of a disorder known as obstructive sleep apnea (OSA). OSA is a highly prevalent condition that is associated with serious health consequences, including cardiovascular disease and neurocognitive impairment. The most commonly observed anatomical difference between OSA and healthy individuals is a more caudally positioned hyoid bone in OSA. While surgical hyoid repositioning therapies have been performed as an attempt to treat OSA, outcomes are unpredictable and highly variable. In this thesis, in a bid to better understand the hyoid's role in OSA and improve treatment outcomes with hyoid repositioning procedures, a previously validated two-dimensional finite element model of the rabbit upper airway was advanced to study the influence of hyoid bone position and surgical repositioning on upper airway patency and tissue mechanics.

**Aims and Methods:** Specifically, the aims of the current study were to investigate the influence of 1) baseline hyoid position (phenotype), 2) surgical hyoid re-positioning, and 3) combined changes in baseline hyoid position and surgical hyoid re-positioning on upper airway collapsibility (quantified as upper airway closing pressure,  $P_{close}$ ), airway lumen geometry (cross sectional area, CSA; anteroposterior diameter, APD) and tissue mechanics (displacement, stress and strain). Simulations involved displacement of the hyoid along cranial, caudal, anterior, anterior-caudal 45° and anterior-cranial 45° directions from 1-4mm (in 1mm increments) for both baseline hyoid position and surgical hyoid repositioning interventions.

**Results:** Changes in baseline hyoid position resulted in a linear increase in  $P_{close}$  (i.e. increased collapsibility) for all directions, ranging between 29-43% at 4mm. Surgical hyoid repositioning outcomes were similarly dependent on both the direction and magnitude of hyoid displacement. Anterior, anterior-cranial and anterior-caudal directions caused the largest decrease in  $P_{close}$ , dropping by ~115% at 4mm. Hyoid

repositioning in the anterior-based directions also led to the greatest airway enlargement (increase in CSA and APD by 35% and 85 to 140%, respectively) and anterior-cranial repositioning generated the highest stress distributions across greater soft tissue areas. Combined baseline hyoid position changes and surgical hyoid repositioning simulations revealed that for a more caudal hyoid baseline position (4mm), like in the OSA condition, anterior-cranial and anterior caudal hyoid repositioning of 2mm (similar to clinical surgical hyoid procedures) were 25% and 8% less effective in decreasing  $P_{close}$ , respectively.

**Discussion:** This unique computational modeling study has predicted that both baseline hyoid position and surgical hyoid re-positioning alter upper airway outcomes, and that these changes are dependent on both the direction and magnitude of hyoid displacement. The original baseline (“normal”) hyoid position was deemed the optimal airway anatomical configuration in terms of airway collapsibility. Position of the hyoid at baseline impacts the effectiveness of surgical hyoid repositioning procedures in reducing upper airway collapsibility. Furthermore, anterior-cranial surgical hyoid repositioning procedures lead to greater improvements in upper outcomes compared to anterior-caudal surgical hyoid repositioning procedures. Study findings have important implications to potentially guide hyoid surgeries to improve OSA treatment outcomes and provide further insight into OSA pathogenesis.

**Keywords:** Upper airway, hyoid bone, computational finite element modeling, obstructive sleep apnea, hyoid repositioning surgery.

## TABLE OF CONTENTS

ACKNOWLEDGEMENTS .....	1
ABSTRACT .....	2
TABLE OF CONTENTS .....	4
ILLUSTRATIONS .....	8
TABLES .....	12
1. INTRODUCTION AND AIMS .....	13
1.1 Introduction .....	13
1.2 Aims .....	17
1.3 Significance and Innovation .....	17
2. LITERATURE REVIEW .....	19
2.1 The Upper Airway .....	19
2.1.1 Overview of Upper Airway Anatomy .....	19
2.1.2 Overview of Upper Airway Functions.....	24
2.1.3 Upper Airway Mechanics .....	25
2.2 Obstructive Sleep Apnea (OSA) .....	30
2.2.1 Overview.....	30
2.2.2 Pathophysiology of OSA .....	31
2.2.3 Upper Airway Mechanics and OSA .....	33
2.3 Hyoid Bone and Upper Airway Patency .....	37
2.3.1 Physiology of the Hyoid Bone.....	37
2.3.2 Role of Hyoid Bone in Upper Airway Patency .....	40

2.4	Computational Model of the Upper Airway.....	49
2.4.1	General Finite Element Technique .....	50
2.4.2	Models of Airway Lumen Only (CFD) .....	51
2.4.3	FEA/FSI models with Simplified Soft Tissue Representation .....	54
2.4.4	FEA/FSI Models Including the Hyoid Bone .....	60
2.5	Anesthetized Rabbit Computational Finite Element Model.....	67
2.5.1	Model Geometry .....	69
2.5.2	Boundary conditions .....	70
2.5.3	Material Properties.....	74
2.5.4	Limitations .....	75
<b>3.</b>	<b>METHODS .....</b>	<b>80</b>
3.1	Overall Study Design .....	80
3.2	Model Redevelopment and Advancement.....	81
3.2.1	Reconstruction and Geometrical Adjustments .....	82
3.2.2	Boundary Condition Definitions.....	84
3.2.3	Meshing and Model Verification .....	87
3.2.4	Current-Original Model Agreement .....	89
3.3	Loading Conditions and Simulations .....	90
3.3.1	Aim 1- Influence of Hyoid Baseline Position (Phenotype) .....	91
3.3.2	Aim 2- Influence of Surgical Hyoid Repositioning for Original Baseline Hyoid Position.....	95
3.3.3	Aim 3- Combined Influence of Baseline Hyoid Position and Surgical Hyoid Repositioning.....	96
3.3.4	Clinically Relevant Simulations .....	96

3.4	FE Analysis Settings.....	98
3.5	Model Outputs .....	98
3.5.1	Upper Airway Collapsibility, Pclose .....	99
3.5.2	Site of Collapse.....	103
3.5.3	Total Tissue Displacement, Stress and Strain.....	103
3.5.4	Lumen Geometry Metrics.....	104
3.6	Model Validation.....	106
4.	RESULTS.....	107
4.1	Comparability to Original Model .....	107
4.2	Upper Airway Collapse at Zero-Baseline Hyoid Position.....	108
4.3	Influence of Baseline Hyoid Position “Phenotype” on Pclose (Aim 1) ..	110
4.4	Influence of Surgical Hyoid Repositioning for Zero-Baseline Hyoid Position (Aim 2) .....	112
4.4.1	Pclose .....	112
4.4.2	Validation of Pclose Outcomes with Experimental Results .....	113
4.4.3	Tissue Displacement, Stress and Strain .....	115
4.4.4	Lumen Geometry Metrics.....	124
4.4.5	Site of Collapse.....	127
4.5	Combined Influence of Baseline Hyoid Position and Surgical Hyoid Repositioning (Aim 3).....	128
4.5.1	Pclose .....	128
4.5.2	Tissue Displacement, Stress and Strain .....	133
4.5.3	Lumen Geometry Metrics.....	140
5.	DISCUSSION AND CONCLUSION.....	144

5.1	Strengths and Key Outcomes .....	144
5.2	Upper Airway Collapsibility and Site of Collapse at Baseline .....	146
5.3	Influence of Baseline Hyoid Position “Phenotype” on Upper Airway Collapsibility (Aim 1).....	147
5.4	Influence of Surgical Hyoid Repositioning for Zero-Baseline Hyoid Position (Aim 2) .....	149
5.4.1	General Overview .....	149
5.4.2	Anterior Hyoid Repositioning .....	150
5.4.3	Caudal Hyoid Repositioning.....	152
5.4.4	Cranial Hyoid Repositioning .....	154
5.4.5	Anterior-Cranial and Anterior-Caudal Hyoid Repositioning .....	156
5.5	Combined Influence of Baseline Hyoid Position and Surgical Hyoid Repositioning (Aim 3).....	160
5.5.1	Overall Impact of Different Hyoid Baseline Positions.....	160
5.5.2	Impact of Caudal Hyoid Baseline Position.....	162
5.6	Clinical Implications .....	164
5.7	Limitations and Critique of Methods.....	167
5.7.1	Original Model Limitations .....	167
5.7.2	Closing Pressure ( $P_{close}$ ) Result .....	168
5.7.3	Hyoid Position Phenotype Changes.....	169
5.7.4	Replication of Hyoid Suspension Surgical Procedures .....	170
5.7.5	Computational Limitations .....	172
5.8	Conclusion and Future Studies .....	173
	<b>REFERENCES .....</b>	<b>175</b>

## ILLUSTRATIONS

Figure

1. Mid-sagittal section of the Human Upper Airway Anatomy.....	20
2. Upper Airway Muscles. ....	24
3. Schematic of the Upper Airway with the Forces that Affect its Patency. ....	26
4. Hyoid Anatomy and Muscle Attachments.....	40
5. Illustration of Hyoid Position in Apneic Male Compared to a Normal Healthy Male. ....	41
6. Illustration of hyomandibular suspension (A) and hyothyroidopexy (B) procedures performed clinically as part of OSA treatment. ....	44
7. Hyoid Bone Displacement in Response to Caudal Tracheal Displacement in a Rabbit Animal Study. ....	46
8. Hyoid Bone Displacement in Response to Mandibular Advancement in a Rabbit Animal Study. ....	48
9. Effect of Hyoid Fixation on Outcomes of Mandibular Advancement Investigated using Computational Model. ....	49
10. Flow Velocity and Pressure Distribution in a Computational Fluid Dynamics (CFD) Model of the Upper Airway. ....	53
11. FEA upper airway models of the velopharyngeal airway region only. ....	56
12. Fluid-Structure Interaction Simplified Soft Tissue Upper Airway Model. ....	58
13. 3-Dimensional Upper Airway Finite Element Model Geometry and Tissue Displacement. ....	60
14. Geometry of FE model of the upper airway with intricate pharyngeal tissue representation.....	61
15. FSI model including key upper airway structures and hyoid bone.....	63
16. Rigid multi-body and FEA models of the head and neck region.....	65
17. Overview of the FRANK model and its response to palatal muscle activation. ....	67
18. Rabbi Upper Airway Finite Element Model Geometry.....	69
19. Illustration of Model Constraints. ....	70
20. Diagram indicating the model’s contact definitions. ....	71



21. Illustration of Model Spring-Defined Muscles.....	73
22. Stress-Strain Curves for the Hyperelastic Yeoh Second-Order Material Models. ....	75
23. Overview of general study design flow. ....	81
24. Models with Different Hyoid Baseline Positions. ....	83
25. Model contact definitions illustrated on diagram of model edges. ....	86
26. Mesh convergence study representing the displacement of a portion of the soft palate in response to anterior-cranial surgical hyoid repositioning simulation vs. the mesh density (number of mesh elements) used.....	88
27. Illustration of the original model with the Mandibular Advancement (MA) and tracheal displacement (TD) displacement loads simulated.....	90
28. Simulations Workflow to Evaluate the Study’s Specific Aims.....	91
29. Model with different hyoid displacement directions studied.....	92
30. Current Model with Illustration of Intraluminal Pressure Load. ....	94
31. Intraluminal negative pressure load applied across 80 substeps (ramped pressure load).....	94
32. Change in penetration results for contact between airway walls due to negative intraluminal pressure (Pua) load. ....	101
33. Airway region delimitation and lumen geometry measurements. ....	106
34. Hyoid displacement result of mandibular advancement simulation from current model compared to the original model outputs. ....	107
35. Identity plot representing the similarities between the current and original models in the change in upper airway geometry for 4.6mm of mandibular advancement (MA). ....	108
36. Upper airway collapse as a result of negative intraluminal pressure simulation for zero baseline hyoid position.....	109
37. Percent change in Pclose ( $\Delta P_{close}$ %; with respect to $P_0$ ) vs. hyoid baseline increments. ....	111
38. Percent change in Pclose ( $\Delta P_{close}$ %; with respect to $P_0$ ) vs. hyoid displacement (surgical repositioning) for zero-baseline hyoid position.....	112
39. Comparison between model outputs and experimental Pclose results for surgical hyoid repositioning simulations from zero-baseline hyoid position.....	113
40. Plots of experimental results and simulation outputs of the percent change in Pclose produced by surgical hyoid repositioning. ....	114

41. Tissue mechanics outcomes for cranial surgical hyoid repositioning simulations. ....	117
42. Tissue mechanics outcomes for anterior surgical hyoid repositioning simulations. ....	118
43. Tissue mechanics outcomes for caudal surgical hyoid repositioning simulations. ....	119
44. Tissue mechanics outcomes for anterior-caudal surgical hyoid repositioning simulations. ....	120
45. Tissue mechanics outcomes for anterior-cranial surgical hyoid repositioning simulations. ....	121
46. Total displacement of upper airway tissues vs. surgical hyoid repositioning load starting from the zero-baseline hyoid position. ....	122
47. Equivalent (Von-Mises) strain distribution in the soft tissues vs. surgical hyoid repositioning load starting from the zero-baseline hyoid position. ....	123
48. Equivalent (Von-Mises) stress distribution in the soft tissues vs. surgical hyoid repositioning load starting from the zero-baseline hyoid position. ....	124
49. Upper airway lumen geometry changes in response to surgical hyoid repositioning from zero-baseline hyoid position. ....	126
50. Contact penetration results showing sites of collapse after Pua simulations. ....	127
51. Change in $P_{close}$ ( $\Delta P_{close}$ %, with respect to $P_0$ ) produced by surgical hyoid repositioning simulations after a 2mm relocation of the baseline hyoid position. ....	131
52. Change in $P_{close}$ ( $\Delta P_{close}$ %, with respect to $P_0$ ) produced by surgical hyoid repositioning simulations after a 4mm relocation of the baseline hyoid position. ....	132
53. Plots showing the effect of the hyoid baseline position modification on the effectiveness of 2mm surgical hyoid repositioning (HR) in the (A) anterior-cranial and (B) anterior-caudal directions. Anterior-cranial and anterior-caudal surgical hyoid repositioning represent hyomandibular suspension and hyothyroidopexy surgical procedures, respectively. ....	133
54. Total displacement of upper airway tissues as a result of surgical hyoid repositioning (HR) starting from a 2mm caudal hyoid baseline position. ....	135
55. Equivalent (Von-Mises) strain distribution in the soft tissues as a result of surgical hyoid repositioning (HR) starting from a 2mm caudal hyoid baseline position. ....	136

56. Equivalent (Von-Mises) stress distribution in the soft tissues as a result of surgical hyoid repositioning (HR) starting from a 2mm caudal hyoid baseline position.....	137
57. Total displacement of upper airway tissues as a result of surgical hyoid repositioning (HR) starting from a 4mm caudal hyoid baseline position.....	138
58. Equivalent (Von-Mises) strain distribution in the soft tissues as a result of surgical hyoid repositioning (HR) starting from a 4mm caudal hyoid baseline position.....	139
59. Equivalent (Von-Mises) stress distribution in the soft tissues as a result of surgical hyoid repositioning (HR) starting from a 4mm caudal hyoid baseline position.....	140
60. Upper airway lumen geometry changes in response to surgical hyoid repositioning from a 2mm caudal hyoid baseline position.....	142
61. Upper airway lumen geometry changes in response to surgical hyoid repositioning from a 4mm caudal hyoid baseline position.....	143

## TABLES

### Table

1. Hyoid Suspension Surgical Outcomes. Preoperative and postoperative mean AHI and success rate of four different studies that considered the role of hyoid suspension (hyothyroidopexy) alone. ....	44
2. Elastic Constraint Properties and Justification.....	71
3. Contacts and Properties.....	72
4. Muscle (spring) Properties. ....	73
5. Bony and Cartilaginous Linear Elastic Material properties.....	74
6. Soft Tissue Hyperelastic (Yeoh second-order) material parameters. ....	75
7. Summary of model contact interfaces and corresponding properties including contact behavior and normal stiffness factor. ....	87
8. Absolute Pclose results for different hyoid baseline positions. ....	111

# CHAPTER 1

## INTRODUCTION AND AIMS

### 1.1 Introduction

The upper airway is complex and highly deformable muscular structure. It has dynamic neuromechanical behavior permitting it to fulfill numerous physiological functions including speech, swallowing and breathing [106, 115]. While upper airway deformability is required for swallowing and speech production, it compromises airway patency (ability to remain open or unobstructed), which is essential for breathing [32]. The loss in the equilibrium of upper airway forces maintaining upper airway patency leads to the collapse of the airway and the development of serious breathing disorders. The hyoid bone is a freely suspended bone in upper airway that serves as an anchor for more than half of the pharyngeal muscles responsible for dilating or stabilizing the airway. Consequently, this unique bone is believed to play a key role in maintaining upper airway patency [41, 75].

The recurrent narrowing or complete collapse of airway during sleep is characteristic of obstructive sleep apnea (OSA). OSA is a highly prevalent disorder that causes reduction in blood oxygen saturation, excess carbon dioxide levels and a repetitive interruption of sleep due to frequent cortical arousals to restore breathing [74, 120]. This sleep disorder has serious consequences such as increased risk of traffic or industrial accidents, cardiovascular disease (hypertension or stroke), diabetes, depression and other neurocognitive impairments [85, 123]. Overall, OSA has been shown to significantly increase the all-cause mortality rate by 3-folds [133]. Existing treatments for OSA are either poorly tolerated (continuous positive airway pressure) or

have variable and unpredictable outcomes (e.g. oral appliances, neurostimulation therapy, upper airway surgeries) [24, 29, 60]. This is likely due to the multitude of factors that can be involved in promoting upper airway collapse, which vary between individuals. As such, upper airway physiology and biomechanics remain incompletely understood. Nonetheless, some of the factors known to promote airway collapse include: unfavorable upper airway anatomy, which leads to a narrower airway lumen, such as increased fat volume in the tongue and neck region [57], retruded mandible or maxilla [30, 99, 102]; increased soft palate length [30, 99]; and more compliant (soft) airway tissues [17], including those associated with decreased end expiratory lung volume [113].

The impact of hyoid bone position and movement on upper airway patency is of particular interest to this thesis. Hyoid bone was consistently found to be positioned more caudally in those with OSA compared to healthy individuals [11, 16, 31, 41, 44, 99, 121]. Hyoid bone position is believed to influence upper airway patency and tissue mechanics. This is because the hyoid has a direct influence on all the muscles anchored to it in terms of muscle angle and length, which affects their contractile properties [3, 44, 117]. The inferiorly located hyoid bone in OSA is therefore thought to alter upper airway behavior by reducing the mechanical effectiveness of dilator muscles and thus increasing airway collapsibility [1, 2, 22]. Numerous studies have shown a significant positive correlation between hyoid position and the severity of OSA (quantified using the apnea-hypopnea index, AHI) [16, 47] as well as upper airway collapsibility (quantified using the critical closing pressure,  $P_{crit}$ ) [41, 99], suggesting that an inferiorly positioned hyoid bone leads to a more collapsible upper airway and higher OSA severity.

In addition to the apparent influence of its baseline phenotypic position, the hyoid bone is thought to play a role in other interventions that are known to impact the upper airway, including tracheal displacement/increasing lung volume and mandibular advancement [1-3, 29, 117]. The hyoid bone has been shown to move in response to applied passive loads of tracheal displacement and mandibular advancement [1-3]. Caudal tracheal displacement and mandibular advancement displace the hyoid bone caudally and anterior-cranially, respectively, leading to regional enlargement in the airway lumen dimensions and stiffening of airway soft tissues [1-3, 29]. This hyoid movement is believed to impact the effectiveness of caudal tracheal displacement or mandibular advancement to reduce upper airway collapsibility by redistributing these loads throughout the airway tissue mass.

Hyoid repositioning surgeries have been performed as a treatment option for OSA by advancing the hyoid bone and suspending it either cranially to the mandible (hyomandibular suspension) or caudally to the thyroid cartilage (hyothyroidopexy) [93, 105]. While hyoid suspension procedures were shown to significantly decrease the AHI in OSA, surgical outcomes were highly variable with success rates ranging from 17% to 78% [83]. Hyoid repositioning in an anterior-based direction was found to reduce airway resistance [14, 45, 95] and airway collapsibility [97] in animal and human cadaveric studies. Nonetheless, the mechanisms underlying the influence of hyoid position (phenotypic or surgically repositioned) on upper airway patency and tissue mechanics are still not known as little attention has been given to investigate mechanistically the impact of the hyoid bone on upper airway properties.

Given the complexity of the upper airway anatomy and of the hyoid structure, it is very challenging to study the precise role of the hyoid in human subjects since it

would require invasive procedures. Animal studies can be an alternative but they are costly, time consuming, and limited by the effect of surgical procedures. Besides, it is impossible to study the effect of the different phenotypic baseline hyoid positions physiologically because changing the hyoid position of an individual/animal involves a surgical procedure and the fixation of the hyoid that alters its natural behavior.

Consequently, the use of computational models is ideal to investigate the mechanical contribution of hyoid bone position or movement on upper airway behavior.

Computational models offer multiple advantages as they allow the study of precise procedures with controlled conditions and permit the acquirement of a multitude of outcomes that cannot be or are difficult to be measured physiologically, such as tissue mechanics (stress and strain).

Upper airway computational models have been previously developed [10, 71-73, 107], but none permit the direct study of hyoid bone position or movement on upper airway mechanics. A two-dimensional computational finite element model of the rabbit upper airway, developed by Amatory and colleagues [1], includes the hyoid bone as well as the other major bony and soft tissue structures and is particularly valuable for this study. In fact, it is the only model capable of predicting upper airway geometry and soft tissue mechanical changes in response externally applied loads such as mandibular advancement and tracheal displacement. However, the model lacked the ability to simulate negative intraluminal pressures to study upper airway collapsibility ( $P_{close}$ ), a prime metric used to define the overall stability of the airway. In addition, the influence of hyoid baseline position (i.e. phenotype) or hyoid repositioning (e.g. surgery) on upper airway outcomes were not considered.



## **1.2 Aims**

The primary aims of this thesis are to investigate:

1. The influence of baseline hyoid position (phenotype) on upper airway patency and tissue mechanics
2. The influence of surgical hyoid repositioning for original baseline hyoid position on upper airway patency and tissue mechanics
3. Combined influence of baseline hyoid position and surgical hyoid repositioning on upper airway patency and tissue mechanics

For that purpose, the original computational finite element upper airway model by Amatory et al. [1] will be redeveloped and advanced using ANSYS Workbench (Release 19.2; Academic Research, Canonsburg, PA) to allow for changes in hyoid bone position and simulation of upper airway collapse. Outcomes that will be quantified include upper airway collapsibility ( $P_{close}$ ), airway geometry (lumen CSA and APD) and tissue mechanics (displacement, stress and strain).

## **1.3 Significance and Innovation**

OSA is a global health concern that requires to be further studied and understood. Being anchored to the majority of the upper airway dilatory muscles, the hyoid bone seems to play a crucial role in the maintaining the upper airway patency during sleep which makes this particular bone a potential target for future OSA therapies.

This study will be the first to investigate the influence of hyoid baseline position on upper airway patency and tissues mechanics. It is also the only study that quantitatively assessed various airway outcomes including collapsibility, lumen

geometry as well as tissue stress and strain in response to surgical hyoid repositioning. Moreover, a particular strength of the current study is its ability to precisely investigate the effect of different hyoid baseline positions (phenotypic characteristic) on upper airway outcomes which is impossible to achieve physiologically.

The project's outcomes will serve as proof of concept in helping clarify the role of the hyoid bone in OSA pathogenesis and guide hyoid repositioning surgeries.

## CHAPTER 2

### LITERATURE REVIEW

#### **2.1 The Upper Airway**

This chapter provides an overview of the upper airway anatomy and functions. It also offers a detailed description of the upper airway mechanical properties along with the conventional metrics used to specify and quantify them. A particular emphasis is placed on the upper airway's breathing function and the mechanism that maintain upper airway patency.

##### ***2.1.1 Overview of Upper Airway Anatomy***

###### **2.1.1.1 Basic Structure**

The upper airway is the first part of the respiratory tract extending from the nasal and oral cavities to the base of the epiglottis and is divided into four regions as shown in Figure 1 . The nasopharynx starts at the posterior nasal choanae and ends with the lower margin of the hard palate, the velopharynx extends from the cranial to the caudal end of the soft palate, the oropharynx is the part between the tip of the soft palate and the tip of the epiglottis and the hypopharynx is the region from the tip of the epiglottis to its base (the glottis) [106].

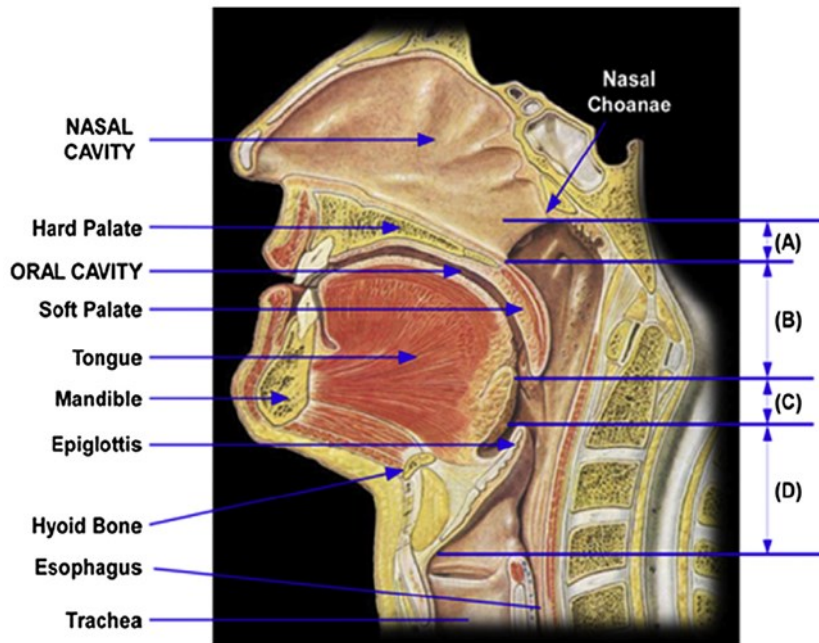


Figure 1: Mid-sagittal section of the Human Upper Airway Anatomy. Representation of a mid-sagittal section of the human upper airway with its subdivisions: (A) Nasopharynx, (B) velopharynx, (C) oropharynx, and (D) hypopharynx. Other major upper airway structures are also shown. *Adapted from Sowho et al [106].*

The pharynx is part of a very complex and elaborate arrangement of bony, cartilaginous and soft tissues known as the pharyngeal tissues. In fact, constrictor muscles form the posterior upper airway wall and part of the lateral wall along with some adipose and glandular tissues. The anterior wall of the airway outlines structures such as the soft palate, tongue, and epiglottis [6].

The position and mechanical properties of the pharyngeal tissues have a direct effect on the behavior of the upper airway. Their active properties involve the pharyngeal reflexes and muscle activity that dilate the airway when needed and their passive properties correspond to the structure.

### 2.1.1.2 Pharyngeal Bony Tissues

The bony components of the upper airway include the **hard palate**, the **mandible** and the **hyoid bone**. The **hard palate** is a fixed horizontal plate of the palatine bone and a part of the maxilla that separates the oral cavity from the nasal cavities (Figure 1). The **mandible** is a U-shaped bone that lies below the maxilla and forms the lower jaw. This bone is mobile and articulates through the temporo-mandibular joint to displace upwards, downwards, or even sideways. The central body of the mandible is a horizontal segment that supports the teeth and the mandibular rami are the quasi-vertical sections that connect to the temporo-mandibular joint to allow the mandible's articulation with the skull. Muscles that are attached to the mandible will be detailed in Section 2.1.1.4. The **hyoid bone** is a mobile bone located at the base of the tongue and almost vertically aligned with the thyroid cartilage. The hyoid bone is a key structure in the upper airway and will be thoroughly described in Section 2.3.1.

### 2.1.1.3 Pharyngeal Cartilaginous Tissues

The cartilaginous tissues of the upper airway are the epiglottis, the thyroid cartilage and the cricoid cartilage. The epiglottis is a thin and elastic cartilage flap that has for main function to close the glottis during swallowing to prevent food from entering the larynx. It is positioned behind the hyoid bone and the base of the tongue and articulates with the thyroid cartilage as shown in Figure 1. The thyroid cartilage is a cartilaginous structure located below the mandible and the hyoid bone that serves as an anchor to some upper airway muscles. It is connected caudally to the trachea and cranially to the hyoid bone through the thyrohyoid membrane. Similarly, the cricoid

cartilage is the first ring of the trachea and the site of attachment of a pharyngeal muscle (inferior constrictor) but also of several muscles of the larynx.

#### 2.1.1.4 Pharyngeal Soft Tissues

The upper airway soft tissues can be divided into two groups: active soft tissue structures (muscles) and passive structures. The passive upper airway soft tissues are mainly adipose and glandular tissues that can vary in size and distribution depending on the individual. However, the upper airway muscles actively modify the upper airway and are concentrated in four areas: the **tongue**, the **soft palate**, the **hyoid bone** and the **pharyngeal walls** [39] (see Figure 2).

The **tongue** is an organ that is made of intrinsic muscles (entirely within the tongue) and extrinsic muscles (originate from other structures and insert into the tongue). The intrinsic tongue muscles alter the shape of the tongue while the extrinsic muscles determine the position of the tongue with respect to the neighboring upper airway structures. Thus, the tongue extrinsic muscles are of interest to us and include the *genioglossus*, the *hyoglossus*, the *styloglossus* and the *palatoglossus*. The *genioglossus* projects from the anterior border of the mandible to the body of the tongue and pulls the tongue anteriorly when activated. The effect that the *genioglossus* has on the upper airway has been widely studied and it was shown that its contraction causes the stiffening and enlargement of the pharyngeal airway [109]. The *styloglossus* connects the styloid process to the superior side of the tongue and the *palatoglossus* originates from the anterior surface of the soft palate and inserts into the lateral part of the tongue to merge with the *styloglossus*. The *styloglossus* and *palatoglossus* muscles are both retracting muscles and act to pull the tongue posteriorly [118] [54].

The **soft palate** is an active structure containing several muscles that control its behavior including the *tensor palatini*, *levator palatini*, *palatoglossus*, *palatopharyngeus* and *musculus uvulae*. These muscles insert into the soft palate but originate from caudal, cranial and posterior parts of the upper airway. The different soft palate muscles act together to either lower the soft palate during nasal breathing to make sure that the velopharynx is open or elevate the soft palate while swallowing to close the velopharynx [118].

The hyoid bone is the anchor to many upper airway muscles that determine its relative position in the upper airway. The **hyoid muscles** will be presented in Section 2.3.1.

Lastly, the **pharyngeal** posterior and lateral walls are made of the superior, middle and inferior *constrictor muscle* sheets that originate from lateral structures and wrap around the airway. The main function of these constrictor muscles is to narrow the upper airway to assist active swallowing [90]. Other minor pharyngeal muscles (*stylopharyngeus* and *salpingopharynx*) serve to raise the pharynx and larynx during swallowing or speech [118].

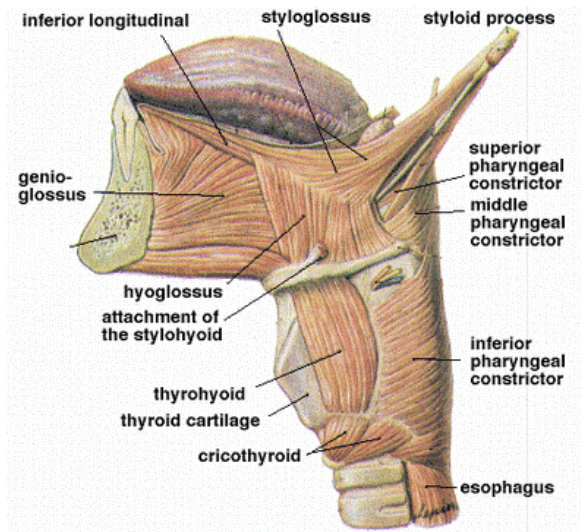


Figure 2: Upper Airway Muscles. Schematic showing some key upper airway muscles constrictor muscles and extrinsic tongue muscles. *Adapted and modified from Kairaitis et al. [62]*

### 2.1.2 Overview of Upper Airway Functions

The upper airway is a muscular tube-like structure that connects the nasal and oral cavities to the larynx and esophagus as mentioned previously. In fact, there are about 24 muscles in the upper airway originating from different structures that regulate the movements of the tongue, soft palate, hyoid bone and pharyngeal walls [39, 106]. The presence of all these muscles allows the upper airway to be a dynamic structure that has a very complex neuromechanical behavior permitting it to fulfill the functions of speech, swallowing and breathing [106, 114]. Throughout this thesis, breathing will be the function of interest for which the upper airway's role is to provide a passage for the air to be delivered in and out of the lungs through the nose or the mouth. However, the high deformability of the upper airway is disadvantageous to respiratory function since it makes the airway prone to close off especially under the negative pressures present during inspiration. Rigid upper airway walls would be ideal for the breathing function but this compromise in structure serves the other upper airway functions: swallowing



and speech production. Speech production, for example, involves elaborate and controlled movements of the upper airway. Thus, the evolution of speech in humans has developed a certain amount of motility to the upper airway that makes it susceptible to collapse [32].

### ***2.1.3 Upper Airway Mechanics***

The behavior of the upper airway is dependent on both active and passive properties of the upper airway tissues. The passive component is based on anatomical and mechanical characteristics of the tissues that form the airway and the active component includes muscle activity and deformations related to the respiratory cycle [17]. In this study, we will focus on understanding the passive upper airway biomechanics.

#### **2.1.3.1 Forces Maintaining Upper Airway Patency**

The most important upper airway property when considering its respiratory function is the upper airway patency. Upper airway patency is the ability of the airway to stay open and unobstructed to allow the passage of air to the lungs and thus permit breathing. Since the upper airway is not a rigid tube, its patency is a balance between forces that promote the airway collapse (falling together of airway walls) and forces that act to maintain its patency as shown in Figure 3. The negative pressure in the airway present during inspiration and the extra-luminal pressure exerted by tissues surrounding the airway act in favor of pharyngeal collapse. In opposition, the dilatory muscle forces and the longitudinal traction that accompanies the increase in lung volume act to maintain the airway open [74]. Therefore, any factor that modifies the above forces can

create an imbalance leading to the airway collapse. For example, the accumulation of fat in the neck and tongue or mandible retrusion increases the extra-luminal tissue pressure [125, 134]. Also, impaired muscle function or control can lead to collapse of the airway [58]. The factors that affect this balance as occurs in sleep disordered breathing are discussed in Section 2.2.3.1.

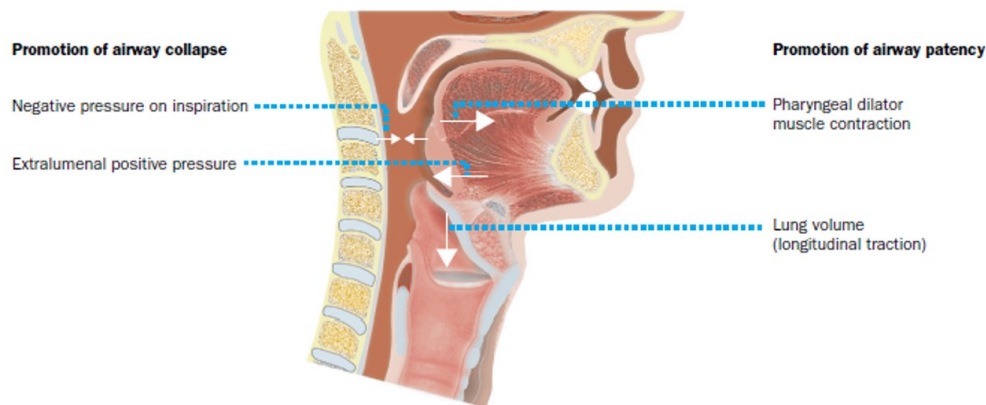


Figure 3: Schematic of the Upper Airway with the Forces that Affect its Patency. The upper airway patency is maintained by a balance of forces. Dilator muscles and longitudinal traction maintain pharyngeal patency while extraluminal positive pressure and inspiratory intraluminal pressure promote its collapse. *Adapted and modified from Malhotra et al [74].*

### 2.1.3.2 Quantification of Upper Airway Mechanics

Upper airway geometry, compliance, collapsibility and tissue mechanical properties are parameters that are typically examined to evaluate upper airway mechanics and provide some insight on the behavior of the given airway.

#### 2.1.3.2.1 Upper Airway Geometry

Upper airway geometry is generally quantified as the upper airway lumen size represented by either the overall upper airway volume or cross-sectional measurements such as the cross-sectional area, antero-posterior diameter and lateral diameter. These dimensions can be acquired from head and neck images, usually CT or MRI, and the

cross-sectional measurements can be presented and examined in various ways depending on the study. In some cases, the cross-sectional metrics are obtained at a single level of the upper airway or at selected levels along its length. In other cases, the metrics are acquired as an average representation of the entire airway or over particular regions often corresponding to the anatomically defined upper airway regions (velopharynx, oropharynx, hypopharynx). The smallest and/or largest cross-sectional size/metrics can also be reported. The lumen size is an important parameter of the upper airway mechanics since it directly affects the amount of airflow that can pass through the airway for a given pressure and thus is a main indicator of the degree of upper airway patency [59].

In a less obvious manner, the airway length also impacts the upper airway mechanics and behavior. The airway length is also measured through imaging techniques but more information about the upper airway's condition is needed before one can determine the influence that the length has on the upper airway's mechanics [7].

#### 2.1.3.2.2 Upper Airway Compliance

The compliance is a parameter that describes the ability of the airway to deform when subjected to intra-luminal pressure changes. In other words, it represents the functional radial stiffness of the airway tissues or their resistance to an applied surface load. The compliance is thus assessed as the amount of change in upper airway lumen size for a given change in intraluminal pressure and can be acquired from imaging or animal studies [109]. In an animal model, the compliance is found by measuring the intraluminal pressure change that corresponds to the amount of volume injected in the airway reflecting the overall lumen size change. When using imaging, the compliance is evaluated by measuring the lumen size change for a particular pressure at any chosen

point or region along the length of the airway which allows the compliance to be obtained at different cross-sectional levels or regions [67, 94]. Consequently, the degree of compliance offers an indication of the effect of intraluminal pressure on upper airway patency and the likeliness and location at which the airway might narrow.

#### 2.1.3.2.3 Upper Airway Collapsibility

The collapsibility is a variable used to determine the upper airway's propensity for collapse and is a key parameter for assessing upper airway mechanics. It can be considered as a measure of the resistance of the upper airway to narrowing or its stability: A more collapsible airway is less stable. To evaluate collapsibility, two intraluminal pressure-based quantities were developed: the critical closing pressure ( $P_{crit}$ ) and the closing pressure ( $P_{close}$ ).

The critical closing pressure ( $P_{crit}$ ) is the “gold standard” for measuring collapsibility and is the estimated nasal pressure that causes upper airway collapse under dynamic conditions (with airflow in upper airway) [25, 103].  $P_{crit}$  represents the pressure at which the airway closes after airflow limitation which is a phenomenon of the dynamic upper airway that occurs when an increase in pressure does not lead to an increase in the airflow anymore. Airflow limitation implies that narrowing in a region of the airway occurs and the airflow become independent of the downstream pressure and dependent on the upstream pressure and the pharyngeal tissue pressure. To measure the critical closing pressure ( $P_{crit}$ ), the following method is performed. The nasal pressure is reduced from a positive value until flow limitation occurs and the value of flow and nasal pressure at airflow limitation is noted. The process is repeated at different stages of the respiratory cycle to get airflow limitation at different flows. A relationship

between the nasal pressure and flow at flow limitation is then derived and plotted.  $P_{crit}$  is obtained when the derived relation intersects with the flow axis (when flow is zero).

The closing pressure ( $P_{close}$ ) is another quantity used to describe upper airway collapsibility and is defined as the intraluminal pressure at which the upper airway collapses in the absence of muscle activity and airflow through the airway [6]. In other words,  $P_{close}$  characterizes the intrinsic pharyngeal tissue pressure component that leads to upper airway collapse. Measuring  $P_{close}$  without the effect of other factors such as the lung volume usually requires invasive procedures that are done in animal models as follows [94]. The upper airway is first isolated at the cranial end of trachea, the system is sealed, and upstream and downstream pressures are monitored. The downstream pressure is decreased progressively while the upstream pressure is recorded. When the airway is open, the upstream pressure decreases with the downstream pressure, but this no longer happens as soon as the airway closes. From this point on, the downstream pressure keeps decreasing but it is no longer transmitted to the upstream pressure that become independent of the downstream pressure. The closing pressure,  $P_{close}$ , is defined as the first downstream pressure at which the upstream pressure stops decreasing. Another method of measuring  $P_{close}$  on anesthetized humans was developed by Isono et al. in a less isolated airway [59]. In this method, a series of pressure drops are induced through a nasal mask and the corresponding lumen cross sectional area at a particular level of the airway is measured using video-endoscopy techniques. The pressure and corresponding area values obtained are fitted and  $P_{close}$  is found by setting the area to zero in the relation found.

#### 2.1.3.2.4 Pharyngeal Tissue Pressure and Strain

Pharyngeal tissue pressure represents the pressure found within the surrounding upper airway tissues. This tissue pressure is an important parameter to be considered for examining upper airway mechanics since it is a major component in the balance of forces that contribute to maintaining upper airway patency (Section 2.1.3.1). The measurement of the pharyngeal tissue pressure cannot be obtained in humans since it requires very invasive procedures. This parameter has been measured in several animal models using pressure transducers implanted in the tissues [2, 3].

Tissue strain is a measure of the deformation per unit length of the upper airway surrounding tissues in a particular situation where they are subjected to a certain load. The measurement of tissue strain experimentally is complex and requires advanced MR imaging and image processing techniques [20].

## **2.2 Obstructive Sleep Apnea (OSA)**

### **2.2.1 Overview**

Obstructive sleep apnea (OSA) is a disorder characterized by the episodic narrowing (hypopnea) or complete collapse (apnea) of the upper airway during sleep. This limits or completely blocks the air flowing into/out of the lungs causing reductions in blood oxygen, excess carbon dioxide, and sleep fragmentation (interruption of sleep due to frequent cortical arousals) [34, 74, 120].

Common consequences of OSA include excessive daytime sleepiness that can cause serious traffic or industrial accidents, cardiovascular disease such as stroke or hypertension, cognitive impairment particularly in memory and new learning, depression and even diabetes [85, 123]. Hence, OSA can have detrimental effects on

both the health and quality of life of individuals suffering from the disorder. Being an increasingly common disorder with a prevalence of around 34% in men and 17% in women aged 30-70 years [84], OSA represents a major global health concern. Therefore, it is important to ensure that diagnosis and treatment of OSA are effective and accessible to all.

The current “gold standard” treatment of OSA is the continuous positive airway pressure (CPAP) applied via a nasal or oronasal mask that provides a constant level of positive pressure to prevent upper airway collapse. This treatment is highly efficacious if used consistently, but due to its obtrusive nature, its adherence rates are often unacceptably low (~ 55%) [60]. Alternative procedures such as oral appliances, upper airway nerve stimulation and upper airway modifying surgeries are thus considered with increasing interest [24, 28]. However, these procedures have variable and non-predictable outcomes with success rates around 50% in general [24, 28]. This variability in OSA treatment outcomes is related to the incomplete understanding of upper airway biomechanics and physiological behavior given that the upper airway is a complex dynamic structure.

### ***2.2.2 Pathophysiology of OSA***

As demonstrated in the previous section (Section 2.1), the upper airway is a complex structure that is highly deformable since the pharyngeal walls have no bony or cartilaginous support apart from the spine posteriorly. This high deformability makes the airway prone to collapse, particularly during sleep, which can lead to sleep disordered breathing.

The mechanism of collapse that occurs in OSA patients is related to an imbalance between the forces that promote collapse and the forces that preserve patency. As described in Section 2.1.3.1, the forces promoting collapse are the negative intraluminal pressure induced by inspiration and the tissue pressure depending on some anatomical factors. The protective mechanisms preventing collapse include first of all an increase in lung volume that tends to keep the airway open by tracheal traction. The pharyngeal dilator muscles also play a very important role in keeping the airway open through reflex pathways. These muscles usually increase their activity in response to stimuli such as negative intraluminal pressure and increased CO<sub>2</sub> or decreased O<sub>2</sub> [34, 74]. During wakefulness, this balance of forces is maintained in healthy and OSA patients and the airway stays open. However, the dilatory muscles' activity and responsiveness to stimuli is relatively decreased during sleep and the upper airway becomes more collapsible [74, 126]. The upper airway of a healthy individual can overcome this fall in muscle activity and maintain upper airway patency all through sleep. On the contrary, pharyngeal collapsibility is increased in OSA patients which causes the airway to narrow and eventually close during sleep [86]. Breathing is thus interrupted, and cortical arousal is often needed to restore normal airflow. A standard way to assess the severity of OSA is by calculating the apnea-hypopnea index (AHI) value defined as the number of apnea and hypopnea events per hour of sleep.

There are numerous anatomical and non-anatomical factors (discussed in the next Section 2.2.3.1) that can affect the upper airway mechanics and cause the airway of OSA patients to be more collapsible. These factors can vary between individuals and the pathological causes of OSA are not yet fully understood. The arousal threshold is another important aspect of OSA pathophysiology as OSA patients often have a low



arousal threshold that participates in the development of the pathology [24]. It has been shown that in some cases, the airflow is restored after the airway had collapsed before cortical arousal occurs [132]. This suggests that delaying arousal in patients with a low threshold could be useful and prevent sleep fragmentation for certain OSA patients. However, further delay in cortical arousal is not possible in patients that have a relatively high threshold already as it might lead to a toxic accumulation of CO<sub>2</sub> [24, 132].

### ***2.2.3 Upper Airway Mechanics and OSA***

#### **2.2.3.1 Factors Affecting Upper Airway Mechanics**

Although the exact upper airway mechanics are not yet fully understood, some factors are known to directly impact the upper airway mechanics and increase its collapsibility. These factors can be considered as common traits contributing to OSA.

##### **2.2.3.1.1 Anatomy**

A poor upper airway anatomy can be a major contributor to alter upper airway mechanics and lead to a more collapsible airway. In fact, some craniofacial criteria such as the position of the mandible, maxilla and hyoid bone have been associated with OSA [13, 80]. Several studies have shown that maxillary and mandibular retrognathism is commonly observed in OSA patients compared to healthy individuals [30, 99, 102]. This structural abnormality crowds the soft tissues behind the mandible in a smaller space and brings the soft palate closer to the posterior pharyngeal wall. The airway lumen size is thus smaller and the pharyngeal tissue pressure higher which compromises the airway patency. Moreover, an inferiorly positioned hyoid bone is also significantly correlated to OSA and will be discussed in Section 2.3.2 in details.

A very common OSA treatment known as mandibular advancement consists in altering the craniofacial anatomy by moving the mandible anteriorly. This can be done with the help of an oral splint that pushes the mandible forward or by means of a maxillo-mandibular advancement surgical procedure. Mandibular advancement has been shown to improve airway lumen dimensions and patency but mandibular advancement treatments have variable and unpredictable success rates [21, 28, 135].

The relative soft tissue size has also been shown to play an important role in upper airway mechanics. An enlarged tongue, longer soft palate or enlarged tonsils were observed in OSA patients [17, 30]. The increase in soft tissue volume leads to an increase in tissue pressure which alters the airway lumen size and collapsibility. Some surgical OSA treatments involve the reduction of the size of some soft tissues such as Uvulopalatopharyngoplasty (UPPP). These procedures are usually part of a multilevel surgery combining several treatment procedures and have unpredictable outcomes [19, 23, 27].

#### 2.2.3.1.2 Body Weight and Neck Circumference

Obesity, usually measured as BMI, is one of the most strongly correlated variables to OSA and an increased collapsibility [134]. Several studies have also shown that patients with a higher BMI tend to also have a higher Apnea-Hypopnea-Index (AHI). Obesity is known to be related to several factors that affect upper airway mechanics depending on the fat distribution of each individual. Firstly, the pharyngeal tissue volume is increased since obesity causes the presence of fat pads in pharyngeal tissues. Moreover, obesity is associated to an expansion in the tongue size and decreased lung volume. All these factors lead to a rise in the forces that promote upper airway collapse. An increase in the neck circumference is also a predictor of OSA that

is linked to the fat deposition in the neck that accompanies obesity [33]. A large neck circumference was shown to decrease the upper airway lumen size and increase upper airway collapsibility [99]. In this context, weight loss is considered as an important part of the treatment plan of OSA patients that are overweight.

#### 2.2.3.1.3 Muscle Activity and Reflexes

The behavior and properties of the upper airway muscles play an important but very complex role in the upper airway mechanics. Several factors influence the upper airway muscles action including the physiological properties of the muscles, the effectiveness of their contraction, the amount of neuromuscular activity and their coupling to other tissues [24, 74, 98]. The genioglossus has been one of the most studied upper airway muscles and its activation is known to be crucial in maintaining airway patency in OSA patients [25, 126]. The reduced genioglossus activity during sleep is directly related to the upper airway collapse in cases. Thus, several OSA treatment are focused on increasing upper airway muscle responsiveness or direct stimulation of some muscles [24, 110, 128].

#### 2.2.3.1.4 Lung Volume and Tracheal Traction

The lung volume has a considerable effect on the forces that impact upper airway mechanics and is altered accordingly in the natural breathing process. During inspiration, the lung volume is enlarged causing an increase in upper airway wall stiffness and the opposite occurs during deflation of the lungs upon expiration. An increase in lung volume has been shown to reduce upper airway collapsibility, increase luminal size and a decrease in lung volume is linked to an increase in OSA severity [52, 68, 74]. Moreover, the level of positive pressure induced by the CPAP treatment is dependent on the lung volume of the patient [51]. The influence of the lung volume on

airway mechanics is thought to be associated with the transmission of traction forces between the chest wall, trachea and pharyngeal tissues [113]. This is shown through the reduced upper airway collapsibility that occurs when downwards tracheal displacement is applied animal models [2, 63].

#### 2.2.3.1.5 Posture and Head/Neck Position

Posture directly alters the way gravitational forces impact the upper airway mechanics. The supine position particularly challenges upper airway patency and studies have shown that the AHI is higher in supine position sleep compared to lateral position sleep for the same patient. Due to their weight, the soft palate, tongue and epiglottis are moved posteriorly in the supine position which might close the airway [28, 91]. The head and neck relative position was also shown to impact upper airway mechanics. Head extension reduced upper airway collapsibility and increased airway lumen size while head flexion increased upper airway collapsibility [80].

#### 2.2.3.2 OSA risk factors

There are many factors that affect upper airway mechanics and play a role in the development of OSA pathology. These factors are patient specific and not always fully understood. Several studies have tried to determine the most common characteristics associated with OSA and four main OSA risk factors were identified. Obesity, poor craniofacial anatomy, male gender and aging have been classified as the risk factors of OSA [134]. Obesity and poor craniofacial anatomy were tackled in detail in the previous section.

#### 2.2.3.2.1 Male Gender Factor

OSA prevalence is of around 34% in men and only 17% in women aged 30-70 years [84]. One explanation to this is the difference in the body fat distribution between males and female leading males to have larger neck circumference in general and central adiposity. The latter causes a reduction in lung volume due to the forces exerted by the fat concentration on the lungs. This will lead to a reduction of caudal traction and an increase in upper airway collapsibility (explained in Section 2.2.3.1.4). Other reasons include the common upper airway morphological differences between males and female and the protective effects that the female sex hormones have on upper airway patency [134].

#### 2.2.3.2.2 Age Factor

Disease prevalence increases by 2 to 3 folds in individuals that are above 65 years old compared to middle aged individuals (30-64 years) [134]. The difference was associated with some changes that usually occur with the aging process such as an increased fat deposition in the neck region and the lengthening of the soft palate. It is also argued that the change in hormones that occur at menopause in females contributes to the increase in the risk of developing OSA [84, 134].

### **2.3 Hyoid Bone and Upper Airway Patency**

#### ***2.3.1 Physiology of the Hyoid Bone***

The hyoid bone is a small U-shaped bone located directly below the tongue (Figure 4). This bone is unique given that it is attached to neighboring bones and structures only through muscle and ligament attachments making the hyoid bone extremely mobile. In fact, about half of the upper airway muscles insert into the hyoid

bone as shown in Figure 4. Mainly, hyoid muscles are divided into the suprahyoid and infrahyoid muscles.

There are 4 pairs of suprahyoid muscles that form the floor of the mouth together with adjacent tissues. The mylohyoid and geniohyoid muscles attach the hyoid bone to the mandible and move the hyoid cranially and anteriorly when they contract. The digastric muscle stretches between the mastoid notch on the inferior surface of the skull to the chin but attaches to the hyoid bone through the intermediate tendon midway between its anterior and posterior belly. This muscle is involved in complex jaw movements and elevates the hyoid bone when it contracts. Lastly, the stylohyoid muscle extends from the styloid process of the temporal bone to the hyoid bone and pulls the hyoid bone upwards and backwards when it contracts.

The infrahyoid muscles are 3 pairs of muscles that attach the hyoid bone to inferior structures and pull the hyoid downwards when they contract. The thyrohyoid muscle attaches the hyoid to the thyroid cartilage, the sternohyoid to the sternum and the omohyoid to the shoulder bone. Together, the infrahyoid and suprahyoid muscles are responsible for the position of the hyoid bone in the upper airway.

Other important muscles that insert into the hyoid bone are extrinsic tongue muscles and pharyngeal constrictor muscles. The middle pharyngeal constrictor, one of the sheets of muscles that form the pharynx, is partly attached to the hyoid bone and is responsible for constricting the middle part of the pharynx. The genioglossus is an extrinsic tongue muscle that originates from the mandible and has a set of inferior fibers that attach to the surface of the hyoid bone. Finally, the hyoglossus muscle is another extrinsic tongue muscle that originates from the hyoid bone and enters the side of the tongue. It is able to flatten the tongue and pull it downwards and backwards [39, 75].

As a matter of fact, one of the main functions of the hyoid bone is to serve as an anchor for the tongue and hold it up through these muscles. The hyoid bone also holds up the larynx through the thyrohyoid membrane that connects the hyoid bone and the thyroid cartilage. Tongue position was found to be highly correlated to hyoid position during eating and to a lesser extent during speech [76]. Moreover, the hyoid bone plays a fundamental role in the movement of the upper airway involved in swallowing for example. The hyoid bone is a central biomechanical component of the swallowing function since a vertical and anterior displacement of the hyoid bone is a marker of swallowing initiation [66]. Lastly, the hyoid bone has been shown to be implicated in the collapse of the upper airway that occurs in obstructive sleep apnea. For the purpose of this thesis, we will focus on the effect the hyoid bone on breathing mechanics and upper airway patency.

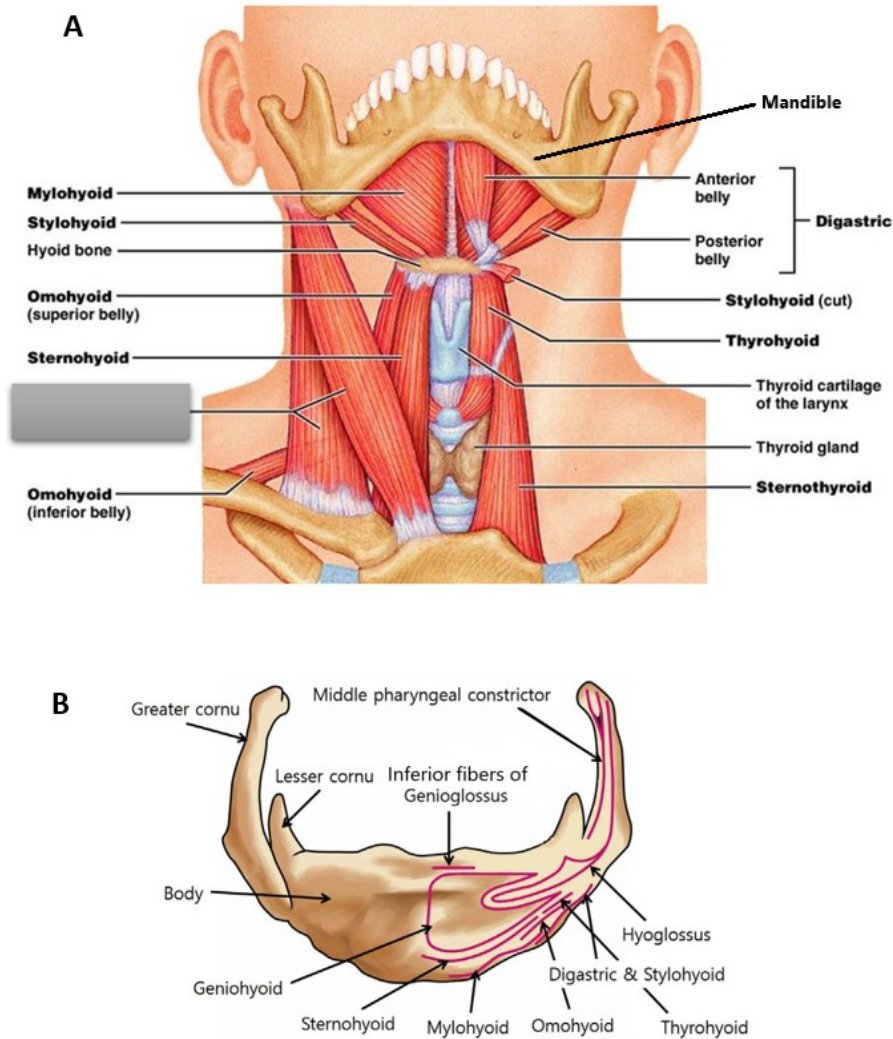


Figure 4: Hyoid Anatomy and Muscle Attachments. A) Schematic representation of the hyoid bone and some of its muscle connections in the neck (anterior view). The mandible, thyroid cartilage and thyroid gland are also shown. Adapted and modified from Marieb [75]. B) Illustration of the anterior view of the hyoid bone with the location of the muscle insertions shown as red outlines. Adapted and modified from Goh *et al* [44].

### 2.3.2 Role of Hyoid Bone in Upper Airway Patency

#### 2.3.2.1 Hyoid Bone and Upper Airway Mechanics

The hyoid bone is a prime structure causing changes to upper airway mechanics and patency since it is attached to several muscles and ligaments that connect it to important neighboring tissues such as the tongue, the epiglottis, the trachea and lateral



pharyngeal musculature as discussed in the previous section. Therefore, a change in the hyoid position affects anatomical characteristics and is likely to alter the effectiveness of the muscles attached to it and lead to modifications in the upper airway mechanics [1, 2, 22, 44]. In fact, a more caudally placed hyoid bone was consistently observed in OSA patients compared to healthy subjects [11, 16, 31, 41, 44, 99, 121]. Among many other studies, a study conducted by Barrera et al demonstrated that the group of individuals that suffers from OSA have a significantly longer distance between the mandibular plane (tangent to the lower border of the mandible and lowest point in the chin) and the hyoid bone when compared to the healthy group (with  $p=0.009$ ) [11]. Moreover, Bilici and colleagues found a significant and positive correlation between the apnea-hypopnea index value (reflecting OSA severity) and the distance from the chin to the hyoid (with  $r=0.368$  and  $p=0.005$ ) [16]. A study by Chi et al demonstrated that an enlargement of the tongue is consistently observed with an inferior hyoid position as shown in Figure 5 [31].

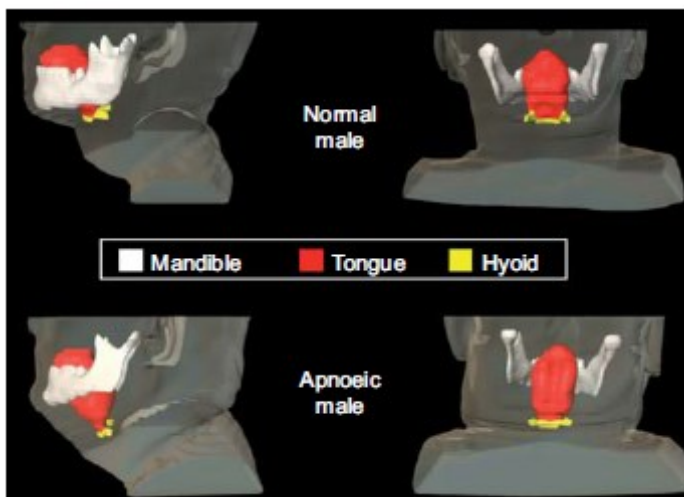


Figure 5: Illustration of Hyoid Position in Apnoeic Male Compared to a Normal Healthy Male. 3-Dimensional reconstruction of the hyoid, tongue and mandible from MRI images of a healthy subject and a patient with sleep apnea shows a more inferior position of the hyoid bone in the apnoeic patient. The tongue volume also appears to be greater in the apnoeic patient. *Adapted from Chi et al [31].*

Although hyoid position was found to be consistently and strongly correlated to OSA, the exact mechanical effect of the hyoid on the upper airway properties remains unclear. However, it is likely that when hyoid position is modified, the angle of the muscles that are attached to it and their length/tension relationship changes leading to different muscle force vectors and even different contractile properties [3, 117]. Since the muscle effectiveness may be altered, an unusual hyoid bone position might result in poor muscle dilatory forces. The change in the muscle dilatory forces will create an instability to the balance between dilatory and collapsing forces required to maintain the airway patency and hence lead to the pharyngeal collapse that occurs in OSA.

Some studies have attempted to relate the hyoid bone position to the parameters describing upper airway mechanics. Studies conducted by Genta et al. and Sfroza et al. have shown a strong positive correlation between the hyoid position and the pharyngeal critical pressure ( $P_{crit}$ ) indicating that a more inferiorly placed hyoid bone leads to a more collapsible upper airway [41, 99]. Furthermore, anterior hyoid advancement was shown to reduce upper airway resistance to airflow and collapsibility [14, 45, 95, 97]. In particular, an animal study conducted in the SUARG research group at AUB [97] quantitatively assessed the effect of surgical hyoid bone repositioning by numerous magnitudes and in different directions on upper airway collapsibility in rabbits. This study demonstrated that anterior displacement of the hyoid bone is the main factor for upper airway collapsibility decrease.

### 2.3.2.2 Hyoid Bone in OSA Surgical Treatment

Playing such a role in the upper airway mechanics and patency, modifying hyoid position has been attempted as a therapeutic surgical management of OSA [23, 105].

Two surgical hyoid repositioning procedures have been used in OSA treatment:

Hyomandibular suspension and hyothyroidopexy that involve first transection of select hyoid bone muscles and then suspension of the hyoid bone either to the mandible or to the thyroid cartilage, respectively (See Figure 6) [15, 44, 92, 93].

Hyoid repositioning surgeries were shown to significantly decrease the apnea-hypopnea index [83]; nonetheless, the surgical outcomes were found to be variable with success rate of approximately 50% [19, 64, 83, 105]. The success is defined as a 50% reduction in apnea-hypopnea index and an apnea-hypopnea index less than 20 usually indicating a mild OSA severity. An evidence-based medicine review by Kezirian et al. presented the outcomes of different studies that investigated the role of hyothyroidopexy alone, as shown in Table 1, demonstrating the variability in the outcomes (success rate range between 17 and 78%) [64]. Moreover, hyoid surgery is most commonly combined with other upper airway surgical procedures in which case it seems to improve the post-surgical outcomes and increase the percentage of surgical success [9, 23]. We can thus conclude that the mechanism of action of the hyoid repositioning surgery is not really understood.

Overall, the number of hyoid repositioning studies is relatively small and no clear comparison in the outcomes of the different hyoid repositioning surgical procedures was done. The comparison between hyomandibular suspension and hyothyroidopexy will be discussed in Chapter 5, Section 5.5.2 and 5.6.

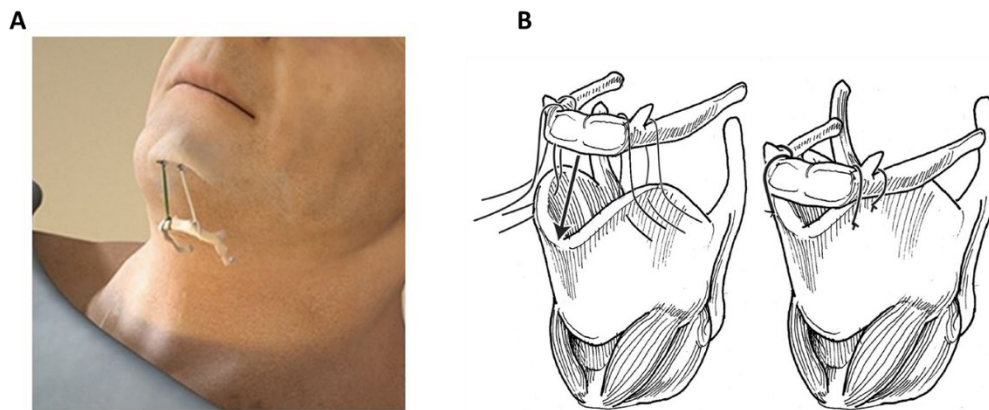


Figure 6: Illustration of hyomandibular suspension (A) and hyothyroidopexy (B) procedures performed clinically as part of OSA treatment. (A) Image showing the hyoid bone anchored to the anterior-most edge of the mandible. (B) Schematic diagram showing the hyoid (top bone) and the thyroid cartilage (bottom) before (left diagram) and after thyrohyoidopexy (right diagram). *Figures A and B are adapted and modified from Van Tassel et al. [119] and Benoist et al. [15], respectively.*

Study	AHI mean, Preoperative	AHI mean, Postoperative	No. of Success** / Total No. of Cases (%)
Vilaseca et al [122]	48.3	29.0*	5/9 (56)
Neruntarat [81]	44.5	15.2*	25/32 (78)
Der Herder et al [35]	32.1	22.2	16/31 (52)
Bowden et al [19]	36.5	37.6	5/29 (17)

\*  $p < .05$ , significant change in AHI.

\*\* Success is defined as 50% or more reduction in AHI and an AHI less than 20.

Table 1: Hyoid Suspension Surgical Outcomes. Preoperative and postoperative mean AHI and success rate of four different studies that considered the role of hyoid suspension (hyothyroidopexy) alone. Two out of the four studies showed a significant postoperative decrease in AHI and the success rates are very different demonstrating the variability in the outcomes of hyoid suspension surgery. Abbreviations: AHI, apnea-hypopnea index. *Adapted and modified from Kezirian et al [64].*

### 2.3.2.3 Hyoid Bone and Other OSA-related Procedures

#### 2.3.2.3.1 Hyoid Bone and Tracheal Displacement

Since the hyoid bone is an exceptionally mobile structure in the upper airway, external passive loads applied to the airway also move this bone. An example of such loads is the caudal displacement of the trachea, a mechanism through which the pharyngeal airway lumen size and collapsibility are affected by an increase in lung volume (Section 2.2.3.1.4) [63]. In an animal study by Amatory et al., the hyoid bone was caudally displaced with caudal tracheal displacement through the thyrohyoid muscle attaching it to the thyroid cartilage. As shown in Figure 7, caudal hyoid movement increases linearly as higher trachea displacement load is applied [2]. The caudal hyoid movement suggests that the suprahyoid muscles are elongated which will stretch and stiffen the concerned airway tissues. Consequently, this caudal hyoid movement is believed to play a major role in redistributing the tracheal displacement loads resulting in regional lumen geometry changes and thus modifications to the upper airway collapsibility.

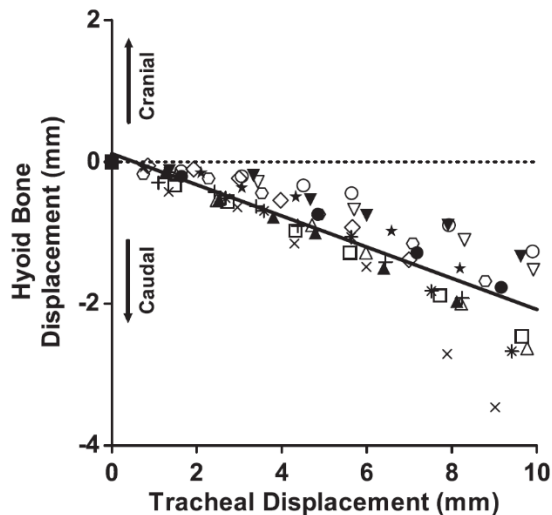


Figure 7: Hyoid Bone Displacement in Response to Caudal Tracheal Displacement in a Rabbit Animal Study. Plot representing the rabbit data for hyoid displacement acquired when caudal tracheal displacement was performed. The hyoid bone is displaced caudally by about 2mm, in a linear fashion, as a result of 10 mm of tracheal displacement. Adapted from Amatoury et al. [2].

#### 2.3.2.3.2 Hyoid Bone and Mandibular Advancement

Mandibular advancement load is applied through an oral appliance and improves upper airway patency in some people with OSA, however surgical mandibular advancement can also be performed [27, 28]. Mandibular advancement is thought to prevent upper airway collapse by enlarging the airway and stiffening pharyngeal soft tissues [1, 3, 21]. Movement of the hyoid bone in response to mandibular advancement is commonly observed in humans primarily in both cranial and anterior directions [29, 40, 69]. Recently, an animal study undertaken in anesthetized rabbits similarly showed cranial-anterior hyoid bone displacement with mandibular advancement (Figure 8) [3]. This study also showed a cranial displacement of the thyroid cartilage in response to mandibular advancement.

If we consider the hyoid anatomy and its muscle attachments, we can imagine that the movement of the hyoid bone is a result of the mandible-originating suprahyoid

muscles, mainly the geniohyoid and mylohyoid muscles. This cranial-anterior hyoid movement will likely also induce the stretching of the infrahyoid muscles resulting in a cranial displacement of the thyroid cartilage and the stiffening of the anterior pharyngeal tissues. In addition, this hyoid movement will likely stretch the middle pharyngeal constrictor muscle and the stylohyoid muscle leading to the stiffening of the lateral pharyngeal walls and enlargement of the lateral airway lumen dimension.

As such, the hyoid movement plays an important role in transferring the external passive mandibular advancement applied loads throughout the airway and redistributing the induced displacement.

A computational finite element model of the passive rabbit upper airway developed by Amatoory et al. [1], that will be described in detail in Section 2.5, was later used to investigate the effect of fixing the hyoid bone on mandibular advancement in terms of tissue displacement, stress and strain. The outcomes of the mandibular advancement simulations with and without fixing the hyoid bone are shown in Figure 9. As a result of hyoid bone fixation, the tissue displacements in response to mandibular advancement were reduced in the tongue and tissue mass but the stresses and strains were increased in that region. The displacements, stresses and strains were also minimal in the tissues caudal to the hyoid bone. Moreover, stresses and strains were reduced in the soft palate. These finite element model predictions reinforce the idea that the hyoid bone plays a key role in the effect that mandibular advancement has on the upper airway, and likely also mandibular advancement efficacy. If hyoid movement is not allowed, the mandibular advancement loads will not be transferred throughout the airway, limiting the enlargement and stiffening of the airway [1, 3].

Additionally, a study by Skinner et al. found that the hyoid initial position (baseline) can be a predicting factor for mandibular advancement success or failure [102]. Therefore, if we better understand the way through which the hyoid bone impacts the efficacy of other OSA treatments (such as mandibular advancement), we could predict to a certain extent these treatment's outcome.

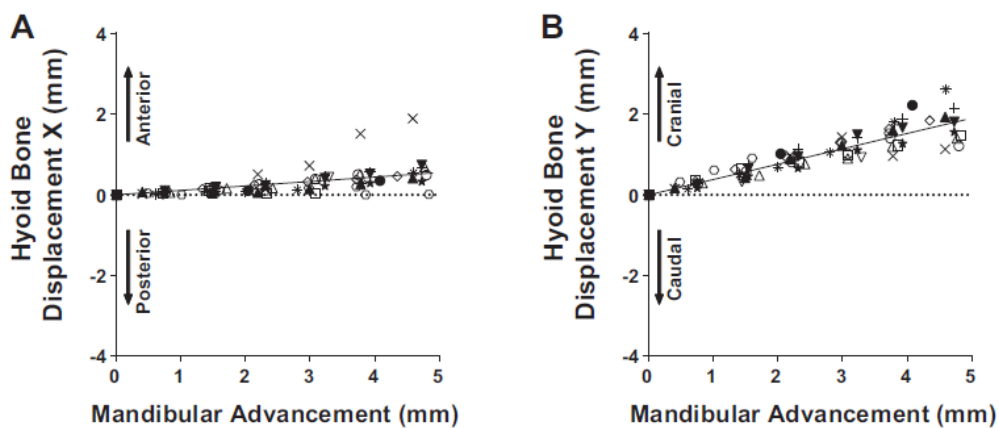


Figure 8: Hyoid Bone Displacement in Response to Mandibular Advancement in a Rabbit Animal Study. Rabbit data shows an effect of mandibular advancement on displacement of hyoid bone in the anterior-posterior direction (A) and the cranial-caudal direction (B). Symbols represent individual rabbit data and solid line represents the linear-mixed effects model. Mandibular advancement results in anterior and cranial movement on the hyoid bone. *Adapted from Amatoury et al. [3].*



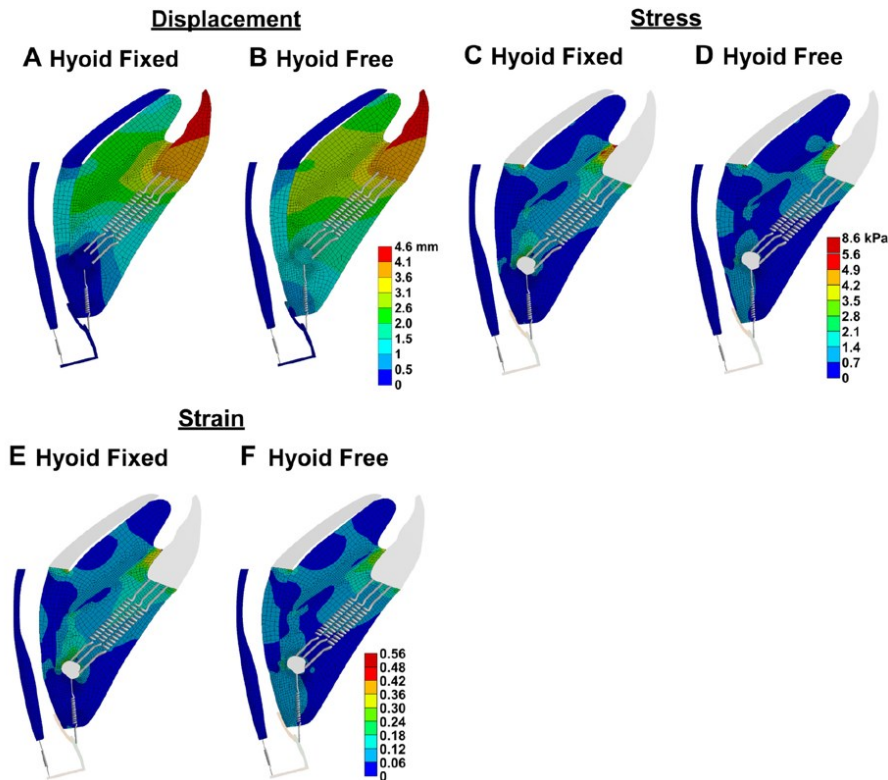


Figure 9: Effect of Hyoid Fixation on Outcomes of Mandibular Advancement Investigated using Computational Model. Tissue displacement, stress and strain outcomes of simulations with 4.6mm mandibular advancement load of the rabbit upper airway computational model are shown once for the fixed hyoid condition (displacement of hyoid is not allowed) and once when the hyoid is left free to move. All tissue mechanics results of the two different conditions are compared (A to F). An immobile hyoid bone limits the effects of mandibular advancement on tissues caudal to the hyoid bone such that the soft tissues are no longer displaced in this region (A vs. B), and with the reduction in stress (C vs. D) and strain (E vs. F), the caudal tissue stiffening effects of mandibular advancement are minimized. *Adapted from Amatoury et al [1].*

## 2.4 Computational Model of the Upper Airway

The complexity of the upper airway continues to limit our precise understanding of upper airway mechanics and the pathogenesis of disorders such as OSA. Numerous human and animal physiological models have been used to study upper airway biomechanics and specifically the mechanisms that lead to the loss of airway patency during sleep. However, studying a precise upper airway underlying mechanism such as

that of the hyoid bone position or movement would require highly controlled and invasive procedures that cannot be performed on humans. Animal models are a good alternative but are still time consuming, logistically challenging, and expensive. Moreover, animal physiological models are limited by the complexity of the anatomy and the undesired physiological responses that surgical procedures might induce. Thus, some procedures and measurements are not feasible in physiological models. Consequently, increasing interest has been directed towards the use of computational models to better understand upper airway physiology and mechanics. Computational models are cost-effective and allow the examination of highly controlled parameters. They also permit the isolation of specific mechanisms and can predict the outcomes of interventions that may not be achievable experimentally.

#### ***2.4.1 General Finite Element Technique***

The most used approach for solving computational models is the finite element method (FEM), a method that relies on dividing the complex model geometry into small interconnected discrete units of simple shapes that form what is referred to as the “mesh”. A finite element model of the upper airway consists of a 2-dimensional or 3-dimensional computer-generated representation of the upper airway lumen and/or the surrounding tissues with defined conditions. Using algorithms, the behavior of the entire modeled structure in response to certain disturbances is approximated by assembling the local behavior of each small mesh element [89]. Thus, this technique is particularly useful for modeling geometries as intricate as biological structures, including the complex upper airway.

Computational fluid dynamics (CFD) is the analysis of fluid flows using the finite element method and allows the investigation of velocity profiles and pressure distribution through a structure with rigid boundaries defined as the fluid domain. Structural finite element analysis (FEA) models represent solid structures (referred to as the solid domain) and provide information on the displacement, stress and strain of these structures in response to applied loads [89]. Fluid-Structure Interaction (FSI) is a coupling between fluid dynamics and structural mechanics that explores the interaction between the airflow and surrounding tissues and allows the understanding of how pharyngeal tissues deform in response to intraluminal pressures elicited by the airflow or vice versa.

#### ***2.4.2 Models of Airway Lumen Only (CFD)***

Over the past decade, finite element models have been widely used to help improve our understanding of upper airway biomechanics. Most of these models are based on computational fluid dynamics (CFD) and describe respiratory airflow dynamics [12, 79, 88, 101, 104, 129, 131, 137, 138]. CFD models consist of the airway lumen geometry representing the fluid domain defined by a “mesh” of the upper airway intraluminal space. The airway lumen geometry is reconstructed through image processing from CT, CBCT or MRI scans and generally includes the lumen from the nasal cavities to the base of the epiglottis. Many of these models have patient-specific geometries describing the exact airway anatomy of the corresponding patient [104, 129, 136, 138]. However, some models have a geometry that is averaged from data of several patients [12] or even an idealized geometry that is computer-generated based on airway dimensions [131]. As shown through the below examples, CFD models can

provide useful information regarding changes in airflow and pressure in the upper airway lumen during a breathing cycle for patients with different airway anatomy or after the simulation of procedures related to OSA treatment.

Differences in the airflow characteristics between patients with various anatomical attributes [79] have been investigated. For instance, a study by Na and colleagues [79] focused on revealing airflow differences between two patients that have opposing facial morphologies in terms of jaw position (one with a retruding mandible and one with a protruding mandible) as shown in Figure 10. The airflow velocity in the upper airway was higher when the jaw was retruding and a rapid pressure drop was observed. This suggests that airway obstruction might be induced in patients exhibiting a retruding jaw as opposed to a protruding jaw where the upper airway cross sectional area and volume are larger.

Some CFD models have also been used to examine the effect of certain OSA related interventions on airflow characteristics [101, 104, 137, 138]. Song et al. studied the changes in upper airway airflow dynamics after the use of mandibular advancement oral appliances in OSA patients to further understand the mechanisms of action of this therapy. In fact, the outcomes showed that at the narrowest region in the upper airway, the cross-sectional area increased considerably with the mandibular advancement oral appliance and the airflow velocity and pressure decreased significantly. These changes suggested that oral appliances make the upper airway less likely to collapse [104]. Similar changes to airway dimensions and airflow dynamics were observed when maxillary skeletal expansion was applied in a CFD analysis developed by Zhao and colleagues [137].

Consequently, pressure and velocity distributions of the airflow in the upper airway obtained in CFD simulations can give an insight on the potential site of collapse in the upper airway. However, CFD models assume that the airway is a rigid-walled tube and that the lumen's surface is fixed while the airway is in reality highly deformable and surrounded by soft tissues. Moreover, CFD models do not allow the study of airway tissue mechanics.

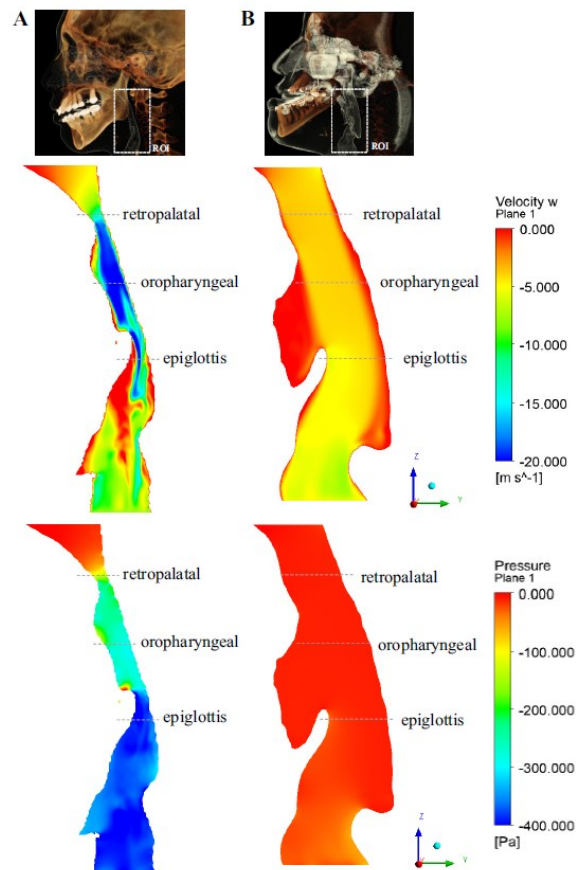


Figure 10: Flow Velocity and Pressure Distribution in a Computational Fluid Dynamics (CFD) Model of the Upper Airway. Example of computational fluid dynamics model outcomes showing the magnitudes and distribution of flow velocity and pressure in the mid-sagittal plane of the upper airway lumen of retruding jaws (A) and protruding jaws (B). Higher airflow velocity and large pressure drop in retruding jaw case (A) suggest that airway obstruction might occur. *Adapted from Na et al [79].*

### ***2.4.3 FEA/FSI models with Simplified Soft Tissue Representation***

Pharyngeal soft and hard tissues make up the upper airway and hence play an important role in upper airway mechanics and behavior. Increasing efforts have been directed in the last few years towards the development of both FE and FSI models that include pharyngeal structures such as soft tissues, bone or cartilage and represent the airway as a collapsible tube. However, given the complexity of the upper airway geometry, most upper airway models have represented the pharyngeal tissues in a simplified manner and excluded major bony structures such as the mandible and hyoid bone. Structural FEA models include the solid structures that form the upper airway (solid domain), without airflow, and allow the study of the displacement, stress and strain of the pharyngeal tissues in response to applied loads [89]. FSI upper airway models incorporate the luminal fluid domain as well as a solid domain representing the surrounding pharyngeal structures.

#### **2.4.3.1 FEA Models**

Existing upper airway FEA models represented mainly represented simplified pharyngeal soft tissues and small regions of the upper airway. For example, a few structural models of the soft palate upper airway region have been developed, with non-linear material models, to study velopharyngeal closure [53, 72, 107].

In a study by Liu et al., a 3-dimensional model of the soft palate region in the upper airway was developed to investigate the effect of palatal implant surgery undertaken to treat OSA on soft palate stiffness [72]. This model is based on a 3-dimensional representation of the soft palate, the part of the pharynx wall that is facing the soft palate as shown in Figure 11 A. Using a Neo-Hookean non-linear material

model to characterize the tissues, this model investigates how different palatal implants affect the soft palate stiffness and improve upper airway collapsibility. Another 3-dimensional FEA model of the soft palate upper airway region was developed by Henrik et al. [53] in the purpose of examining the biomechanical properties of the velopharynx in OSA patients. Non-linear material properties were also used to model the soft tissue behavior and collapse of the airway was observed at the level of the lateral attachment of the soft palate (Figure 11 B).

Srodon et al. developed a 2-dimensional model of an oblique coronal section of the upper airway at the level of the soft palate with the objective of investigating passive changes in some muscles and their effect on velopharyngeal closure [107]. This model's geometry, shown in Figure 11 C, is based on MRI images of a female subject and a modified Neo-Hookean non-linear material model is used to describe the behavior of the different types of palate tissues (fibrous, muscle and glandular). This model included more pharyngeal tissues such as the tongue and the levator veli palatini muscle; however, the tissues and muscle connections not included in the coronal slice were disregarded. These models only provide information on one isolated region of the upper airway and neglect other pharyngeal structures and factors that impact upper airway mechanics.

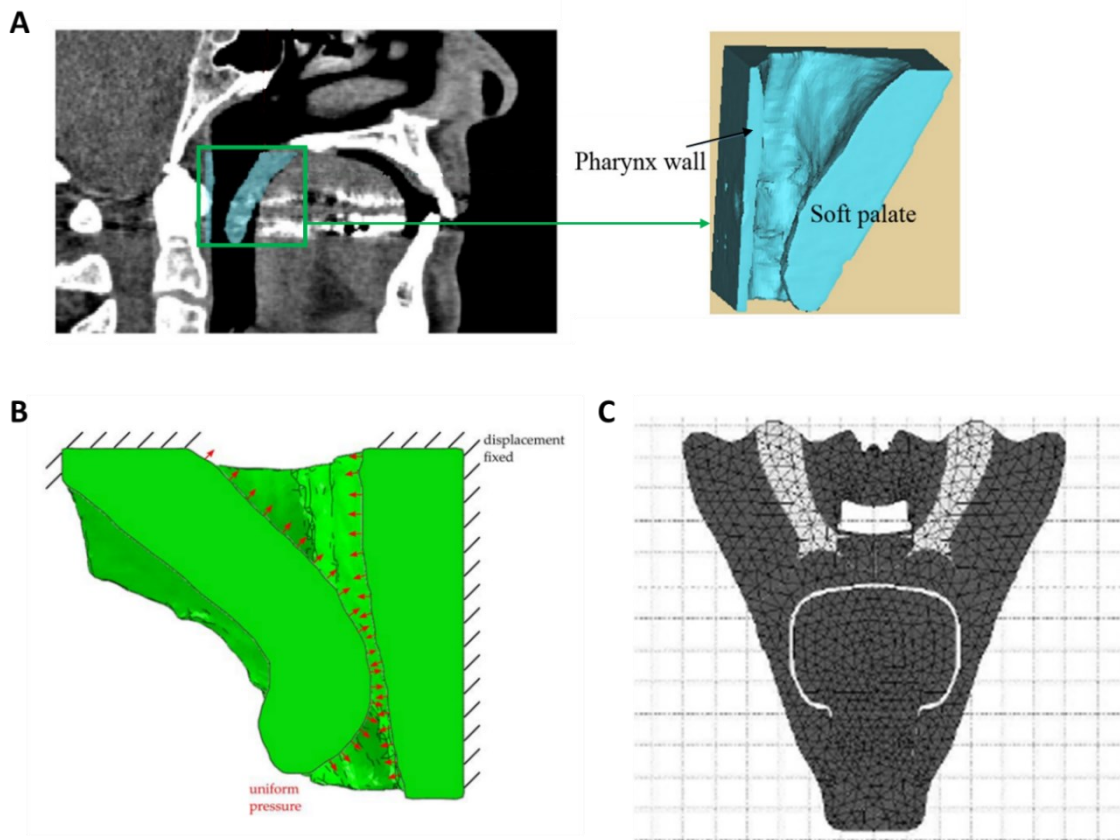


Figure 11: FEA upper airway models of the velopharyngeal airway region only. (A) 3D geometry reconstruction of portion of upper airway including the soft palate and facing pharyngeal posterior wall from a patient specific CT image. (B) Deformed state of FE model of the soft palate and velopharynx after a uniform negative intraluminal pressure is applied at the airway walls. (C) 2-dimensional finite element model reconstructed from the MRI coronal section at the level of the soft palate. *Figures (A), (B) and (C) are adapted and modified from Liu et al. [72], Henrik et al. [53] and Srodon et al. [107], respectively.*

### 2.4.3.2 FSI Models

#### 2.4.3.2.1 Very simplified pharyngeal soft tissue representation

In most FSI upper airway models, pharyngeal structures were simplistically modeled to avoid overcomplicating these Multiphysics models by representing the complex and highly non-linear upper airway tissues. In most cases, the solid domain of FSI models was represented by a uniform thickness around the airway walls representing the pharyngeal soft tissues [8, 10, 65, 71, 88, 136].



The FSI model developed by Le et al. [71] is an example of such models. It was reconstructed from MRI scans of the head and neck of a healthy women: The fluid domain consisted of the patient specific airway lumen from the nasal cavities to the trachea and the solid domain was a made of a uniform wall thickness around the airway perimeter representing the pharyngeal soft tissues as shown in Figure 12 A. The inner airway walls define the interface between the fluid and solid domain and are loaded by to the pressure that the airflow exerts on them. The airway walls are accordingly deformed and follow a non-linear material model (Neo-Hookean model) to reproduce the hyperelastic behavior of soft tissues. Le et al.'s model was used to examine the influence of breathing cycles, airway wall thickness and pharyngeal wall material stiffness on upper airway collapse. The results were found to be independent of the breathing pattern and an increase in the soft tissue thickness or the soft tissue material elasticity led to a decrease in the airway wall compliance. Figure 12 B illustrates the pressure distribution and airway deformation for a particular combination of airway wall thickness and material stiffness at a specific time during a linear breathing cycle. At the level of the soft palate the airway walls were significantly deformed inwards and the distance between the opposing airway walls became smaller than 0.5mm which was considered as a collapse of the airway walls in that study. According to that model, the airway collapsed at a pressure of around -5 cmH<sub>2</sub>O at the level of the soft palate. Moreover, to validate the outcomes of the model, a physical collapsible airway replica was fabricated and used to obtain experimental measurements.

Other FSI airway models with a patient specific lumen and uniform thickness pharyngeal walls were used to investigate how the sleeping position affects upper airway collapse [8], and observe changes produced in upper airway behavior and

occlusion in response to mandibular advancement [10, 88, 136]. A study by Barber et al. [10] demonstrated the success of mandibular advancement splint treatment by showing that the upper airway deformation was smaller and no collapse occurred post-treatment. Nevertheless, representing the structural domain of the upper airway by a uniform thickness around the airway walls does not portray the actual behavior of upper airway structures because the tissue distribution around the pharynx is highly asymmetric and the bone attachments restrict the soft tissue motion.

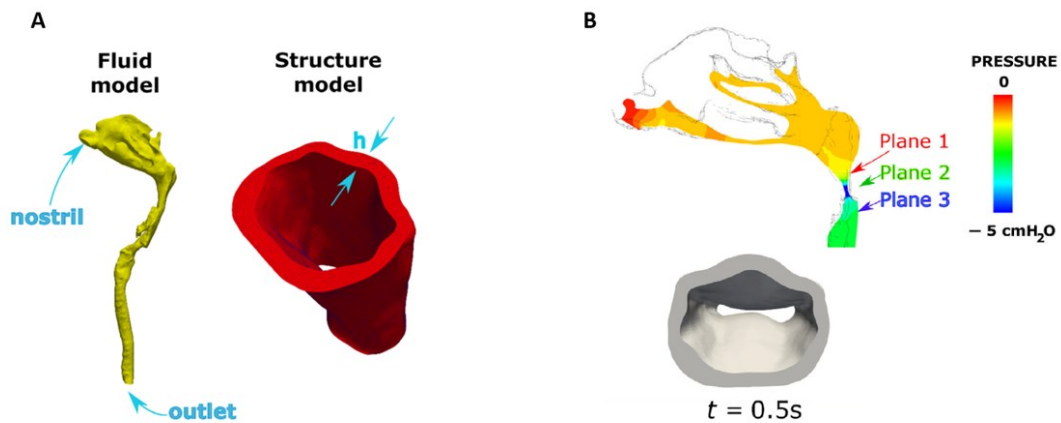


Figure 12: Fluid-Structure Interaction Simplified Soft Tissue Upper Airway Model. Example of an upper airway fluid-structure interaction model geometry (A) and simulation outcomes (B). (A) The fluid domain geometry (in yellow) is reconstructed from MRI images and the structure domain geometry (in red) is a simplification of the pharyngeal soft tissues represented by a wall with uniform thickness,  $h$ . (B) Model outcomes after simulating inspiration at a specific time point ( $t=0.5s$ ) and thickness ( $h=2mm$ ) showing the pressure field (top) and the collapsible pharyngeal wall (bottom). Airway collapse occurs at plane 2. *Adapted and Modified from Le et al. [71].*

#### 2.4.3.2.2 Additional pharyngeal soft tissue representation

Some upper airway FSI models worked on including an accurate representation of more pharyngeal soft tissue structures to allow the evaluation of tissue mechanics of these structures in addition of airflow properties. As such, studies by Pirnar et al. and

Sun et al. [87, 112] developed fluid-structure interaction models with a more realistic and detailed solid domain but focused only on the velopharyngeal region of the airway as was the case in simplified FEA models discussed in the previous section (Section 2.4.3.1). These models included the soft palate, uvula and some posterior velopharyngeal tissues and were used to explain mechanisms of pharyngeal collapse and snoring by observing airway narrowing and soft palate flutter during inspiration. Even though these models were able to provide useful information regarding the interaction between airflow and velopharyngeal tissues, linear elastic material properties were assumed and further work needs to be done to validate these models.

Dhaliwal et al. [36] developed a 3-dimensional FSI model of the entire upper airway length that realistically represented some soft tissue structures from MRI scans of OSA patients such as the base of the tongue, the epiglottis, the soft palate, the uvula, the palatine tonsils and the pharyngeal walls as shown in Figure 13 A. Non-linear material properties were applied and the model allowed the prediction of the degree and site of maximal collapse in OSA patients. An example of the tissue displacement results is shown in Figure 13 B. Although this model's results were interesting, they lacked proper validation and important upper airway bony structures such as the hyoid bone were left out.

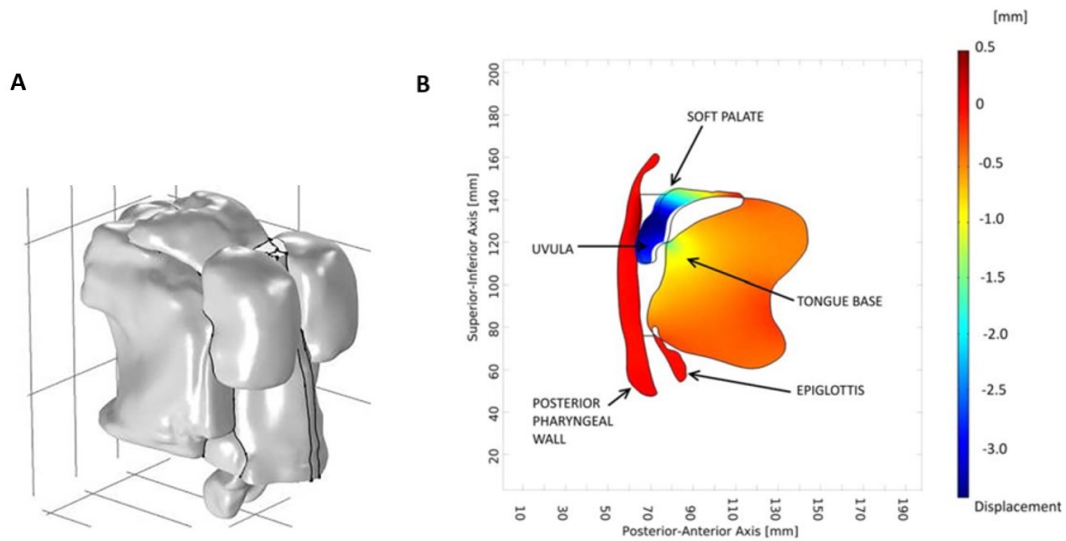


Figure 13: 3-Dimensional Upper Airway Finite Element Model Geometry and Tissue Displacement. Example of a patient-specific upper airway finite element model reconstructed from MRI scans. (A) 3-Dimensional geometry of the upper airway model including the base of the tongue, the palatine tonsils, the soft palate, epiglottis, uvula and the pharyngeal walls. (B) Results from the simulation showing the displacement of the various modeled structures in a mid-sagittal cross section of the finite element model. *Adapted and modified from Dhaliwal et al [36].*

#### 2.4.4 FEA/FSI Models Including the Hyoid Bone

##### 2.4.4.1 FEA Models

Apart from the rabbit upper airway FEA model [1], that will be further discussed in the following section (Section 2.5), only one single FEA upper airway model including the hyoid bone was found in literature.

In fact, a study by Carrigy et al. [26] developed a finite element model of the passive human upper airway with an intricate 3D anatomical representation of the head and neck of a healthy patient based on CT scan images. The purpose of the study was to find suitable moduli of elasticity for muscle and adipose tissue for modeling pharyngeal mechanics to a very detailed 3D model of the human upper airway. More specifically, pharyngeal tissue deformation due to negative airway pressure was examined. All

material properties were assumed to be linear elastic. Although the upper airway structures were thoroughly modeled, collapse of the upper airway was not achieved, and model outcome were not validated. Too many upper airway structures were included in that model including the skull, spine, hyoid, ligaments/tendons, adipose tissue, muscles and even the thyrohyoid membrane representing not only upper airway but also face and neck structures (Figure 14). This indeed leads to unnecessary model complexity that increases the computational cost of the study since the effect of many of the included structures could be represented through boundary conditions.

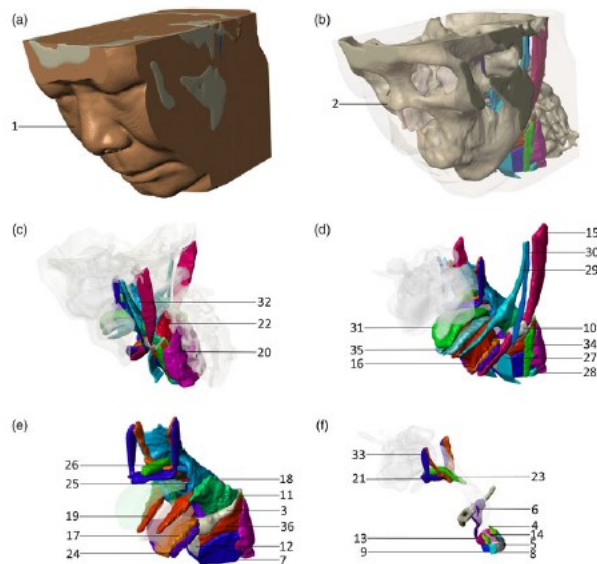


Figure 14: Geometry of FE model of the upper airway with intricate pharyngeal tissue representation. The numerous soft tissues included in the model are differentiated through different colors and number-labels. The corresponding structure names are not shown here and can be found in Table 1 of [26]. *Adapted from Carrigy et al. [26].*

#### 2.4.4.2 FSI Models

Similarly to FEA models, there is a very limited number of FSI upper airway models that include a complete and realistic representation of pharyngeal tissues with the key hyoid bone structure.

The most recent model currently is a fluid-structure interaction model of the whole upper airway (with the exception of the nasal cavity) developed by Liu et al. with the purpose of identifying the location, severity and characteristic of airway collapse in OSA patients [73]. The model was reconstructed from CT scans of a patient suffering from OSA and included the pharynx, its posterior and lateral walls, the epiglottis, the soft palate, the tongue, other soft tissues located under the tongue (mainly adipose tissue) and the hyoid bone. Flow simulations were performed with ambient inlet pressure and sinusoidal outlet pressure varying between 0 and -2000 Pa in 1.66s. The model geometry as well as the deformation at four different points along the airway in the midsagittal plane are shown in Figure 15 A and B, respectively. In this study, complete collapse of the upper airway was observed at the tip of the soft palate region at a pressure of about -14 cmH<sub>2</sub>O which is considerably larger than the collapse pressure found in other models. While providing initial insight into which areas of the OSA airway are prone to collapse, this model assumed linear elastic material properties for the soft tissues, disregarding the large soft tissue deformation produced in the actual physiological airway. Moreover, model validation was not undertaken and the passive influence of other upper airway muscles was included in the study.

Another FSI model, developed by Huang et al. [55, 56], was based on a simpler 2-dimensional representation of the upper airway tissues in the midsagittal section of a healthy individual, including the tongue (with active genioglossal muscle contraction), hard palate, soft palate, epiglottis, hyoid bone and mandible (Figure 15 C). The purpose of the model was to simulate tongue movement and airway collapse and assess the impact of various OSA related manipulations such as mandibular advancement, palatal resection and soft palate stiffening on pharyngeal mechanics and collapse. Results

indicated that the active upper airway during sleep collapsed a -13 cmH<sub>2</sub>O pressure and all interventions simulated yielded a more negative pressure meaning that the airway collapsibility was reduced. While the model provided insight into the effect of tongue muscle activity and various OSA interventions on pharyngeal collapse, some pharyngeal structures such as the glandular or adipose tissues were excluded and the hyperelastic behavior of the airway soft tissues was disregarded (linear elastic behavior assumed). Furthermore, model outcomes corresponded reasonably well to clinical data when such data was available but they were not directly validated against experimental results.

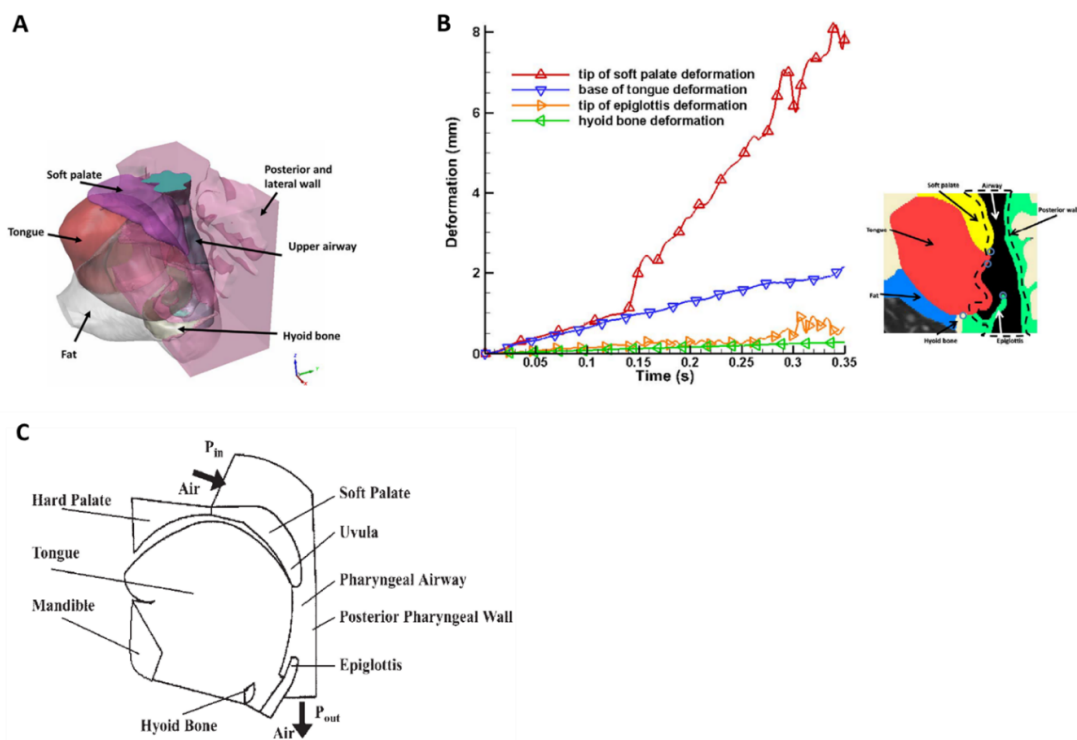


Figure 15: FSI model including key upper airway structures and hyoid bone. (A) 3D geometry of the structural domain model that includes the posterior and lateral airway walls, the hyoid bone, the epiglottis, the soft palate, the tongue and adipose soft tissues located under the tongue. (B) Deformation vs. time plot of the tip of the soft palate, base of the tongue, hyoid bone and tip of the epiglottis in the midsagittal section of 3D model shown in (A) during a breathing cycle. (C) 2D midsagittal FSI upper airway model including the soft and hard palate, uvula, posterior pharyngeal wall, epiglottis, hyoid bone, tongue and mandible.  $P_{in}$ = the pressure at the inlet,  $P_{out}$ = pressure at the outlet of

the airway defining the driving pressure for airflow. *Figures (A) and (B) adapted and modified from Liu et al [73] and figure (C) adapted from Huang et al. [55].*

#### 2.4.4.3 Rigid Multi-Body and FEA Models

Rigid multi-body models are composed of various rigid and elastic bodies interconnected through joints and are used to describe the motion of non-deformable bodies relative to one another based on kinematic mechanics. Multi-body models representing the bones, joints and point-to-point muscles of the head and neck area have been developed to simulate facial gestures, speech, chewing and swallowing [48, 50, 116]. Multi-body skull-jaw-hyoid models (Figure 16 A) with actuated muscles are of particular interest for studying upper airway mechanics and the influence of the hyoid bone. These models have permitted the study the hyoid biomechanics during chewing [48] and swallowing [50, 116].

However, representing only the rigid and non-deformable upper airway structures results in an inaccurate simulation of upper airway functions as the pharyngeal soft tissues play a crucial role in the upper airway. Increasing attention has been directed towards adding soft tissues to multi-body models to create tightly coupled FEM-rigid body models capable of physically modeling the dynamic interactions when soft tissues and hard bodies are connected and interact. As a first step towards this goal, Stavness et al. [108] added a 3-dimensional finite element model of the tongue to the hyoid-jaw rigid multi-body complex (Figure 16 B) governed by a hybrid physical simulation technique that combines multibody physics with 3D finite element analysis. This jaw-tongue-hyoid model simulated chewing through the activation of muscles and demonstrated the coupled dynamics of the deformable tongue and the rigid jaw and hyoid structure.



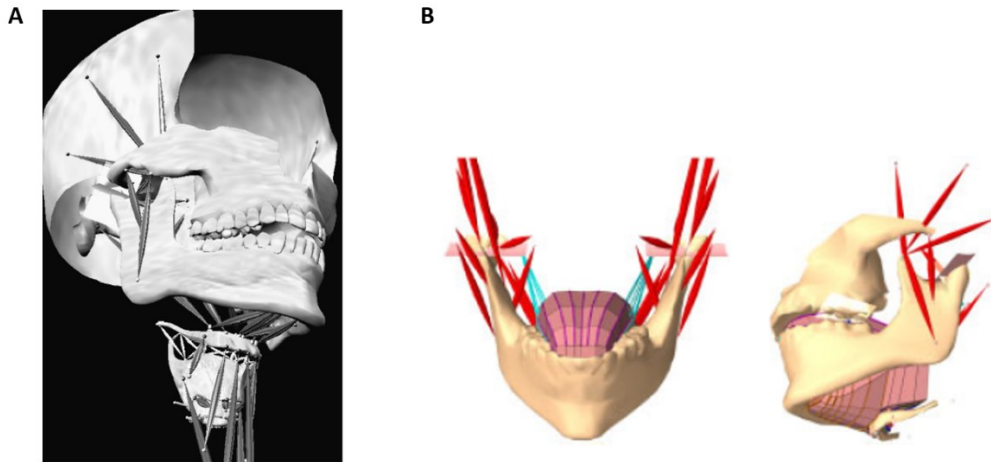


Figure 16: Rigid multi-body and FEA models of the head and neck region. (A) Illustration of a dynamic rigid multi-body model of the skull, jaw, hyoid and thyroid with point-to-point muscles. Adapted from Hannam et al. [48] (B) Front and oblique views of the jaw-tongue-hyoid model. Adapted from Stavness et al. [108]

Anderson et al. [4] later further developed this coupled FEM/multi-body model to become a reference template biomechanical model of the head and neck referred to as the functional reference anatomical knowledge (FRANK) template. The model is composed of a combination of rigid bodies, finite element models, point-to-point muscles, joints and “skin” meshes and is able to replicate the kinematics related to orofacial movements and mechanisms, essentially swallowing, chewing and speech production. This model includes the key upper airway structures: the bony tissues such as the spine, maxilla, mandible, hyoid, thyroid, epiglottis; the deformable soft tissues such as the tongue, soft palate, pharyngeal wall, larynx and masseter; and the muscles and ligaments that connect these structures together. The model’s geometry is illustrated in Figure 17 A. However, the lack of some upper airway components in the model causes discontinuities in the geometry that make the airway lumen not accurately defined. An airway skin mesh is parametrically defined to get rid of the gaps present

between tissues and to better delineate the airway. Ideally, this model would be used as a reference template to construct a patient-specific model based on the FRANK model. However, given its high complexity, it is very challenging to create a patient specific model from the FRANK model.

A more recent study by Anderson et al. used the FRANK upper airway model to explore the effect of the levator veli palatini (LVP) and palatoglossus muscles on velopharyngeal constriction [5]. Activation of these palatal muscles led to velopharyngeal collapse and activation of the palatoglossus muscle caused anterior flexion of the uvula Figure 17 B. These results give an insight on the movement of the soft palate involved in speech production; however, the model needs to be further improved to be able to simulate breathing and upper airway collapse that can occur during a breathing cycle. Additionally, the soft palate and pharynx are assumed to follow a linear elastic rather than a hyperelastic material model and large deformations impacts the model's stability. Moreover, the model was derived from different data sources which is a possible drawback and might cause some incoherence in the model.

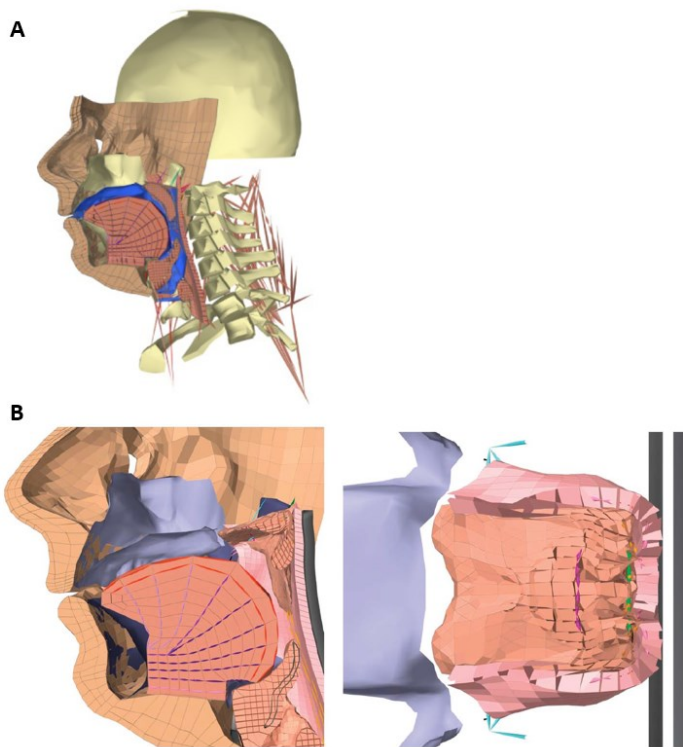


Figure 17: Overview of the FRANK model and its response to palatal muscle activation. (A) Midsagittal view of the FRANK model showing the internal soft tissues (tongue, soft palate, airway walls), airway skin mesh (Blue color), some bony structures and muscles. (B) Midsagittal and transverse cutaway view of the model at the velopharynx level after levator veli palatini muscle activation. Complete velopharyngeal closure can be observed: the soft palate posteriorly displaced. *Adapted and modified from Anderson et al. [4, 5].*

## 2.5 Anesthetized Rabbit Computational Finite Element Model

In this thesis, the model created by Amatory and colleagues [1] will be re-developed and advanced in order to investigate the influence of the hyoid bone on upper airway mechanics and collapsibility (thesis aims are detailed in Chapter 1.2)

This model is a two-dimensional (2D) computational finite element model of the passive rabbit upper airway and pharyngeal tissues that was developed and validated based on an anesthetized rabbit model with the purpose of investigating mechanistically the influence of mandibular advancement and lung-volume related tracheal

displacement on the upper airway. The model examined upper airway biomechanics under passive (no muscle activity) and static (without airflow) conditions.

Compared to the other FE computational models found in literature, Amatoory et al.'s model [1] presents several advantages that illustrate its importance in the context of this thesis. As a matter of fact, this model is one of the very few that include the hyoid bone as well as many of the key pharyngeal tissues (bony and soft tissues). The passive influence of many upper airway muscles is also incorporated, even those that are not present in the midsagittal plane modeled. Moreover, the invasive rabbit upper airway experimental studies performed in parallel to the model development allowed the unique and thorough optimization of model boundary conditions and the direct validation of model outcomes against experimental data.

Finally, the model successfully simulated mandibular advancement and tracheal displacement and was able to predict upper airway lumen geometry changes and tissue mechanics in response to these interventions. In fact, the model predictions were in agreement with the experimental data obtained from the animal study in its response to mandibular advancement, tracheal displacement and a combination of the two procedures. Furthermore, the model supported the idea that the hyoid bone influences considerably the upper airway tissue mechanics by showing that its fixation during mandibular advancement or tracheal displacement has an impact on model outcomes (shown in Figure 9). However, the direct effect of changing the hyoid position was not directly considered and the model was not able to simulate negative intraluminal pressures to examine upper airway collapsibility ( $P_{close}$ ). Additionally, its current geometry does not allow changes in the hyoid baseline position.

The model definitions are presented in detail in this section.

### 2.5.1 Model Geometry

The model geometry was reconstructed from mid-sagittal CT scans of the head and neck of a New Zealand White rabbit by image segmentation, processing and smoothing. The obtained model geometry is shown in Figure 18 and includes upper airway bony tissues (mandible, hard palate and hyoid bone), cartilaginous tissues (thyroid cartilage and epiglottis) and soft tissues (tongue, soft palate, constrictor muscles, geniohyoid and mylohyoid muscles). The rest of the soft tissues mainly including adipose and glandular tissue are lumped into a single structure named the tissue mass. A rectangular base plate is also added to the lower edge of the thyroid cartilage for some muscles connections and to provide a surface for caudal tracheal displacement application.

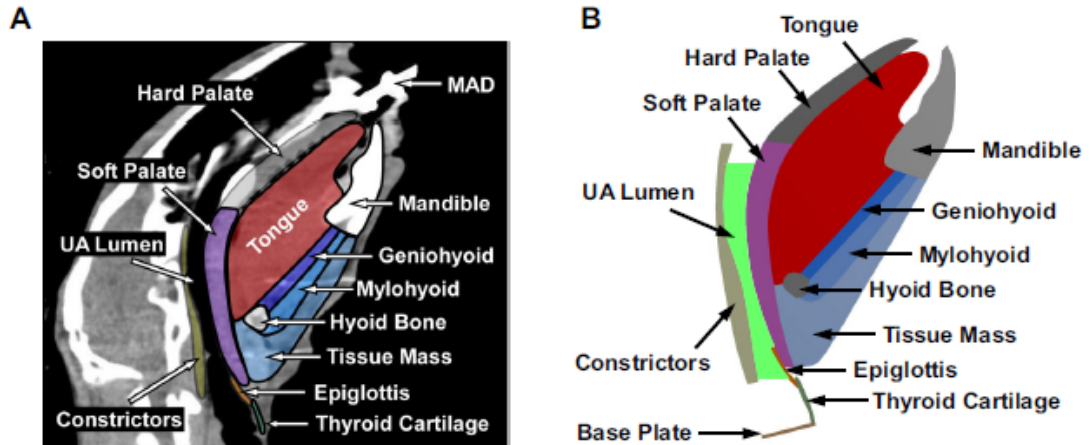


Figure 18: Rabbit Upper Airway Finite Element Model Geometry. The model geometry reconstruction is represented. (A) Mid-sagittal computed tomographic (CT) image of a representative rabbit used for model geometry reconstruction showing in color the tissues that will be included in the model. (B) Reconstructed two-dimensional finite element model geometry of the rabbit upper airway from the level of the nasal choanae to the glottis. All the structure included in the model are labeled. Abbreviations: MAD, mandibular advancement device; UA, upper airway. *Adapted from Amatoury et al [1].*

### 2.5.2 Boundary conditions

The boundary conditions were defined from anatomy and physiological experimentation. These include the constraints, contacts and spring connections.

The constraints are graphically illustrated in Figure 19 and consist of fixed supports, frictionless supports and elastic constraints applied to allow the model to replicate experimentally observed behavior under the two different loads investigated (mandibular advancement and tracheal displacement). The properties and justification of the elastic constraints applied are detailed in Table 2.

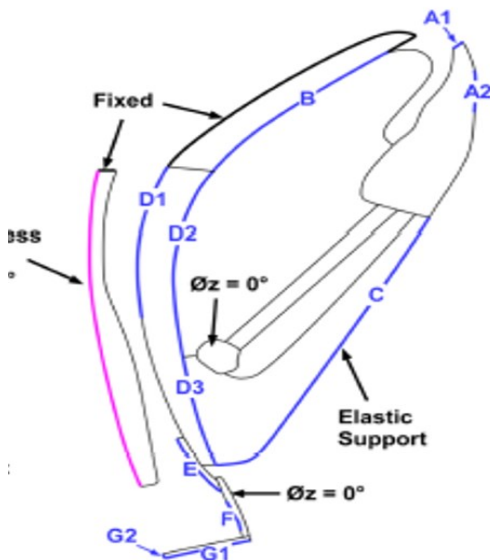


Figure 19: Illustration of Model Constraints. Diagram of all the boundaries of the model to indicate the location of different constraints: Dark black outlines indicate fixed support, pink outline indicates frictionless support and no rotation condition ( $\theta_z = 0^\circ$ ) is applied to the constrictors, thyroid cartilage and hyoid bone. The blue outlines indicate elastic supports and are labeled from A1 to G1. The same labeling is found in Table 2 that explains and justifies the elastic support properties. *Adapted from Amatory et al [1].*

Tissue	Boundary	Elastic Foundation Stiffness, mN/mm <sup>2</sup>	Function	Physiological Representation	Source*
Mandible	A1	2,000	Limit caudal displacement	Mandible supports (e.g., temporal-mandibular joint and muscle attachments)	TD
	A2		Limit AP displacement		
Tongue	B	1	Limit caudal displacement	Tongue supports provided by tongue muscle attachments	TD
Tissue Mass	C	0.5	Limit overall displacement	Skin	MA, TD
Soft palate	D1	0.8	Limit AP displacement	Palatal muscle supports (tensor palatini and levator palatini)	MA, TD
	D2	0.1			
	D3	0.1			
Epiglottis	E	5	Limit AP displacement	Lateral epiglottis structure and thyroid supports	MA, TD
Thyroid Cartilage	F	50	Limit AP displacement	Lateral thyroid structure, ligament and tissue supports	MA, TD
Base plate	G1	100	Limit CC displacement	Trachea and attachments, including tracheal cannula in experiments (3, 4)	MA
	G2	50	Limit AP displacement		

\*The Source column indicates the experimental intervention(s) that provided the information (i.e., from midsagittal image sequences) for inclusion of the elastic support in the model.

Table 2: Elastic Constraint Properties and Justification. The boundary for each tissue is labeled from A1 to G2 and its location is indicated in Figure 19. Abbreviations: TD, tracheal displacement; MD, mandibular advancement; AP, anteroposterior; CC, cranial-caudal. *Adapted from Amatoury et al [1].*

The contacts determine the interaction between the different parts of the model.

The contact definitions of the model are shown in Figure 20 and the properties and justification of these contacts of these contacts are shown in Table 3.

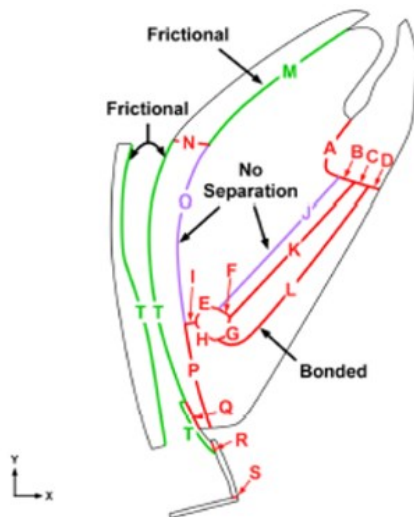


Figure 20: Diagram indicating the model's contact definitions. Red outlines indicate bonded contact definitions, purple outlines indicate no separation contact and green outlines indicate the frictional contact definitions. The letter labels (from A to T) are used in Table 3 to describe the contact interfaces and their properties. *Adapted from Amatoury et al [1].*

Interface	Label*	Behavior	Source **
Mandible/attached tissues	A-D	Bonded	Anatomy/observed behavior (MA, TD)
Hyoid bone/attached tissues	E-H	Bonded	Anatomy/observed behavior (MA, TD)
Tongue/tissue mass	I	Bonded	Assumed
Tongue/geniohyoid	J	No Separation	Observed behavior (MA, TD)
Geniohyoid/mylohyoid	K	Bonded	Assumed
Mylohyoid/tissue mass	L	Bonded	Assumed
Tongue/hard palate	M	Frictional, $\mu = 0.2$	Observed behavior (MA, TD; $\mu$ optimized to tongue displacement)
Hard palate/soft palate	N	Bonded	Anatomy
Soft palate/tongue	O	No separation	Observed behavior (MA, TD)
Soft palate/tissue mass	P	Bonded	Assumed
Soft palate/epiglottis	Q	Bonded	Observed behavior (MA, TD)
Thyroid cartilage/epiglottis	R	Bonded	Anatomy
Thyroid cartilage/base plate	S	Bonded	NA
Soft palate-epiglottis/constrictors	T	Frictional, $\mu = 0.1$	Assumed

\* The label points to the location of the interface in the model shown in Figure 20.

\*\*The Source column indicates the reason for the contact condition.

**Table 3: Contacts and Properties.** Description and justification of contact properties associated with each interface. Abbreviations: TD, tracheal displacement; MD, mandibular advancement; NA, not applicable;  $\mu$ , Friction coefficient. *Adapted from Amatory et al [1].*

Finally, one dimensional elastic spring connections were added to anatomically relevant positions to represent the passive action of the pharyngeal muscles as shown in Figure 21. The muscles represented are the stylohyoid, thyrohyoid, sternohyoid, sternothyroid, genioglossus (transverse fibers), geniohyoid and mylohyoid. The geniohyoid and mylohyoid muscles are represented by surface bodies and springs to allow the definition of the muscle direction. The spring properties are all shown in Table 4.



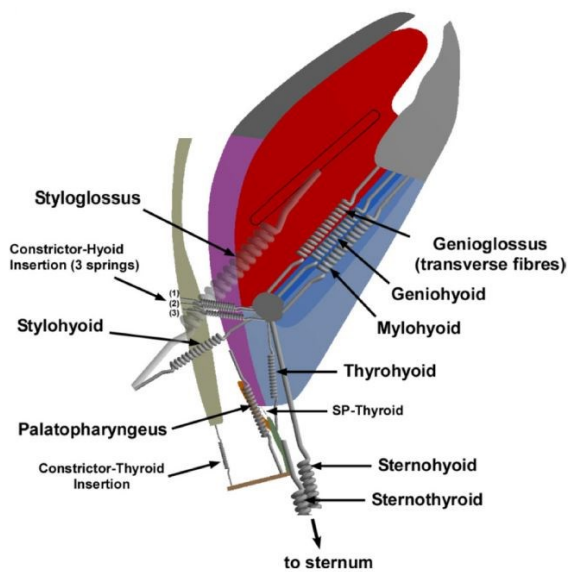


Figure 21: Illustration of Model Spring-Defined Muscles. Spring connections are added to represent the passive action of upper airway muscles. The annotations give the name of the muscle represented by each spring and the stiffness properties of each spring is shown in Table 4. Note that the styloglossus spring is shown transparent for clarity. Abbreviations: SP, soft palate. *Adapted from Amatoury et al [1].*

Spring (Muscle)*	Stiffness, N/mm	Source**	Stiffness Value Optimization***
Genioglossus (transverse fibres)	0.3	Anatomy	Hyoid bone displacement
Geniohyoid	0.15	Anatomy	Hyoid bone displacement
Mylohyoid	0.15	Anatomy	Hyoid bone displacement
Styloglossus	0.001	Anatomy	Thyroid cartilage displacement
Stylohyoid	0.6	Anatomy	Hyoid bone displacement
Thyrohyoid	0.25	Anatomy	Hyoid bone displacement
Sternohyoid	0.2	Anatomy	Thyroid cartilage displacement
Sternothyroid	0.2	Anatomy	Hyoid bone displacement
Soft palate-base plate	0.0005	Representative anatomy (palatopharyngeus)	Soft palate displacement
Constrictors-hyoid (1)	0.1	Anatomy	Hyoid bone displacement
Constrictors-hyoid (2)	0.1	Anatomy	Hyoid bone displacement
Constrictors-hyoid (3)	0.5	Anatomy	Hyoid bone displacement
Constrictors-base plate	0.008	Representative anatomy (constrictors to thyroid)	Constrictors longitudinal deformation
Soft palate-thyroid	0.00001	Experimental observation (TD)	Soft palate longitudinal deformation
Tissue mass-thyroid	0.005	Representative anatomy (connective tissue)	Tissue mass boundary displacement

\*Spring locations in the model are shown in Figure 21.

\*\*The source indicated what the spring definition is based on.

\*\*\*The experimental outcomes used for the spring stiffness value optimization.

Table 4: Muscle (spring) Properties. Summary of all the spring stiffness parameters used in the finite element model to represent the passive action of upper airway muscles. Abbreviations: TD, tracheal displacement. *Adapted from Amatoury et al [1].*

### 2.5.3 Material Properties

The material properties assigned to the model were based on values found in literature [42, 130]. The bony and cartilaginous parts were assigned incompressible linear elastic material properties shown in Table 5. The thyroid cartilage and the base plate were assumed to have bone material properties to avoid deformations from artificially generated moments during simulated caudal tracheal displacement.

Tissue	E*, MPa	$\nu^{**}$	Literature Source
Hyoid bone mandible	17,000	0.49	Yamada 1970 (72)
Hard palate base plate			
Thyroid cartilage	17,000	0.49	Assumed (see text)
Epiglottis	2.4	0.49	Yamada 1970 (72)

\*E, Young's Modulus. \*\*  $\nu$ , Poisson's ratio.

Table 5: Bony and Cartilaginous Linear Elastic Material properties. Properties used in the finite element model for the hyoid bone, the mandible, the hard palate, the thyroid cartilage, the epiglottis and the base plate are those of linear elastic material. *Adapted from Amatoury et al [1].*

For the soft tissue material properties, the Yeoh second-order strain energy function (Equation 1), a nonlinear hyperelastic material model was used. This model was previously used in a tongue model [42]. The function parameters chosen for different tissues after model optimization are shown in Table 6. Furthermore, Figure 22 shows the stress-strain curves describing the hyperelastic material model used in this model.

Equation 1 – Yeoh second-order strain energy function

$$W = C_{10}(I_1 - 3) + C_{20}(I_1 - 3)^2 + \frac{1}{d_{10}}(J - 1)^2 + \frac{1}{d_{20}}(J - 1)^4$$

Tissue	$\nu$	$C_{10}$ , Pa	$C_{20}$ , Pa	$d_{10}^*$	$d_{20}^*$
Tongue, Soft palate	0.49	1,628	770	1.24	2.61
Tissue mass, Geniohyoid, Mylohyoid	0.45	1,532	725	6.75	14.30
Constrictor body	0.45	4,005	1,896	2.58	5.46

\*(Pa<sup>-1</sup>) x 10<sup>-5</sup>

Table 6: Soft Tissue Hyperelastic (Yeoh second-order) material parameters. Parameters of hyperelastic tissue model chosen after optimization to be applied to the upper airway soft tissues such as the tongue, soft palate, tissue mass, geniohyoid, mylohyoid and constrictor body. *Adapted from Amatory et al [1].*

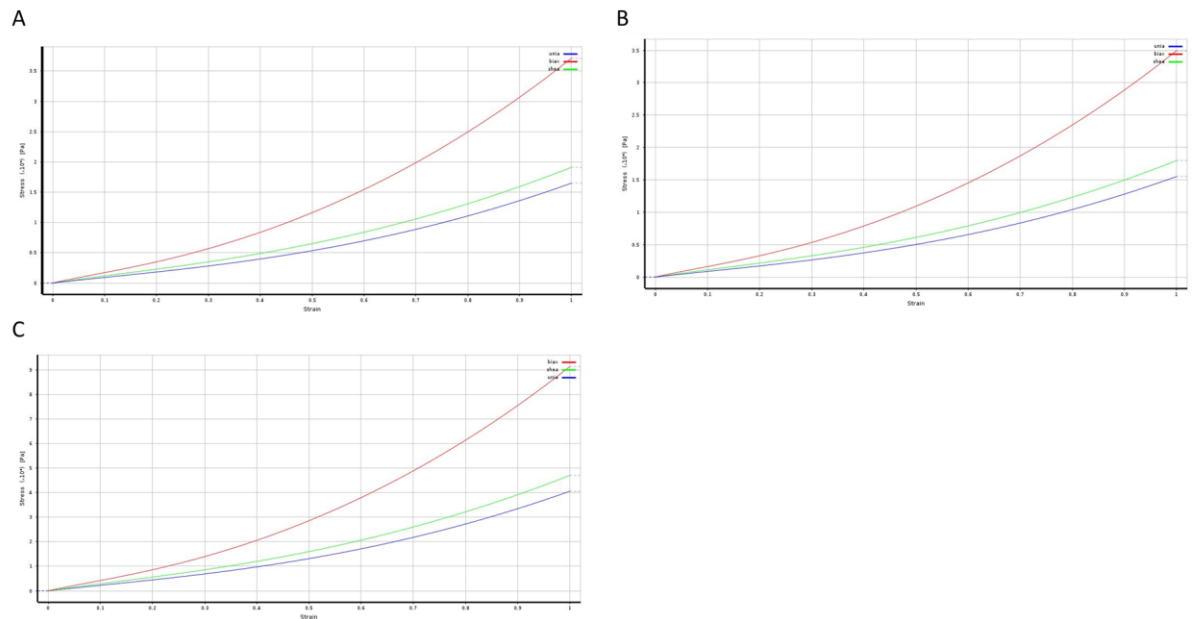


Figure 22: Stress-Strain Curves for the Hyperelastic Yeoh Second-Order Material Models. The stress-strain curves represent the material behavior for the (A) tongue and soft palate tissues, (B) the tissue mass, geniohyoid and mylohyoid and (C) the constrictors under uniaxial (red curve), biaxial (blue curve) and shear (green curve) loading.

### 2.5.4 Limitations

The limitations of the model by Amatory et al. [1] used in this thesis are summarized in this section. See Amatory et al. for further details.

#### 2.5.4.1 Rabbit Upper Airway

Different animals have been used to explore upper airway physiology such as mice, rats, cats and dogs. However, the rabbit can be considered to be the most suitable animal model for upper airway. First of all, there is a high similarity between the rabbit and the human upper airway, particularly in the mobility of the hyoid bone. The rabbits are the only non-primate that have a freely suspended hyoid bone as humans do [2, 127]. Another valuable aspect of the rabbit's upper airway is that the airway is also prone to collapse since the pharyngeal soft and hard tissues present are similar to the ones in the human upper airway.

Some minor differences in the airway anatomy include a longer soft palate in rabbits and thus a bigger velopharynx. Moreover, there are some evident craniofacial differences between humans and rabbits which makes the results from this model not directly translatable to humans. However, developing a rabbit upper airway model has beneficial aspects since the invasive procedures performed in the animal model allowed an accurate definition of boundary conditions that provides insight on the tissue interactions in humans. The experimental studies also permitted a comprehensive verification of model behavior that would not have been possible in humans. Moreover, rabbit animal experiments have been extensively used to study the upper airway and numerous studies were found in literature to further assess the model outcomes. It is also worth noting that results of rabbit studies have previously been highly correlated with human studies. Therefore, the current rabbit model can be used as a basis to develop a human upper airway model after the refinement of some model properties.

#### 2.5.4.2 Passive Airway

The model does not incorporate nor muscle activity nor airflow but rather replicates the behavior of the passive upper airway of anesthetized and tracheostomized rabbits, as it was the case in the animal experimental studies used to develop and later valid the model. Thus, important respiratory reflexes are disregarded and the model does not entirely represent the in vivo upper airway behavior. Nonetheless, since upper airway muscle activity is reduced during sleep [17, 38], the passive upper airway behavior is particularly relevant in the context of sleep-disordered breathing.

#### 2.5.4.3 Simplification from 3D to 2D

The model is a 2D representation of the midsagittal section of the upper airway. Simplifying the complex 3D upper airway geometry to a 2D plane eliminate the possibility of obtaining lateral airway information. However, given the highly non-linear aspect of the model (hyper-elastic materials, complex boundary conditions), including the 3D geometry leads to a substantial increase in the computational cost. Existing 3D upper airway computational models usually have other simplified model properties, such as linear elastic materials or the exclusion of upper airway structures, to avoid the excessive computational expense (Section 2.4).

While the current model is reduced to 2D, it incorporates the impact of many structures outside the modeled midsagittal plane through the projection of out of plane muscle connections and thoroughly defined boundary conditions. In fact, the model was developed and optimized to represent the 3D behavior of the rabbit upper airway and was previously shown to successfully predict the upper airway behavior in response to mandibular advancement and tracheal displacement loads [1]. These results confirm the

ability of the model to reproduce the key biomechanical behaviors of the animal model examined (3D). Therefore, this 2D model can provide useful initial information regarding the complex upper airway interactions.

#### 2.5.4.4 Model definition assumptions

##### 2.5.4.4.1 Anatomical simplifications

Some simplifications were made to the tissue representations in the original model. The division between the superior, middle and inferior constrictor muscles was not considered and the constrictors were represented as one single body. The glandular tissues, adipose tissues and neck strap muscles were also all lumped together and embodied by the tissue mass in the model. Furthermore, the airway mucosa was not included in the model. Despite these simplifications, the model was able to reproduce experimental results and replicate the behavioral responses of the passive airway tissues.

##### 2.5.4.4.2 Boundary conditions

The model boundary conditions were defined on the basis of experimentally observed tissue behavior in response to mandibular advancement and tracheal displacement loads due to the lack of true contact behavior quantifications in literature. Overall, the boundary conditions and spring connections were able to reproduce the 3D airway behavior. However, some boundary conditions such as the bonded and no-separation contact between the soft palate and the tongue, tissue mass and epiglottis do not represent the true physiological conditions.

#### 2.5.4.4.3 Material Properties

The material properties of the model were defined and optimized to replicate the experimental results of the previous rabbit animal experimental study. The lack of available data on material properties of rabbit upper airway soft tissues, particularly the constrictor muscles, makes it difficult to evaluate the legitimacy of these properties.

## CHAPTER 3

### METHODS

#### 3.1 Overall Study Design

In order to accomplish the aims of this study, the rabbit upper airway 2-dimensional computational finite element model developed by Amatoury and colleagues [1] will be redeveloped, enhanced and utilized to examine the effect of hyoid bone position and movement on different upper airway outcomes using ANSYS Workbench (Release 19.2; Academic Research, Canonsburg, PA). The original model is discussed in detail in Section 2.5. An overview of the study design is illustrated in Figure 23.

The original model will first be redeveloped to allow intraluminal pressure simulation and thus permit the quantification of passive upper airway collapsibility ( $P_{close}$ ; negative pressure at which the upper airway closes). The model will be further enhanced to allow the representation of different hyoid baseline positions. However, it is important to note that the redeveloped model should preserve the behavior of the original model in response to mandibular advancement and tracheal displacement simulations since these interventions were validated against physiological experiments in the previous study [1].

The second phase of the study involves performing a set of model simulations associated with each of the project's specific aims. For Aim 1, simulation of upper airway collapse for different hyoid baseline positions will be performed. For Aim 2, a hyoid displacement load in different directions and magnitudes will be added to simulate hyoid surgical repositioning for the original baseline hyoid position. Finally,



for Aim 3, the same surgical hyoid repositioning loads will be applied starting from different baseline hyoid positions to investigate the combined effect of changes in baseline hyoid position and surgical hyoid repositioning on upper airway outcomes. All simulations will be discussed in detail in Section 3.3.

In addition to collapsibility ( $P_{close}$ ), upper airway model outcomes will include airway lumen geometry (airway dimensions and cross-sectional area) and tissue mechanics outcomes (tissue displacement, stress and strain).

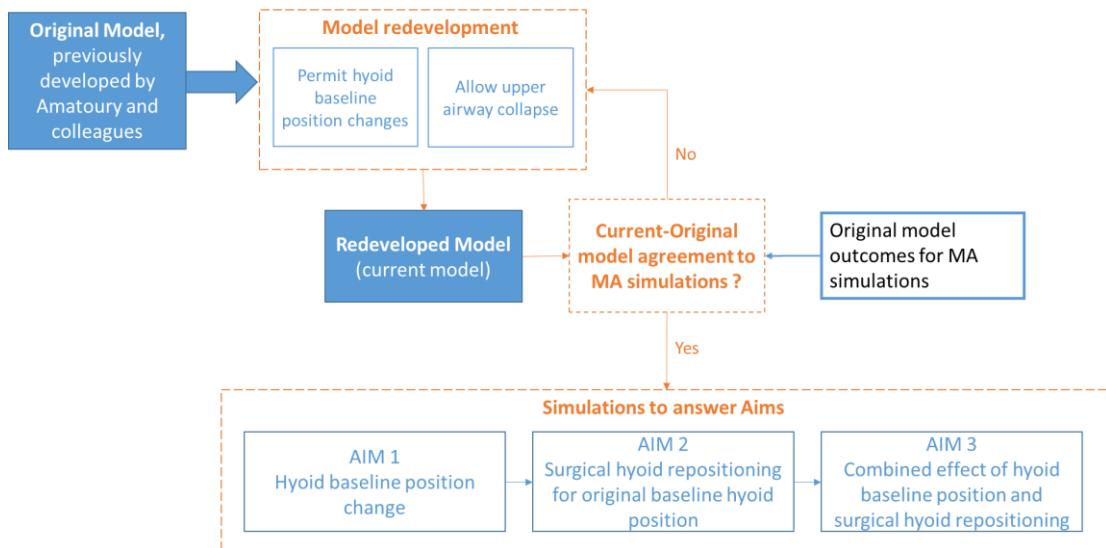


Figure 23: Overview of general study design flow. The original model developed by Amatory and colleagues [1] will be redeveloped and then used to perform a set of simulations to answer the specific aims of this study.

### 3.2 Model Redevelopment and Advancement

The aims of this thesis require the examination of the effect of changing hyoid baseline position, a phenotypic characteristic of an individual’s upper airway. Indeed, this investigation cannot be performed in a physiological model (animal or human). Changing hyoid baseline position involves altering hyoid position without changing the mechanical properties of the tissues connected to it. Thus, this needs to be a geometrical

modification of the model, pre-simulation, and cannot be achieved by means of an applied load.

On the other hand, simulating upper airway collapse involves the adjustment of select model definitions (boundary conditions, mesh) and analysis settings (discussed in Section 3.4) to allow the solution to converge for the high deformations that occur with this simulation. While modifications to the original model definitions are necessary for the purpose of this thesis, they are limited by the fact that the current model should still successfully simulate mandibular advancement and predict the outcomes (deformation, tissue mechanics and lumen geometry) associated with this procedure as in the original model, even after the modifications are made. In this section, the original model definitions that were modified in the current model will be detailed.

### ***3.2.1 Reconstruction and Geometrical Adjustments***

The model geometry was initially reconstructed from the segmented geometry contours of the original model from Amatoory et al. [1] using ANSYS Design Modeler. Surface bodies were built to replicate the upper airway structure of the original model shown in Figure 18. Geometrical changes were required to allow the hyoid baseline position to be modified and the surrounding structures to adapt to this change. The original hyoid baseline position is referred to as the zero-baseline position in this thesis. The hyoid bone surface was reconstructed with respect to a new plane, different from the plane on which the other structures were defined. Thus, shifting in the hyoid baseline position was achieved through the offset of this new plane. The upper airway structures that are in contact with the hyoid bone such as the tongue, geniohyoid and mylohyoid muscle surfaces had to be redrawn to ensure that the model geometry

remains an anatomically coherent airway structure after the changes in hyoid baseline position. For example, caudal change in the hyoid baseline position also implies that the base of the tongue is extended downwards and the angle and length of the surfaces representing the geniohyoid and mylohyoid are changed. Therefore, the lower tongue edges and the points where the geniohyoid and mylohyoid surfaces attach to the hyoid bone were redefined in Design Modeler with respect to the hyoid bone position to allow these structures to move in parallel with the hyoid as shown in Figure 24.

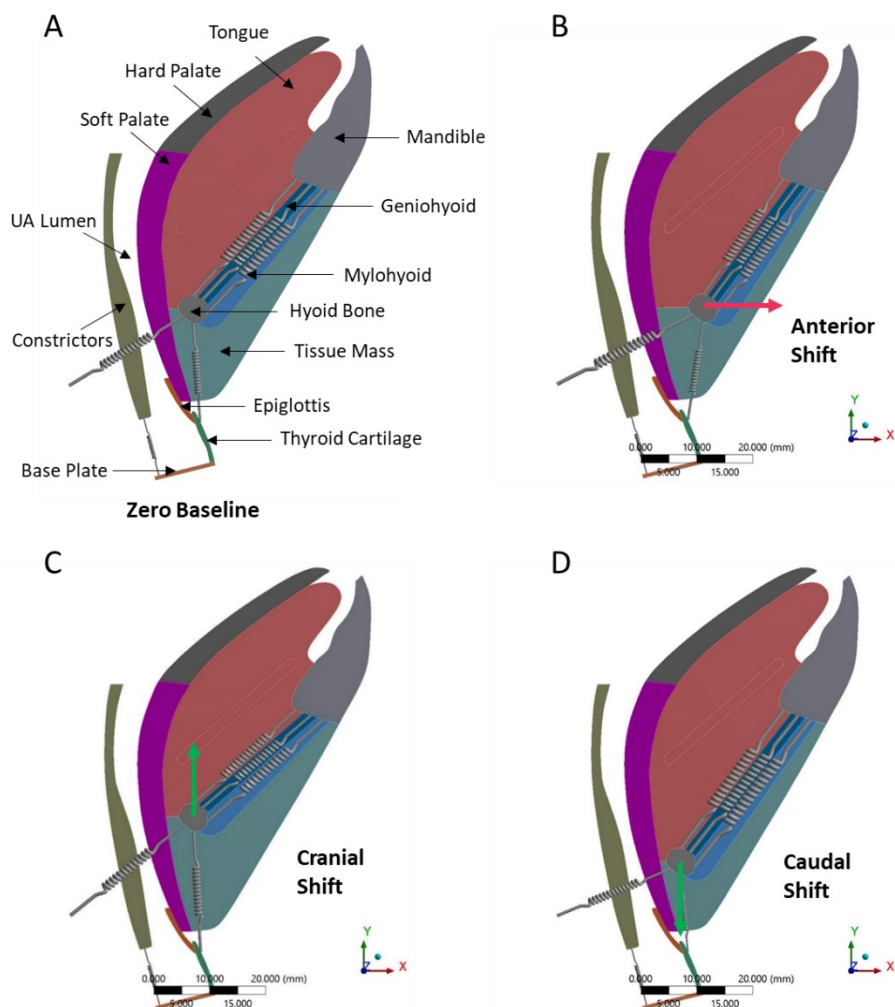


Figure 24: Models with Different Hyoid Baseline Positions. Figure showing the model geometry and the spring connections attached to the hyoid bone for hyoid baseline position shifted by 4mm in different directions. A) Model with the original hyoid

baseline position, zero-baseline hyoid position B) Model with an anterior hyoid baseline position. C) Model with a cranial hyoid baseline position. D) Model with a caudal hyoid baseline position. Only select spring-represented muscles (genioglossus, geniohyoid, mylohyoid, thyrohyoid, stylohyoid and constrictor-thyroid insertion) are shown in the figure to improve visibility.

### **3.2.2 *Boundary Condition Definitions***

Boundary conditions such as spring connections were slightly altered to adapt to the geometrical change in hyoid baseline position and contact definitions were adjusted to allow solution convergence of the intraluminal negative pressure (Pua) simulations for upper airway collapsibility quantification.

#### **3.2.2.1 Spring Connections**

All the spring connections that are attached to the hyoid bone were redefined with respect to a new coordinate system based on the hyoid bone that moves along with it. That way, the linear elastic springs' length and angle are altered according to the different hyoid positions, replicating the behavior of the upper airway muscles when the hyoid bone is displaced. Figure 24 illustrates how select springs adapt to the shifted hyoid baseline positions. Furthermore, the springs' behavior is changed from tension-compression to tension-only as this is more representative of the passive muscle's mechanical properties (much stiffer in tension than in compression) [18, 124].

#### **3.2.2.2 Contacts**

Contacts of the current model are based on the ones from the original model and are summarized in Figure 25 and Table 7.

The first step of adapting the model to Pua simulations and solving the convergence issues consisted in updating the contact interfaces depending on the

relative tissue movements during the different simulations. The displacement of the tongue with respect to the hard and soft palate was the most noticeable change in tissue structure produced by Pua and surgical hyoid repositioning (See Chapter 4). In fact, the tongue slides considerably backwards with the negative pressure load while the hard palate remains fixed. This causes the edges of the tongue that were previously in contact with the hard palate to become in contact with the soft palate during the airway collapse simulation. Furthermore, in some directions of hyoid displacement, the tongue is slightly moved anteriorly and some tongue edges at the interface with the soft palate come into contact with the hard palate after tissue deformation. Therefore, the no-separation contact originally defined between the soft palate and tongue (Labeled O in Figure 25) and the frictional contact between the hard palate and tongue (Labeled M in Figure 25) were redefined to include the whole upper boundary of the tongue to adapt for the tongue displacement.

The next step involved troubleshooting with the Newton-Raphson non-linear diagnostics tool to identify the sources of instability that caused the simulation solution to fail in each case. The Newton-Raphson residuals indicated that the interface between the tongue and soft palate as well as the area where hyoid, tongue and geniohyoid surfaces are joined had the highest force imbalances. Thus, adjustments were made to the normal contact stiffnesses at the problematic areas (set to 1 by default). This is a variable that controls the amount of penetration between two bodies in contact: the higher the normal contact stiffness, the less the penetration of the bodies into each other is permitted. Therefore, the hyoid to geniohyoid bonded contact stiffness is increased to a factor of 2 in order to reduce the penetration of the geniohyoid surface into the hyoid bone. Similarly, the contact stiffness factor of the no separation contact between the soft

palate and the tongue is increased to 1.55. These changes were found to be the best to allow solution convergence for a maximum number of simulations of surgical hyoid repositioning and Pua starting from different hyoid baseline positions. The normal stiffness factors used in the current model are summarized in Table 7.

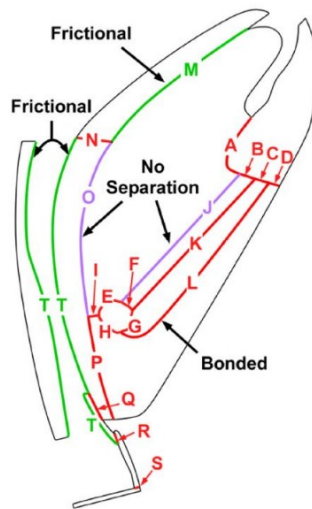


Figure 25: Model contact definitions illustrated on diagram of model edges. Red outlines indicate bonded contact definitions, purple outlines indicate no separation contact and green outlines indicate the frictional contact definitions. The letter labels (from A to T) are used in Table 7 to describe the contact interfaces and their properties. *Adapted from Amatoury et al [1].*

Interface	Label	Behavior	Stiffness Factor
Mandible/attached tissues	A-D	Bonded	1
Hyoid bone/attached tissues	E and G-H	Bonded	1
Hyoid bone/geniohyoid	F	Bonded	2
Tongue/tissue mass	I	Bonded	1
Tongue/geniohyoid	J	No Separation	1
Geniohyoid/mylohyoid	K	Bonded	1
Mylohyoid/tissue mass	L	Bonded	1
Tongue/hard palate*	M	Frictional, $\mu = 0.2$	1
Hard palate/soft palate	N	Bonded	1
Soft palate/tongue*	O	No separation	1.55
Soft palate/tissue mass	P	Bonded	1
Soft palate/epiglottis	Q	Bonded	1
Thyroid cartilage/epiglottis	R	Bonded	1
Thyroid cartilage/base plate	S	Bonded	1
Soft palate-epiglottis/constrictors	T	Frictional, $\mu = 0.1$	1

Table 7: Summary of model contact interfaces and corresponding properties including contact behavior and normal stiffness factor. Note that 1 is the default stiffness factor value. Contacts described in red represent the contacts for which the stiffness factor was modified from the original model. The mark \* indicates that the contact interface was modified from the original model. The label (second column) points to the location of interface shown in Figure 25. *Adapted and modified from Amatoury et al [1].*

### 3.2.3 Meshing and Model Verification

The mesh was generated using the ANSYS meshing capabilities. Two-dimensional 4-node quadrilateral plane strain elements were preferred because these elements adapt well to large deformation produced by the hyperelastic and nearly incompressible soft tissues represented in the current model. The default pure displacement element formulation was applied and the element technology used was the simplified enhanced strain formulation to prevent shear locking (inaccurate representation of curvature of a material present under bending).

The initial baseline mesh, as well as the deformed mesh after surgical hyoid repositioning (5mm magnitude in all directions) and Pua, were checked for visible errors but also evaluated according to mesh metrics such as skewness and general

element quality. Mesh metrics of different element sizes were assessed and compared for the different simulation scenarios. Moreover, the mesh was refined at the edges around the hyoid bone since higher strains were found in the area. Additional mesh refinement was performed at the edge between the hyoid and the geniohyoid surface and the edge between the hyoid and tongue to allow solution convergence for Pua simulations.

Finally, a mesh convergence study was performed to verify that the model is independent of the mesh density, as shown in Figure 26. The model output used is the antero-posterior displacement (along the X-axis) of a portion of the soft palate located right behind the hyoid bone since it was found to be the site of collapse. Anterior-cranial surgical hyoid repositioning of a 4mm magnitude was simulated for the mesh convergence study since it produced large tissue displacements and stress and is a clinically relevant procedure as discussed in Section 3.3.4. The final mesh was chosen based on the mesh metrics and mesh convergence study and consisted of 3970 elements with 3910 quadrilateral elements and 63 triangular elements.

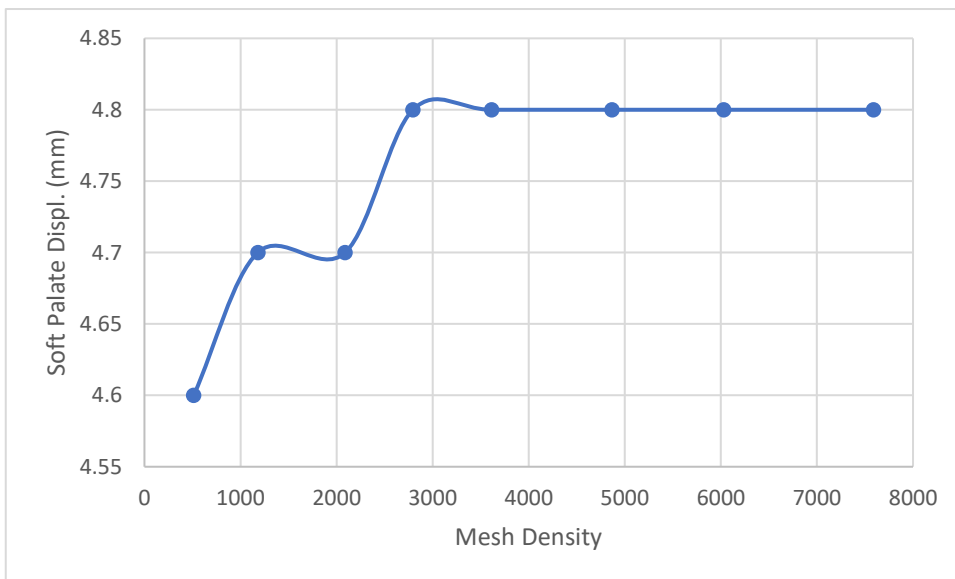


Figure 26: Mesh convergence study representing the displacement of a portion of the soft palate in response to anterior-cranial surgical hyoid repositioning simulation vs. the



mesh density (number of mesh elements) used. The selected portion of soft palate is located behind the hyoid bone and a 4mm hyoid displacement magnitude was chosen for the hyoid repositioning simulation. Convergence was reached at a mesh density of 3613 elements.

#### ***3.2.4 Current-Original Model Agreement***

The original model was developed to simulate mandibular advancement and tracheal displacement loads, with output outcomes validated to experimental data (as discussed in Section 2.5). In the current study, the model was redeveloped and enhanced to be used for a different purpose. Nonetheless, we chose to attempt to maintain the validity of the model to MA and TD. For this reason, the modifications made to the model definitions were as minor as possible.

After the model was reconstructed and redeveloped, mandibular advancement and tracheal displacement simulations of the original model were replicated in the current model. A mandibular advancement displacement load of 4.6 mm was applied at an angle of 75° with the +Y-axis (vector's X and Y components are 4.4 and 1.2 mm respectively) and a tracheal displacement load of 5.6 mm at an angle of 155° to the +Y-axis (vector's X and Y components are 1.9 and -5.3 mm respectively) as shown in Figure 27. Being the major model outcome of the previous study, the hyoid displacement results obtained in the current model were compared to the outcomes of the original model. The upper airway geometrical metrics (airway length, midsagittal area and antero-posterior diameters) were also compared in the different models. This allowed the estimation of the impact that the modifications made to the current model have had on mandibular advancement and tracheal displacement simulation outcomes. The plots showing the comparison between the original and the current model outputs are presented in Section 4.1.

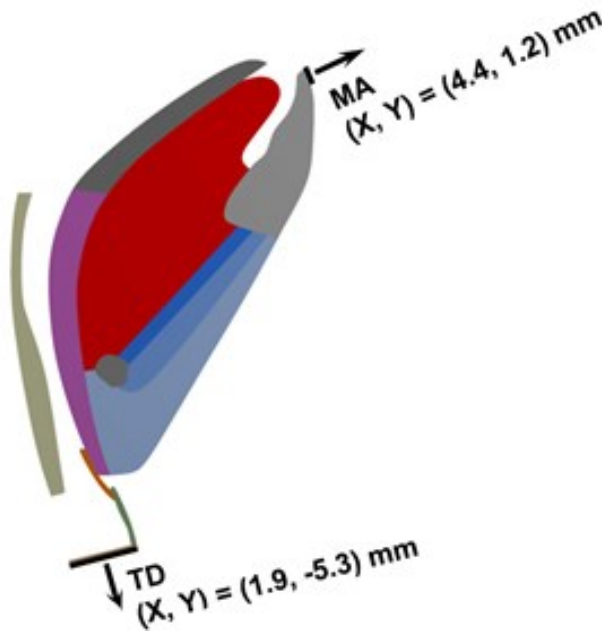


Figure 27: Illustration of the original model with the Mandibular Advancement (MA) and tracheal displacement (TD) displacement loads simulated. MA and TD load direction and component magnitudes (X,Y) applied and simulated in the original model and replicated in the current model are shown. *Adapted from Amatoury et al. [1].*

### 3.3 Loading Conditions and Simulations

The redeveloped model will be used in a series of simulations in order to accomplish the different aims of this Thesis. The flow diagram in Figure 28 summarizes the simulations that will be undertaken and model outputs examined for each aim.

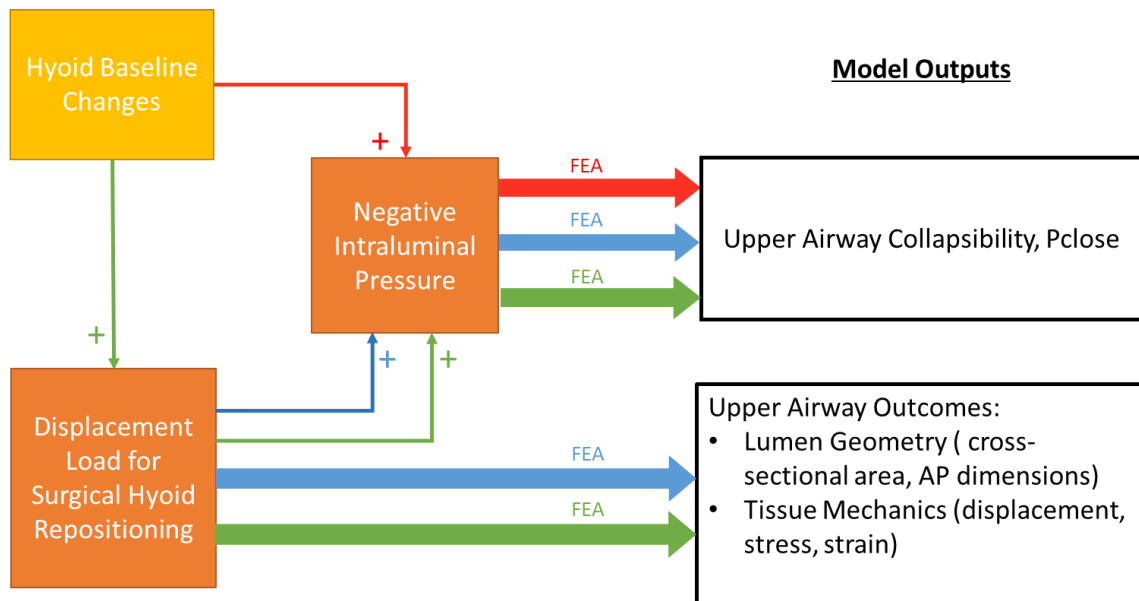


Figure 28: Simulations Workflow to Evaluate the Study's Specific Aims. The loads applied to the model are shown in the orange boxes and the changes in geometry in the yellow box. Red arrows represent the simulations undertaken for Aim 1, blue arrows for Aim 2 and green arrows for Aim 3. The model outputs (including lumen geometry, collapsibility and tissue mechanics) are obtained and examined for FEA simulations. Abbreviations: FEA, finite element analysis; AP, antero-posterior. Pclose is the closing pressure defined as the pressure at which the upper airway collapses (first point of direct contact between opposite walls of upper airway).

### 3.3.1 Aim 1- Influence of Hyoid Baseline Position (Phenotype)

#### 3.3.1.1 Changes in hyoid baseline position

The first aim of this study was to investigate the effect of hyoid baseline position (i.e. hyoid position phenotype) on upper airway outcomes. As a result of the geometrical model enhancements performed, offsetting the hyoid baseline position of the model directly from the geometry (not through a load) can be achieved in Design Modeler. Hence, the hyoid baseline position will be displaced up to 5mm in increments of 1mm along the cranial (+Y-axis), anterior (+X-axis), caudal (-Y-axis), anterior-caudal 45° and anterior-cranial 45° directions (see Figure 29). Anterior-caudal 45° and anterior-cranial 45° consist of an anterior component and a cranial or caudal component

to make a direction vector at 45° angle from the +X-axis and will be referred to as anterior-cranial and anterior-caudal in the rest of this thesis.

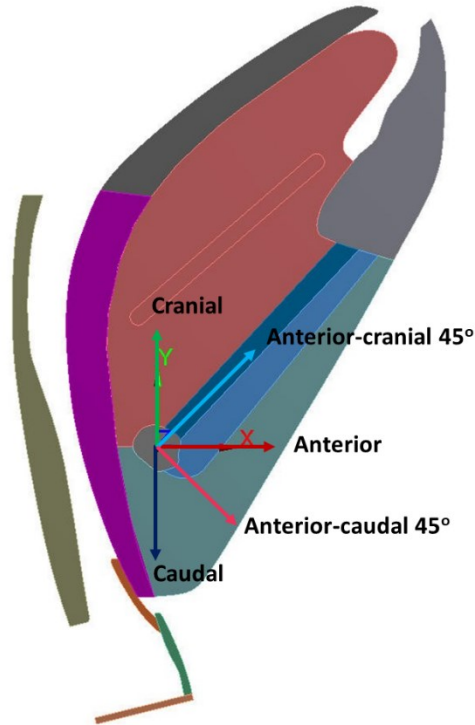


Figure 29: Model with different hyoid displacement directions studied. The anterior direction (red vector) is along the +X axis, cranial direction (green vector) along the +Y axis, caudal direction (blue vector) along the -Y axis. Anterior-cranial 45° vector (cyan vector) has both an anterior and cranial component and forms a 45° angle with the axes. Anterior-caudal 45° vector (magenta vector) has both an anterior and caudal component and forms a 45° angle with the axes.

### 3.3.1.2 Intraluminal Negative Pressure (Pua) Load

For each hyoid baseline position, a negative intraluminal pressure (Pua) load was applied to simulate upper airway collapse. Pua was applied at the walls of the upper airway lumen defined by the anterior boundary of the constrictor body and the posterior boundaries of the soft palate, epiglottis and thyroid cartilage as shown in Figure 30.

A uniformly distributed negative pressure load of -9000 Pa (-91.8 cmH<sub>2</sub>O) was gradually applied to the airway walls. This pressure magnitude is much larger than the

upper airway physiological pressures, as discussed in Sections 5.2 and 5.7.2, because the model behavior was stiffer than the actual physiological airway. The pressure load of -9000 Pa was found to be the smallest pressure that produced airway collapse for all different hyoid baseline positions and hyoid repositioning procedures while still allowing solution convergence of the simulations.

Pua simulation is completed over a single load step using 80 substeps which permits the gradual application of the pressure by increments of 112.5 Pa (~1.15 cmH<sub>2</sub>O) as shown in Figure 31. Defining the number of substeps for the Pua load was important for two major reasons. On the one hand, increasing the number of substeps meant applying this large pressure more gradually which aided the solution convergence of this simulation with large deformations. On the other hand, the quantification of model collapsibility ( $P_{close}$ ), one of the primary model outputs, is dependent on that number of substeps since the  $P_{close}$  measurement error is defined as half the smallest Pua increment. After testing for different number of substeps, 80 was found to be the ideal number of substeps for solution convergence as well as accuracy of  $P_{close}$  determination with a measurement uncertainty of  $\pm 0.58$  cmH<sub>2</sub>O.

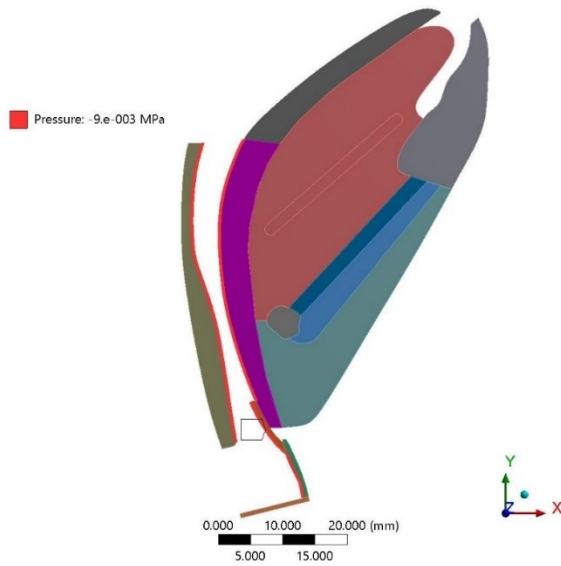


Figure 30: Current Model with Illustration of Intraluminal Pressure Load. Negative intraluminal pressure load applied on airway boundaries delineated in red in direction normal to the edges and pointing inwards as shown by arrows.

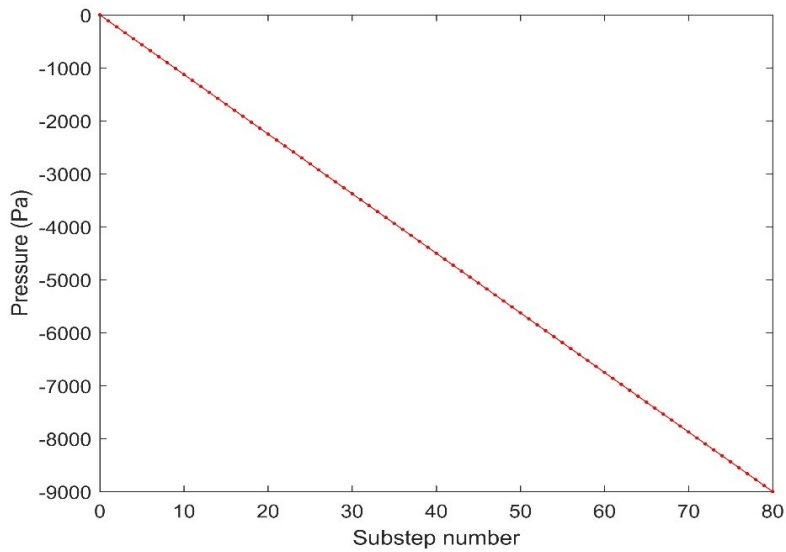


Figure 31: Intraluminal negative pressure load applied across 80 substeps (ramped pressure load). Plot showing the gradual incrementation of pressure applied with respect to the substep number.

### ***3.3.2 Aim 2- Influence of Surgical Hyoid Repositioning for Original Baseline Hyoid Position***

The second aim involves assessing the effect of surgical hyoid repositioning on upper airway collapsibility and tissue mechanics.

A displacement load was applied on the hyoid bone to simulate surgical hyoid repositioning. The hyoid displacement load was applied at the centroid of the hyoid bone surface specifying the direction and magnitude of hyoid displacement. The displacement load also ensured that the hyoid is fixed in its new position after it is displaced, as it is the case in the hyoid repositioning surgeries. The magnitude of hyoid displacement applied was from 1 to 5mm with a 1mm increment and is applied along the cranial (+Y-axis), anterior (+X-axis), caudal (-Y-axis), anterior-caudal 45° (equal anterior and caudal displacement component) and anterior-cranial 45° (equal anterior and caudal displacement component) to replicate the hyoid bone movement performed experimentally in the rabbit experimental animal study (See Figure 29) [97]. Surgical hyoid repositioning simulations were solved over 1 step using 4 substeps (0.25mm hyoid displacement increment per substep).

As a second phase, Pua is applied exactly as described in Section 3.3.1.2 to combinations of hyoid baseline position and surgical hyoid repositioning procedure to simulate upper airway collapse. This multiple load simulation was solved over 2 steps:

- Step 1 (4 substeps): Surgical hyoid repositioning load
- Step 2 (80 substeps): Pua load

### ***3.3.3 Aim 3- Combined Influence of Baseline Hyoid Position and Surgical Hyoid Repositioning***

The third aim involves assessing the combined effect of hyoid baseline positions changes and surgical hyoid repositioning on upper airway collapsibility and tissue mechanics.

Starting from different hyoid baseline position created for the Aim 1 (see Section 3.3.1), a displacement load will be applied on the hyoid bone to simulate surgical hyoid repositioning exactly as is done in Aim 2. The directions and magnitudes of the hyoid displacement load applied as well as the analysis settings of the simulations are detailed in Section 3.3.2.

### ***3.3.4 Clinically Relevant Simulations***

Amongst the numerous loading conditions and simulations performed, select conditions were established to be of particular interest to this study since they represent clinically relevant physiological scenarios.

First of all, the caudal shift in the hyoid baseline position is considered since the hyoid bone was consistently found to be inferiorly positioned in OSA patients compared to healthy individuals [11, 16, 31, 41, 44, 99, 121]. A study by Chi et al. reported that there is a 6.2% difference in the hyoid-to-nasion vertical distance between apneic and normal individuals [30]. Taking the vertical distance in the current model from the fixed superior boundary of the hard palate to the centroid of the hyoid bone at baseline, a 6.2% change in dimension translates into a ~2mm shift in the hyoid baseline position. Thus, a caudal hyoid baseline position change of 2mm increment in this study mimics



OSA phenotypical characteristics. A 4mm hyoid baseline increment is also chosen to be of interest to examine the impact of a doubled baseline increment.

Moreover, two types of surgical hyoid repositioning procedures have been performed clinically as OSA treatment options: hyomandibular suspension and hyothyroidopexy which consist in anchoring the hyoid bone either cranially to the mandible or caudally to the thyroid cartilage, respectively [92, 93]. Although these surgical procedures are performed crudely with no specific guidance (angle and magnitude of hyoid displacement not specified), an anterior hyoid advancement component seems to be consistently present in both procedures [15] and the magnitude of advancement is generally between 1 and 2cm [119]. Anterior-cranial and anterior-caudal surgical hyoid repositioning loads are therefore chosen to mimic hyomandibular suspension and hyothyroidopexy, respectively. From the study by Chi et al. [30], an 8mm change in hyoid baseline in the human physiological airway translated into a 2mm change in the current airway model. Thus, the 1 to 2cm advancement was approximated by a hyoid displacement magnitude between 2 and 5mm in the model. The 2mm and 4mm hyoid displacement increments were selected for consistency with the hyoid baseline increments.

Consequently, anterior-cranial and anterior-caudal hyoid repositioning simulations applied for the caudal hyoid baseline position are of particular clinical relevance since they mimic the scenario of applying surgical hyoid repositioning treatments for OSA patients.

### **3.4 FE Analysis Settings**

The finite element analysis was performed under a static structural system with 2-dimensional plane strain conditions using the ANSYS Mechanical solver. Large deformation effects were enabled due to the presence of non-linear hyper-elastic materials and expected large deformation. The FE analysis settings particular to the solution of the different simulations are described with the load conditions of these simulations in Section 3.3. The simulations were executed on virtual machine system with a 32-Core Processor (AMD EPYC 7551 ~2 GHz) and 32 GB RAM.

It is important to point out that analysis settings play a role in facilitating the solution convergence for the Pua simulations. Foremost, the maximum number of equilibrium iterations per substep was doubled from 25 to 50 (using the NEQIT APDL command), which allows the solver to have a greater number of chances to attempt solution convergence. Additionally, increasing the number of substeps used for the Pua load application helps the solution to converge since the pressure is applied gradually, in smaller increments as discussed in section 3.3.1.2.

### **3.5 Model Outputs**

The current model was able to provide numerous outputs including upper airway collapsibility ( $P_{close}$ ) when Pua load was applied. Changes in airway lumen geometry (cross-sectional area, CSA and antero-posterior diameter, APD) and tissue mechanics (displacement, stress and strain) are also measured in response to the different surgical hyoid repositioning load simulations (refer to Figure 28).

Given the large number of possible scenarios to be studied, select simulations were chosen for each of the model outputs based on the most clinically relevant conditions (Section 3.3.4). These select simulation will be listed below for each output.

### ***3.5.1 Upper Airway Collapsibility, $P_{close}$***

#### **3.5.1.1 $P_{close}$ Measurement Technique**

The closing pressure,  $P_{close}$ , is a major outcome of this study and quantifies the collapsibility of the modeled upper airway, i.e. the pressure at which the upper airway closes.  $P_{close}$  is quantified in the model as the pressure at which the opposing airway walls first come into direct contact. The contact between the anterior side of the constrictors and the posterior boundaries of the soft palate, epiglottis and thyroid cartilage was monitored throughout Pua load step using the post-processing *contact tool* in ANSYS Workbench.

Based on the ANSYS Mechanical contact algorithm, the penetration result of the contact between the opposing airway boundaries provides information on when the initial direct contact occurs between the airway edges. More specifically, a non-zero penetration result signifies that the boundaries of the airway have directly touched each other. Since there is a gap between the upper airway walls in the initial state of the simulation, the penetration is initially zero (Figure 32 A). Throughout the gradual application of the Pua load, the airway walls come closer to each other and eventually touch, which leads to a non-zero contact penetration value at the point of contact (Figure 32 B). Consequently, the pressure at which the first non-zero penetration value occurs is taken as  $P_{close}$ .

$P_{close}$ , cannot be defined as a direct solution output in ANSYS Workbench. Instead the time vs. contact penetration results are exported from ANSYS Workbench and  $P_{close}$  is computed from the time at which the first non-zero contact penetration between the airway walls occurs in the Pua load step. Since Pua load is linearly applied across time (Figure 31),  $P_{close}$  can be obtained using the below equation:

$$P_{close} = t \cdot P_t \cdot cf \quad (\text{eq. 1})$$

where  $t$  is the time at which the penetration becomes greater than zero,  $P_t$  is the total intraluminal negative pressure applied (-9000 Pa) and  $cf$  is the Pascals (Pa) to centimeters of water (cmH<sub>2</sub>O) units conversion factor used to obtain the  $P_{close}$  result in cmH<sub>2</sub>O.

The process of obtaining the  $P_{close}$  results manually is complex and time consuming and was therefore automated through a workbench macro script as described in the next section (Section 3.5.1.2)

In this study,  $P_{close}$  will be mainly expressed as the percent change in  $P_{close}$  ( $\Delta P_{close}$ , %) with respect to the zero-baseline  $P_{close}$ . In some cases the percent change in  $P_{close}$  is measured with respect to  $P_{close}$  of different baseline positions. This will be further detailed in Chapter 4.

$P_{close}$  outcomes were computed for Pua simulations for the following scenarios:

- Zero hyoid baseline position
- Hyoid baseline position changes in the 5 directions and 5 increments each (Section 3.3.1.1)
- Surgical hyoid repositioning in all 5 directions and 5 increments each for zero hyoid baseline position (Section 3.3.2)

- Surgical hyoid repositioning in all 5 directions and 5 increments each for 2mm and 4mm changes in hyoid baseline position in all 5 directions

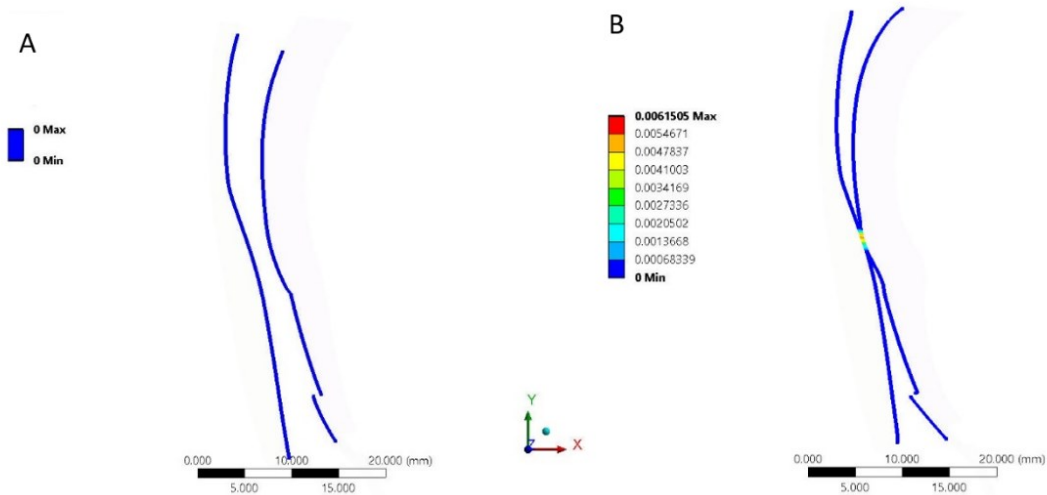


Figure 32: Change in penetration results for contact between airway walls due to negative intraluminal pressure ( $P_{ua}$ ) load. Upper airway lumen boundaries with color-coded contours map of penetration values (in mm) between the opposing airway walls in the initial undeformed state of the upper airway (A) and at the moment closure first occurs (B).

### 3.5.1.2 Automation of Simulations and Pclose Output Acquisition

Although the individual simulations are quite simple and require only a couple of minutes to solve, the large number of simulations and the complex process of obtaining Pclose results reinforce the need for automating the simulations and Pclose result acquisition.

As a first step of automating the simulations, a parametric study was designed in ANSYS Workbench that takes as input the X and Y components of either the geometrical hyoid baseline position offset (Aim 1) or the hyoid displacement load (Aims 2 and 3). In both cases about 25 different design points are specified that define

the combinations of X and Y displacement vectors representing all the directions and increments of hyoid displacement studied. The output parameter of the parametric study was set to be the maximum penetration result of the contact between the opposing airway boundaries. The time at which the penetration result is computed was set as another input to be able to evaluate the contact penetration result at each substep of the Pua load step.

Since Pclose could not be obtained using a predetermined command in ANSYS Workbench and set as an output parameter of the parametric study, further scripting was required to automate the Pclose determination process described above. More specifically, an ANSYS Workbench journal file (.wbjn file) was created and a macro script was written using a Python-based j-script language. A python source file was used to launch ANSYS Workbench in Batch mode and run the macro script.

The macro script was developed to solve the parametric study designed in a specific Workbench project file. Iterating over the different time increments (substeps) of the Pua load application, the penetration result output corresponding to the different time increment was evaluated. The time step iteration loop was stopped when a condition defined as the “penetration result is strictly greater than zero” was met, since a non-zero penetration value implied that direct contact between the airway walls occurred. Thus, the last time increment before exiting the loop was used to calculate Pclose from the equation previously described (Section 3.5.1, equation 1) and the Pclose result was recorded in a text file. This process was repeated for each design point of the parametric study (different combinations of direction and increment of hyoid displacement). The macro script was organized such that each run of the code produced five different output text files (.txt file) corresponding to the five different directions of

hyoid displacement and each file included the displacement magnitudes for that specific direction from 1 to 5mm (first column) with their respective Pclose results (second column). These output files were then processed in Matlab to generate the desired Pclose output plots.

### ***3.5.2 Site of Collapse***

The location at which the initial upper airway collapse occurs along the airway's length was also examined in some cases using the penetration result of the airway boundaries at the instant of collapse (time of first non-zero penetration value). The site at which collapse occurs for different loading conditions were compared by aligning these results and projecting lines along all different scenarios to observe the relative location of the site of collapse.

In this study, the site of collapse was evaluated for the below conditions:

- Zero baseline hyoid position
- Surgical hyoid repositioning of 2 and 4mm magnitude in all 5 directions for zero baseline hyoid position

### ***3.5.3 Total Tissue Displacement, Stress and Strain***

The displacement of upper airway structures in response to the applied loads were obtained using the total deformation solution in ANSYS Workbench and displayed as color-coded displacement contours and deformed mesh. Displacement vectors were also visualized to indicate the direction of the deformation at the mesh nodes.

The equivalent (von Mises) stress and strain distributions in the upper airway tissues were also evaluated and visualized as a color-coded contours map. Stress is a quantification of the force experienced by the tissues and is expressed as the force per unit area. Strain is a dimensionless measure of the amount of deformation experienced by the tissues in response to the applied stress.

Tissue displacement, stress and strain outcomes were examined, in this study, for a few selected simulation scenarios:

- Surgical hyoid repositioning simulations in all 5 directions with 2mm and 4mm hyoid displacement increment for zero-baseline hyoid position
- Surgical hyoid repositioning simulations in the anterior-cranial (hyomandibular suspension) and anterior-caudal (hyothyroidopexy) directions by 2 and 4mm magnitudes from a caudal hyoid baseline position shift of 2mm (mimicking OSA).
- Surgical hyoid repositioning simulations in the anterior-cranial (hyomandibular suspension) and anterior-caudal (hyothyroidopexy) directions by 2 and 4mm magnitudes from a caudal hyoid baseline position shift of 4mm (position lower than average OSA phenotype).

#### **3.5.4 *Lumen Geometry Metrics***

The changes in upper airway geometry produced by the different loads were assessed by measuring the lumen dimensions and cross-sectional area. After the FE simulation, the deformed model geometry was exported from ANSYS (in Parasolid format) into the 3D CAD design software, SOLIDWORKS, where the upper airway lumen contour was created. The measurements of the upper airway lumen cross-



sectional area (CSA), and antero-posterior diameter (APD) were performed in SOLIDWORKS based on the airway geometry region delimitations from the rabbit experimental study by Amatoury et al. [1].

The cross-sectional area (CSA) was measured as the area within the mid-sagittal airway contour delimited as shown in Figure 33.

The antero-posterior diameters (APD) were measured along the airway's lumen length (at 1.2mm increments; [1]). The upper airway was divided into 3 regions along its length, R1, R2, and R3 starting from the cranial boundary. Region R1 represents the base of the tongue region and is delimited by the nasal choanae (cranial airway boundary defined) and the upper surface of the hyoid bone. The second region, R2, extends from the superior surface of the hyoid bone to 1.5 mm above the superior face of the epiglottis. This region represents the hyoid bone region. Region R3, epiglottal region goes from the lower boundary of R2 to the base of the epiglottis. The APD measurements were calculated as the average of the APD dimensions for each one of the regions defined.

All the measurements are expressed as the percent change from the zero-baseline undeformed airway measurements ( $\Delta\text{Length, \%}$ ;  $\Delta\text{CSA, \%}$ ;  $\Delta\text{APD, \%}$ ).

Lumen geometry outputs were obtained for the exact same simulations used for tissue displacement stress and strain outputs listed above (Section 3.5.3)

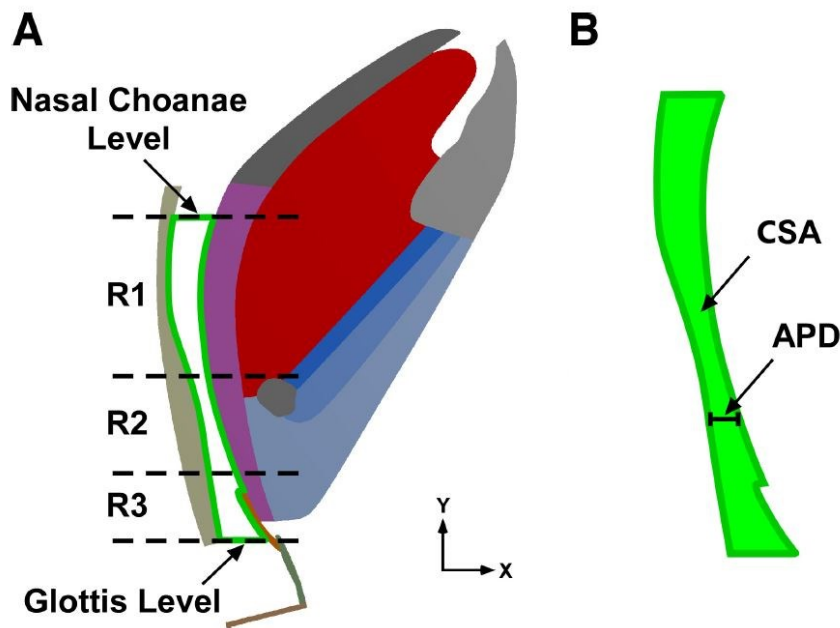


Figure 33: Airway region delimitation and lumen geometry measurements. A) FE model geometry with airway regions (R1-R3) delimitations and lumen contour (green) extending from the glottis to the nasal choanae. B) Measurements of upper airway cross sectional area (CSA) and antero-posterior diameter (APD). Note that APD was sampled along the airway at 1.2 mm increments and the mean value was calculated from each region. *Adapted from Amatoury et al. [1].*

### 3.6 Model Validation

The model was validated against the experimental data obtained from an animal study conducted in our research group that performed surgical hyoid repositioning on rabbits [97]. Hence, the  $P_{close}$  model outputs for surgical hyoid repositioning simulations starting from the zero-baseline hyoid position were compared to the  $P_{close}$  obtained experimentally. More precisely, for each direction and increment of hyoid displacement, the percent change in  $P_{close}$  with respect to the baseline  $P_{close}$  ( $\Delta P_{close}$ , %) obtained from the model simulations were compared to mean  $\pm$  95% confidence interval of these outcomes obtained experimentally.

# CHAPTER 4

## RESULTS

### 4.1 Comparability to Original Model

The hyoid displacement results produced in the current model are compared to the results of the original model in response to the same mandibular advancement simulation load (4.6mm at a 75° angle to the +Y-axis) [1]. The results from the current model are in agreement with the ones from the original model with a maximum difference of 0.05mm in hyoid displacement produced for a 4.6 mm mandibular advancement (See Figure 34). Furthermore, the change in upper airway lumen geometry in response to mandibular advancement produced in the current model are very closely matched to those produced in the original model (see Figure 35). Therefore, the current model was able to replicate the validated behavior of the original model in response to mandibular advancement simulations.

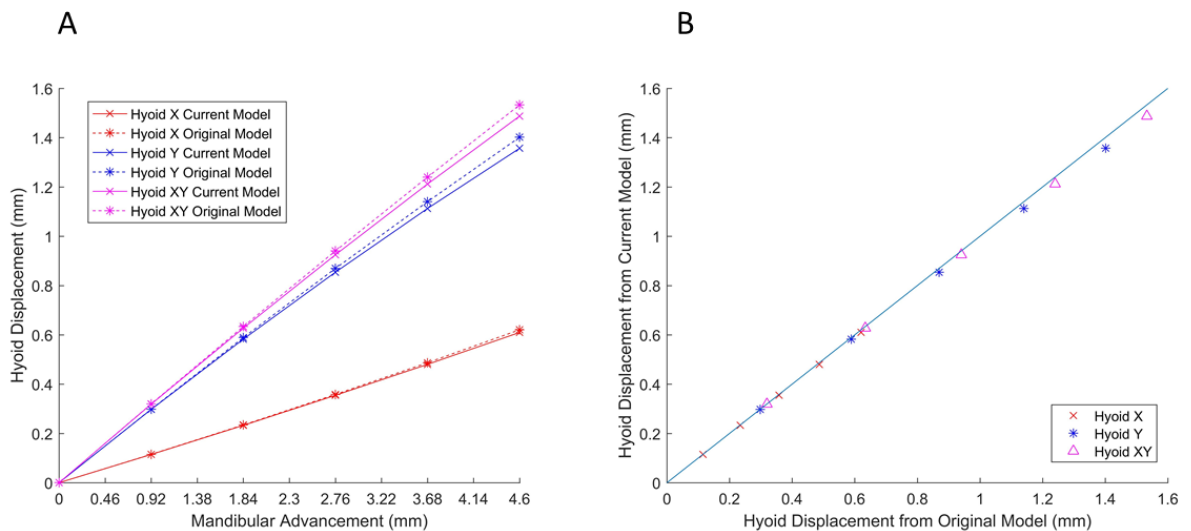


Figure 34: Hyoid displacement result of mandibular advancement simulation from current model compared to the original model outputs. (A) The values of hyoid

displacement components (X and Y) and resultant displacement vector in response to mandibular advancement simulation are represented as a function of mandibular advancement increment for current and original model. (B) Identity plot illustrating the close association between the hyoid displacement results presented in graph A.

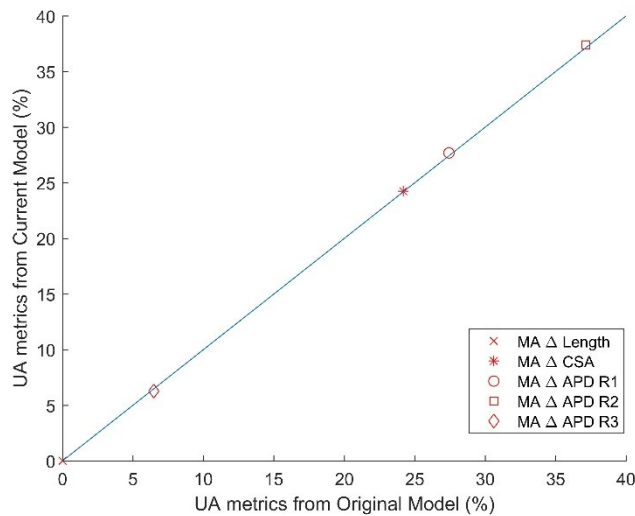


Figure 35: Identity plot representing the similarities between the current and original models in the change in upper airway geometry for 4.6mm of mandibular advancement (MA). The resulting percent change in upper airway length ( $\Delta$ Length), cross-sectional area ( $\Delta$ CSA) and anteroposterior diameters ( $\Delta$ APD; for regions R1-R3) from the current model are directly compared to those obtained from the original model.

#### 4.2 Upper Airway Collapse at Zero-Baseline Hyoid Position

Simulating upper airway intraluminal negative pressure when the hyoid bone is in its original position (referred to herein as “zero-baseline hyoid position”) led to upper airway collapse with a closing pressure ( $P_{close}$ ) of approximately 40.15 cmH<sub>2</sub>O. As shown in Figure 36, the first point at which airway closure occurs is located behind the hyoid bone at the level of the superior surface of the hyoid (boundary between regions

R1 and R2). The baseline  $P_{close}$  value corresponding to the unchanged hyoid position model is referred to as  $P_0$  in the following sections.

The upper airway soft tissue displacements created by the intraluminal negative pressure load applied are represented in Figure 36-B. The largest displacement occurred in the soft palate and tongue that are pulled backwards by approximately 2 mm until the soft palate and constrictors are pressed against each other and the airway lumen is closed. Very slight movement was produced in the constrictors body (since they are fixed at the top to represent their attachment to the occipital bone). Likewise, the bony upper airway structures such as the mandible, hard palate and thyroid cartilage were not displaced by the intraluminal negative pressure load applied.

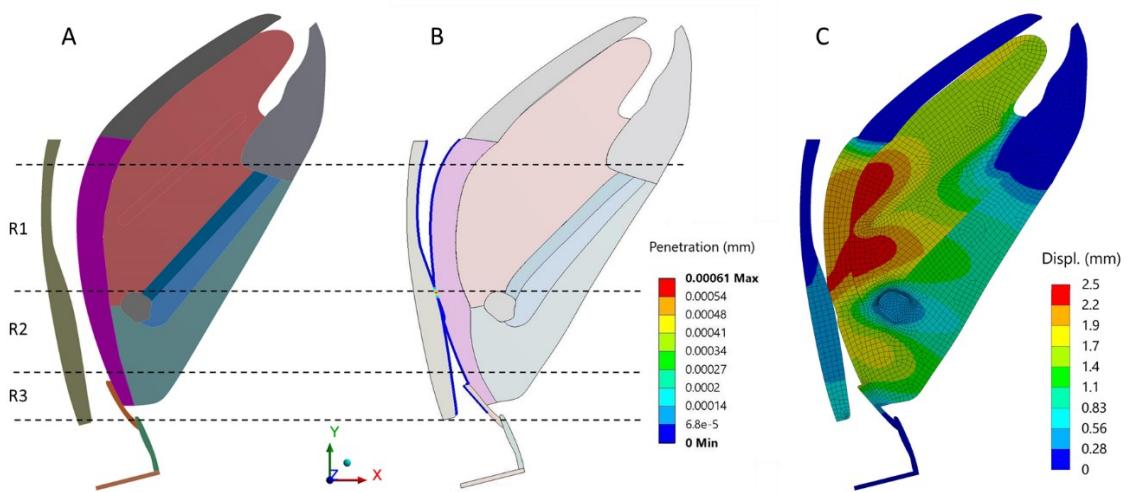


Figure 36: Upper airway collapse as a result of negative intraluminal pressure simulation for zero baseline hyoid position. Model in the undeformed state (A) and at the instant of initial airway closure (B) with the R1-R3 regions delimitations. The penetration result of the contact between the lumen boundaries (B) indicates that initial closure (point of maximum penetration here) occurs at the boundary between regions R1 and R2. Resultant tissue displacement represented as a color-coded contours map shown on the deformed mesh when the intraluminal negative pressure applied is equal to  $P_0 \sim 40.15$  cmH<sub>2</sub>O (C).

### 4.3 Influence of Baseline Hyoid Position “Phenotype” on $P_{close}$ (Aim 1)

When the hyoid baseline position is altered,  $P_{close}$  increases for all directions and increments of hyoid baseline shift. Figure 37 presents the percent change in  $P_{close}$  compared to the baseline  $P_{close}$  ( $P_0$ ) as a function of the increment of hyoid baseline position change for different directions.  $P_{close}$  is increasing quasi-linearly with the increment of baseline position shift.

The smallest change in  $P_{close}$  is for the cranial direction (35% increase) and the highest for anterior-caudal and anterior-cranial directions (~50% increase). A caudal relocation of the hyoid baseline position, representing a common phenotypical characteristic of obstructive sleep apnea patients, causes a 23% increase in  $P_{close}$  for a 2mm baseline increment and ~35% increase in  $P_{close}$  for 4mm.

The absolute values of the  $P_{close}$  obtained for the different baseline positions are summarized in Table 8. Individual position  $P_{close}$  baselines are used in section 4.5.1.2 to describe the effectiveness of surgical hyoid repositioning ( $\Delta'' P_{close}$  %) while  $P_0$  baseline is used for all other calculations of the percent change in  $P_{close}$  ( $\Delta P_{close}$  %). Note that the absolute  $P_{close}$  values from the model are much larger than physiological closing pressure as discussed in Section 5.2

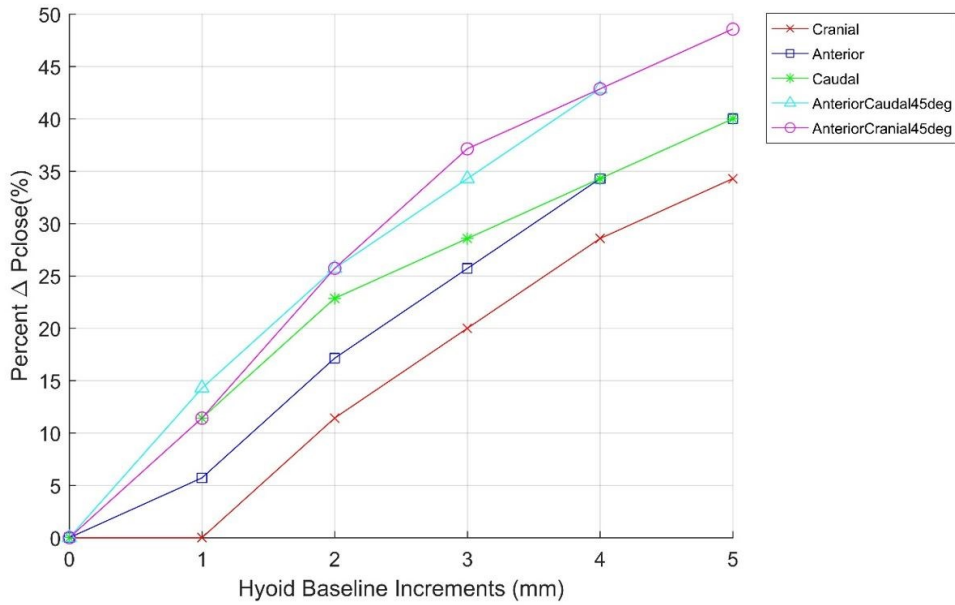


Figure 37: Percent change in Pclose ( $\Delta P_{close}$  %; with respect to  $P_0$ ) vs. hyoid baseline increments. The hyoid baseline position is altered by 1 to 5mm in the cranial, anterior, caudal, anterior-cranial 45° and anterior-caudal 45° directions. All changes in hyoid baseline position produced an increase in Pclose relative to zero-baseline position.

Hyoid Baseline relocation Direction Increment (mm)	Absolute Baseline Pclose Values (cmH2O)				
	Cranial	Anterior	Caudal	Anterior-Caudal	Anterior-Cranial
0	$P_0 = -40.15$				
1	-40.15	-37.86	-35.56	-34.42	-35.56
2	-35.56	-33.27	-30.97	-29.83	-29.83
3	-32.12	-29.83	-28.68	-26.39	-25.24
4	-28.68	-26.39	-26.39	-22.94	-22.94
5	-26.39	-24.09	-24.09	N.A. *	-20.65

\* Geometrically not possible to shift hyoid baseline position to this point (Hyoid becomes too close to the inferior boundary of the model and mylohyoid structure goes beyond the delimiting boundaries of the model).

Table 8: Absolute Pclose results for different hyoid baseline positions. Zero baseline Pclose ( $P_0$ ), shaded in red, is used to determine the percent change in Pclose ( $\Delta P_{close}$  %) in the next sections. The individual position baseline Pclose values in the green cells are used in section 4.5.1.2 to obtain the change in Pclose with respect to shifted hyoid baseline position Pclose ( $\Delta'' P_{close}$ ).

## 4.4 Influence of Surgical Hyoid Repositioning for Zero-Baseline Hyoid Position (Aim 2)

### 4.4.1 $P_{close}$

Simulations of surgical hyoid repositioning with a hyoid displacement load (starting from the zero-baseline position) were both magnitude and position dependent (Figure 38). The change in  $P_{close}$  was progressive at each increment (linear-like behavior) for all directions and the largest change was produced for hyoid displacement directions with an anterior component. In fact, surgical hyoid repositioning in anterior, ant-cranial and ant-caudal directions resulted in the greatest decrease in  $P_{close}$ , reaching up to 130% decrease at 5mm of hyoid displacement. Hyoid repositioning in the cranial direction produced a relatively smaller decrease in  $P_{close}$  of  $\sim 40\%$  for 5mm increment of cranial hyoid displacement. On the contrary, caudal hyoid repositioning caused an increase the  $P_{close}$  of up to 30%.

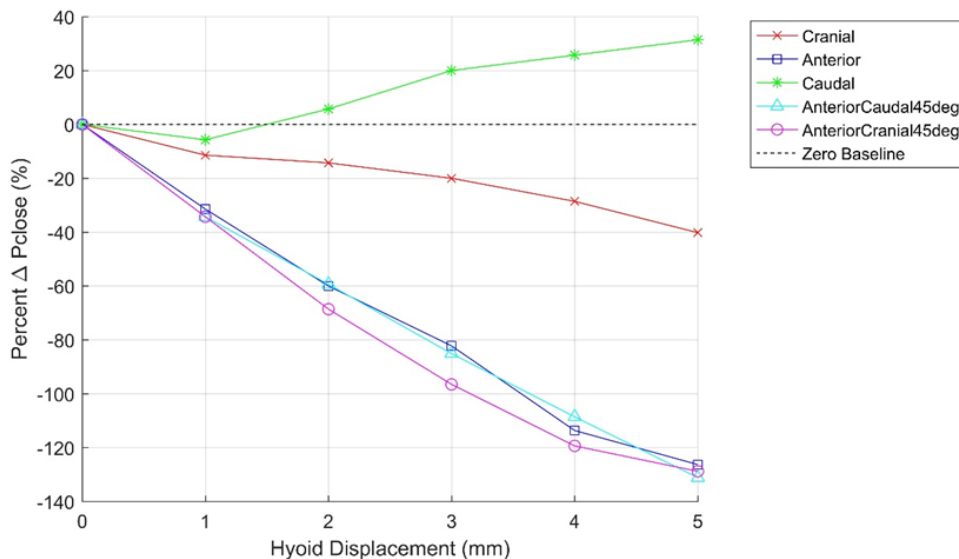


Figure 38: Percent change in  $P_{close}$  ( $\Delta P_{close}$  %; with respect to  $P_0$ ) vs. hyoid displacement (surgical repositioning) for zero-baseline hyoid position. Hyoid displacement applied from 1 to 5mm for cranial, anterior, caudal, anterior-cranial 45° and anterior-caudal 45° directions. Hyoid displacement is applied on the model from the initial zero-baseline hyoid position.



#### 4.4.2 Validation of Pclose Outcomes with Experimental Results

The model outputs revealed similar changes in Pclose in response to surgical hyoid repositioning as the experimental results from the rabbit animal study [97]. Figure 39 shows plots of the change in Pclose obtained from the model outputs and from the experimental results of the rabbit study, side by side. The pattern of change in Pclose for the different surgical hyoid repositioning directions and increments observed in the model was generally similar to the pattern observed in the animal study. The percentage change produced is slightly overestimated in the model for the caudal and cranial hyoid repositioning procedures while it is slightly underestimated for the anterior, anterior-cranial and anterior-caudal directions. However, the results obtained from the model simulations are still within the 95% confidence interval of the experimental Pclose for all directions and increments of hyoid displacement, except for select increments in the caudal direction and the 5mm increment of cranial hyoid repositioning, as shown in Figure 40.

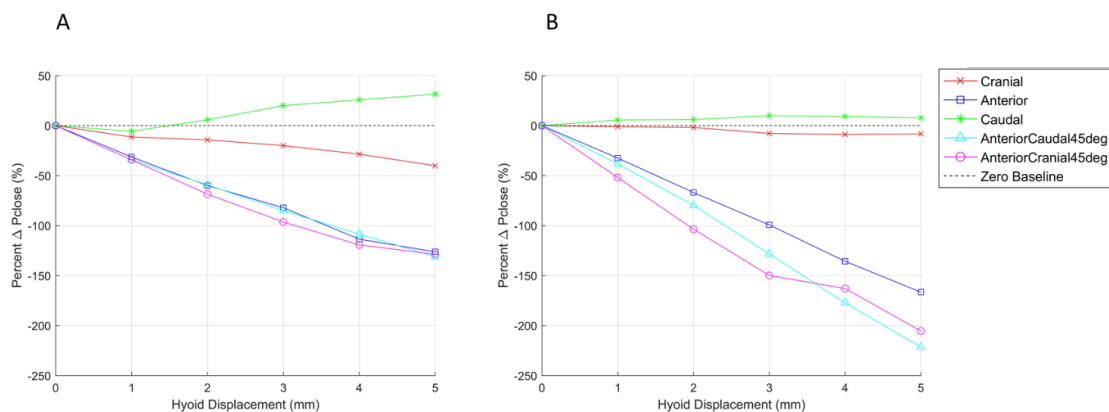


Figure 39: Comparison between model outputs and experimental Pclose results for surgical hyoid repositioning simulations from zero-baseline hyoid position. (A) Percent change in Pclose obtained from the model simulations and (B) from the experimental results of surgical hyoid repositioning procedures performed in anaesthetized rabbit studies. The hyoid was surgically displaced by 1 to 5mm in the cranial, anterior, caudal, anterior-cranial 45° and anterior-caudal 45° directions.

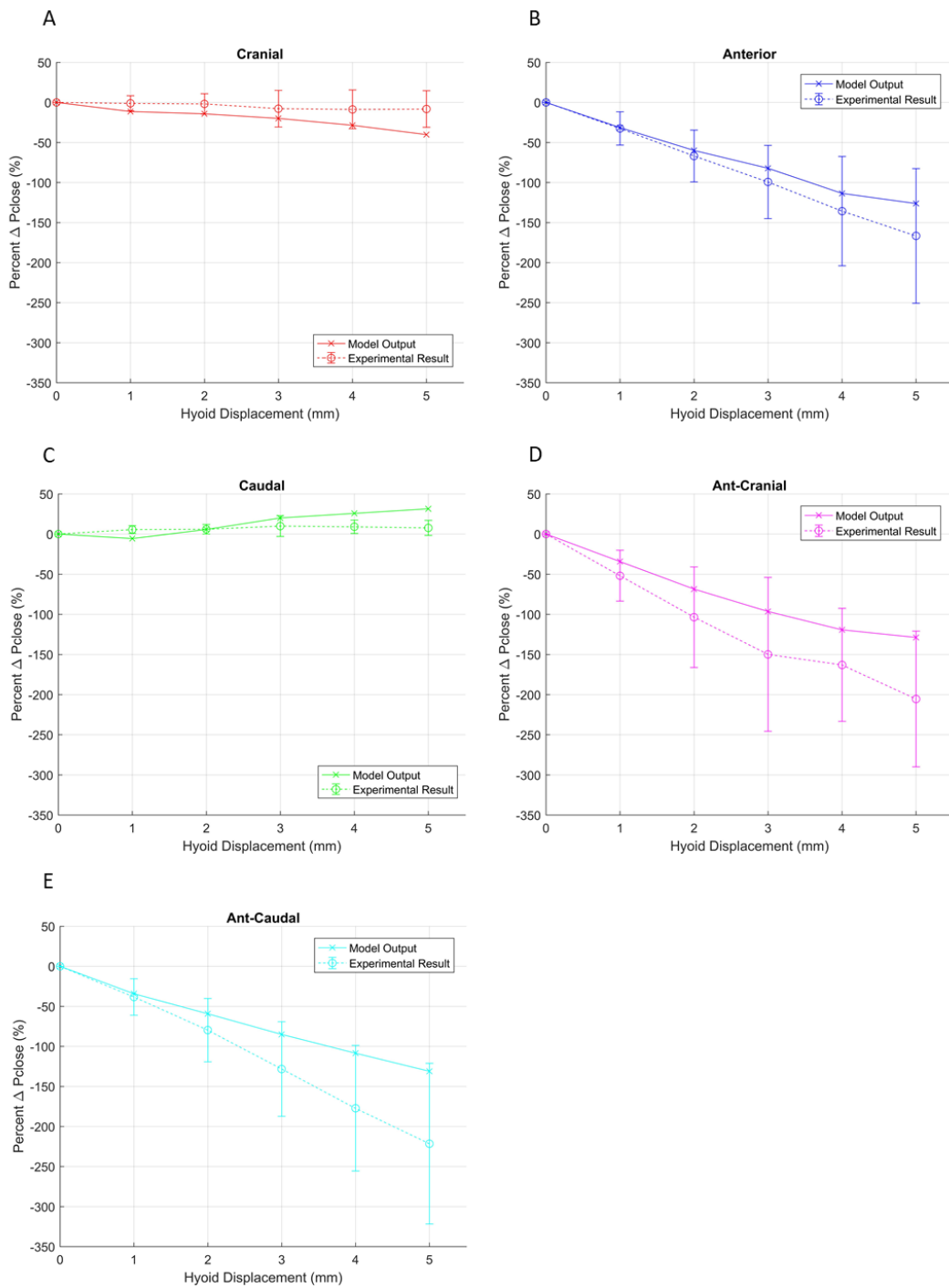


Figure 40: Plots of experimental results and simulation outputs of the percent change in Pclose produced by surgical hyoid repositioning. Hyoid is displaced by 1 to 5mm in the Cranial (A), Anterior (B), Caudal (C), Anterior-Cranial (D) and Anterior-Caudal (E) directions. The experimental results are plotted with the 95% confidence interval bars represented. All the model percent change in Pclose outputs are contained in the confidence interval of the experimental data except for the results of some increments of caudal and cranial hyoid repositioning simulations.

#### ***4.4.3 Tissue Displacement, Stress and Strain***

The resultant overall displacement, stress and strain distributions of the upper airway tissues are computed for select increments of surgical hyoid repositioning, 2 and 4mm, since they are considered to be similar to the magnitude of hyoid displacement induced in the clinically performed hyoid repositioning surgical procedures (as explained in Section 3.3.4).

##### **4.4.3.1 Influence of Hyoid Repositioning Load Magnitude**

Simulating different increments of surgical hyoid repositioning for each direction revealed that a larger increment leads to higher magnitudes of tissue displacement, stress and strain, while maintaining the same distribution across the soft tissues as demonstrated in Figure 41 to Figure 45.

##### **4.4.3.2 Influence of Hyoid Repositioning Load Direction**

Figure 46 shows the total tissue displacement contour maps for the higher increment (4mm) surgical hyoid repositioning in the five different directions. Generally, most of the soft tissue structures (tongue, soft palate, tissue mass, geniohyoid and mylohyoid surfaces) were deformed in response to hyoid repositioning with the largest movements being around the hyoid bone. The constrictor body and bony structures were however not displaced. Anterior, anterior-caudal and anterior-cranial hyoid displacements resulted in the highest deformation of the soft palate region behind the hyoid bone in the anterior direction, which visibly widened the airway lumen in that area. Movement of the entire tongue tissue, from its base to tip, is provoked with hyoid repositioning in all directions except the anterior direction. In fact, anterior hyoid

repositioning caused the translation of soft tissues in a smaller region concentrated around the hyoid bone with no movement produced in most of the tongue tissue and the soft palate portion located above that region. Caudal hyoid repositioning led to the accumulation of the soft tissues located below the hyoid bone and the posterior deformation of the soft palate which causes the narrowing of the airway lumen region behind the hyoid bone.

Similarly, the stress and strain produced in response to hyoid repositioning are mainly located at the base of the tongue, the soft palate and the tissue mass regions around the hyoid bone and are highest at the boundaries of the hyoid (see Figure 47 and Figure 48). A rise in stress and strain is also seen at the intersection between the soft tissues and the mandible. Anterior-cranial hyoid repositioning was found to produce larger stress and strain over a broad area of soft tissues extending from the soft palate region inferior to the hyoid bone to the boundary with the mandible including the tongue and, geniohyoid and mylohyoid area and tissue mass.

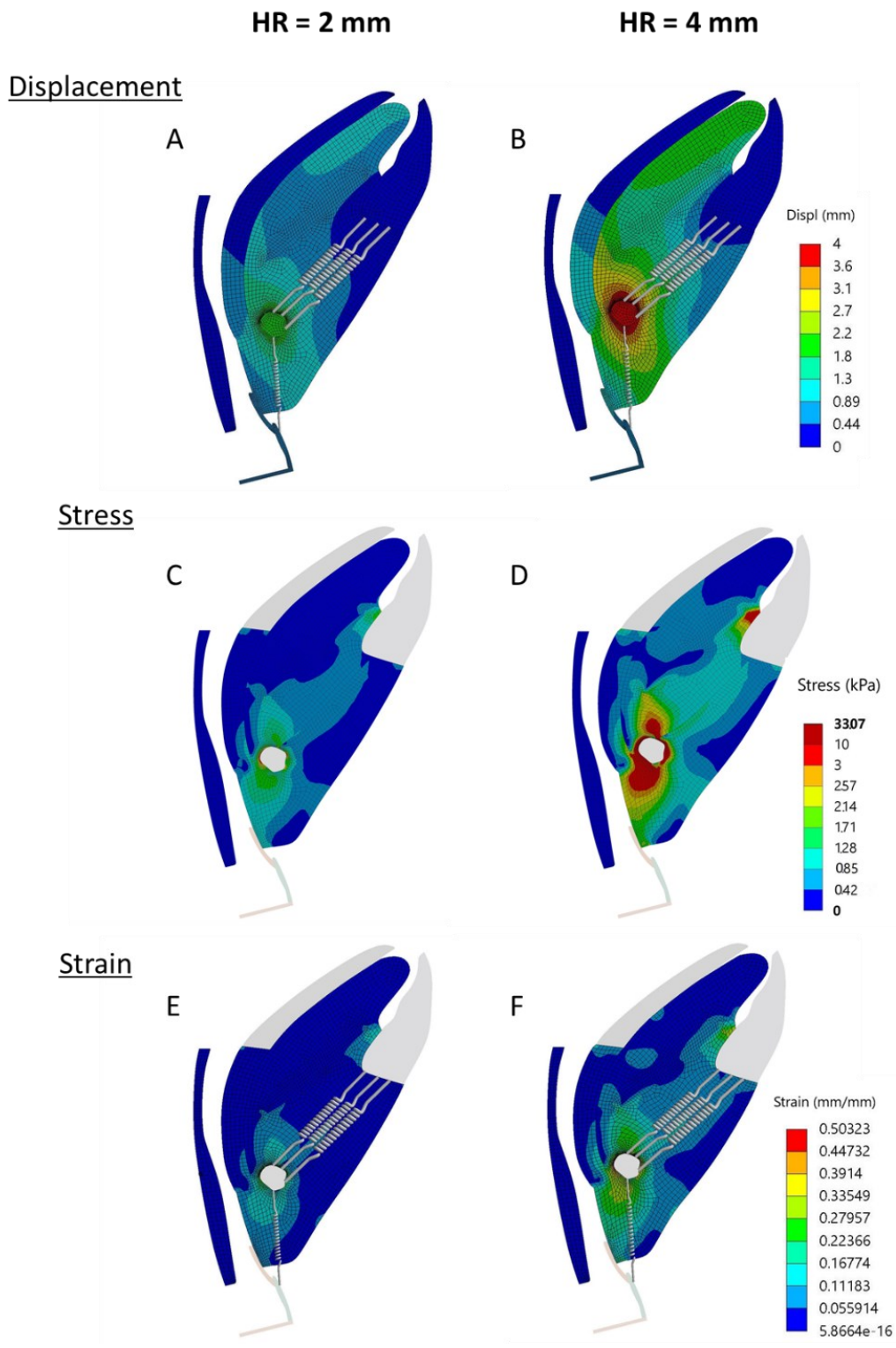


Figure 41: Tissue mechanics outcomes for **cranial surgical hyoid repositioning** simulations. Total displacement (A, B), stress (C, D) and strain (E, F) distributions are represented for 2mm (A, C, E) and 4mm (B, D, F) of surgical hyoid repositioning (HR) load. Note that only select spring-represented muscles (genioglossus, geniohyoid, mylohyoid and thyrohyoid) are shown in the figure and the rest are hidden to improve visibility of the simulation results.

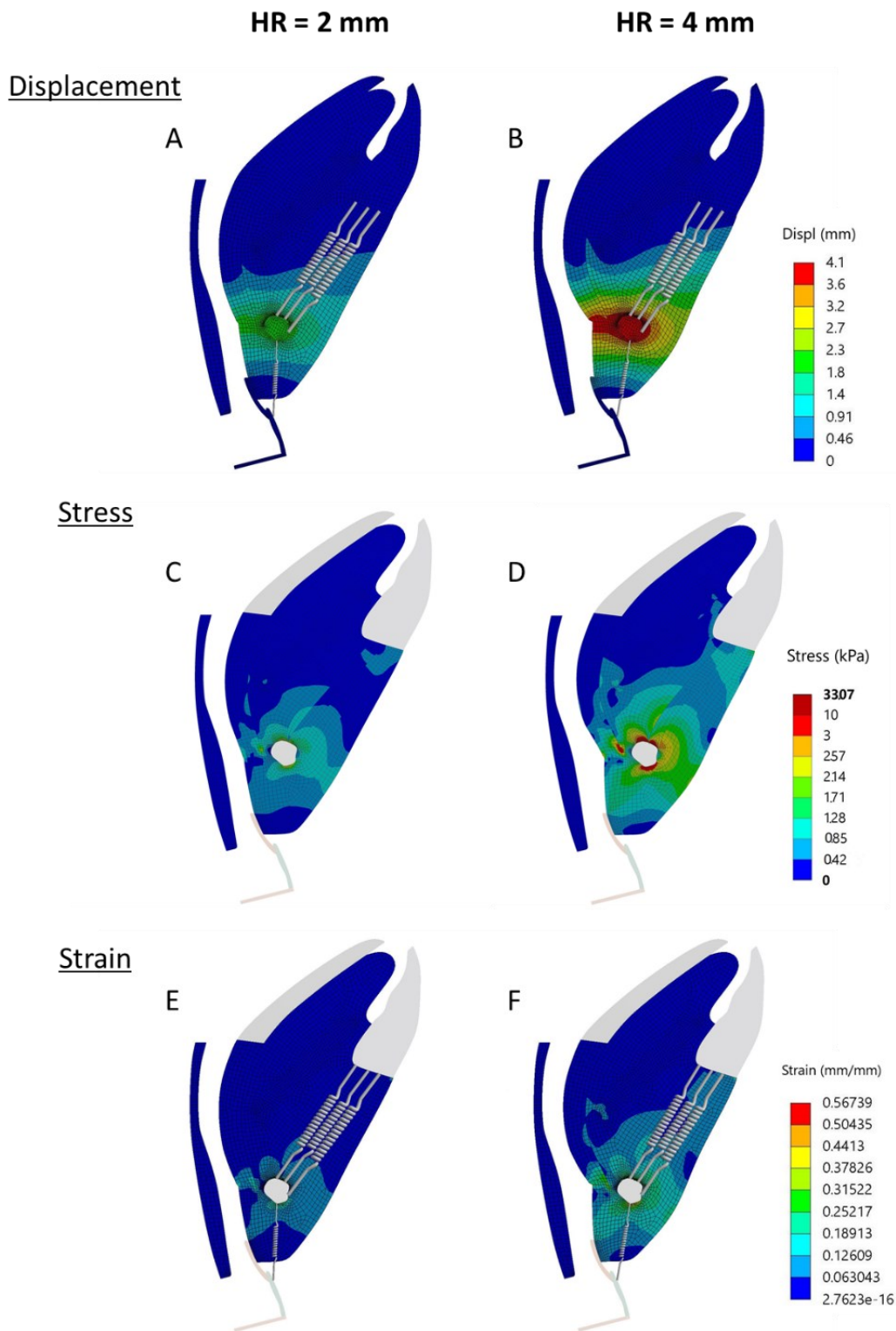


Figure 42: Tissue mechanics outcomes for **anterior surgical hyoid repositioning** simulations. Total displacement (A, B), stress (C, D) and strain (E, F) distributions are represented for 2mm (A, C, E) and 4mm (B, D, F) of surgical hyoid repositioning (HR) load. Note that only select spring-represented muscles (genioglossus, geniohyoid, mylohyoid and thyrohyoid) are shown in the figure and the rest are hidden to improve visibility of the simulation results.

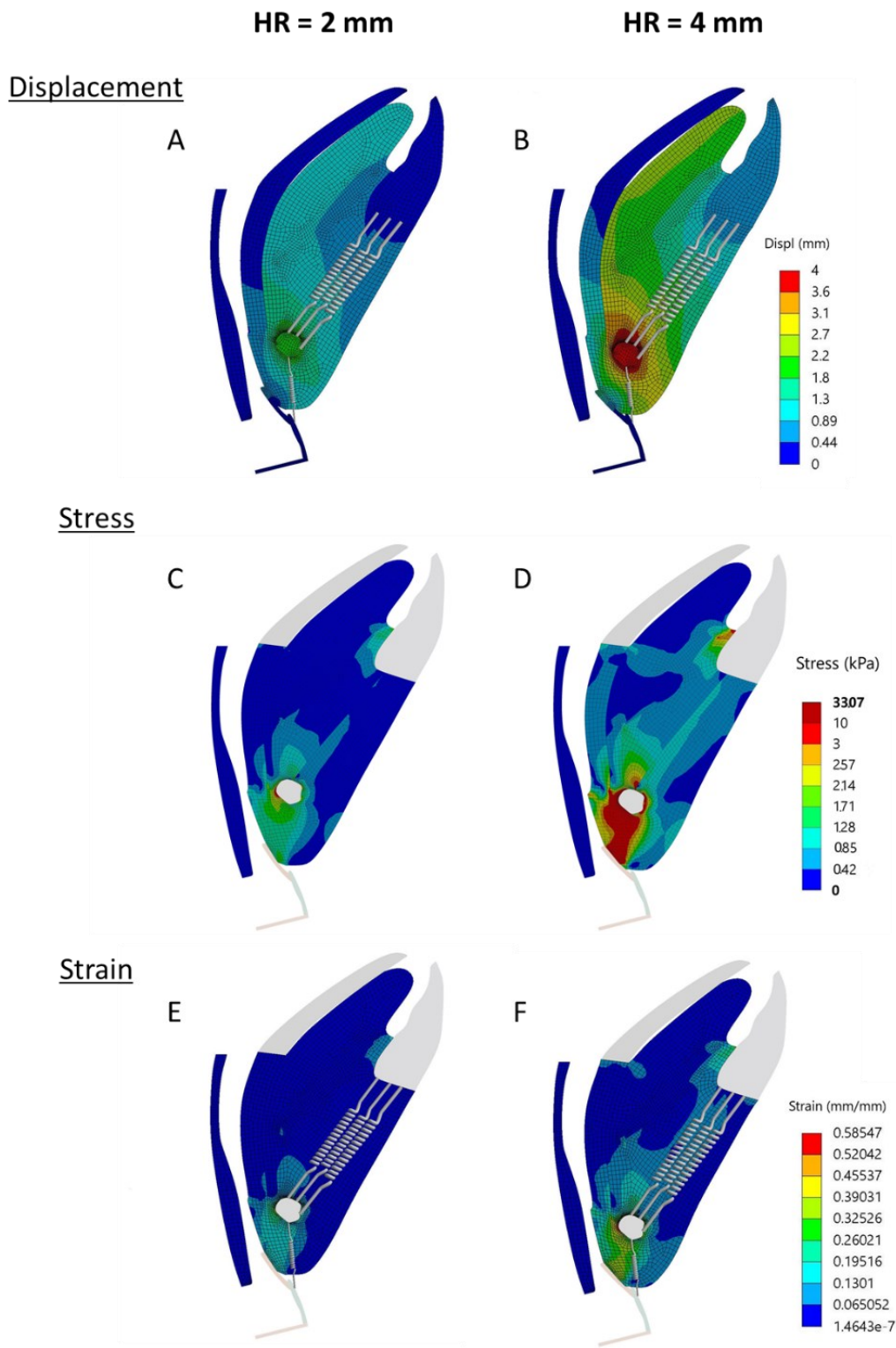


Figure 43: Tissue mechanics outcomes for **caudal surgical hyoid repositioning** simulations. Total displacement (A, B), stress (C, D) and strain (E, F) distributions are represented for 2mm (A, C, E) and 4mm (B, D, F) of surgical hyoid repositioning (HR) load. Note that only select spring-represented muscles (genioglossus, geniohyoid, mylohyoid and thyrohyoid) are shown in the figure and the rest are hidden to improve visibility of the simulation results.



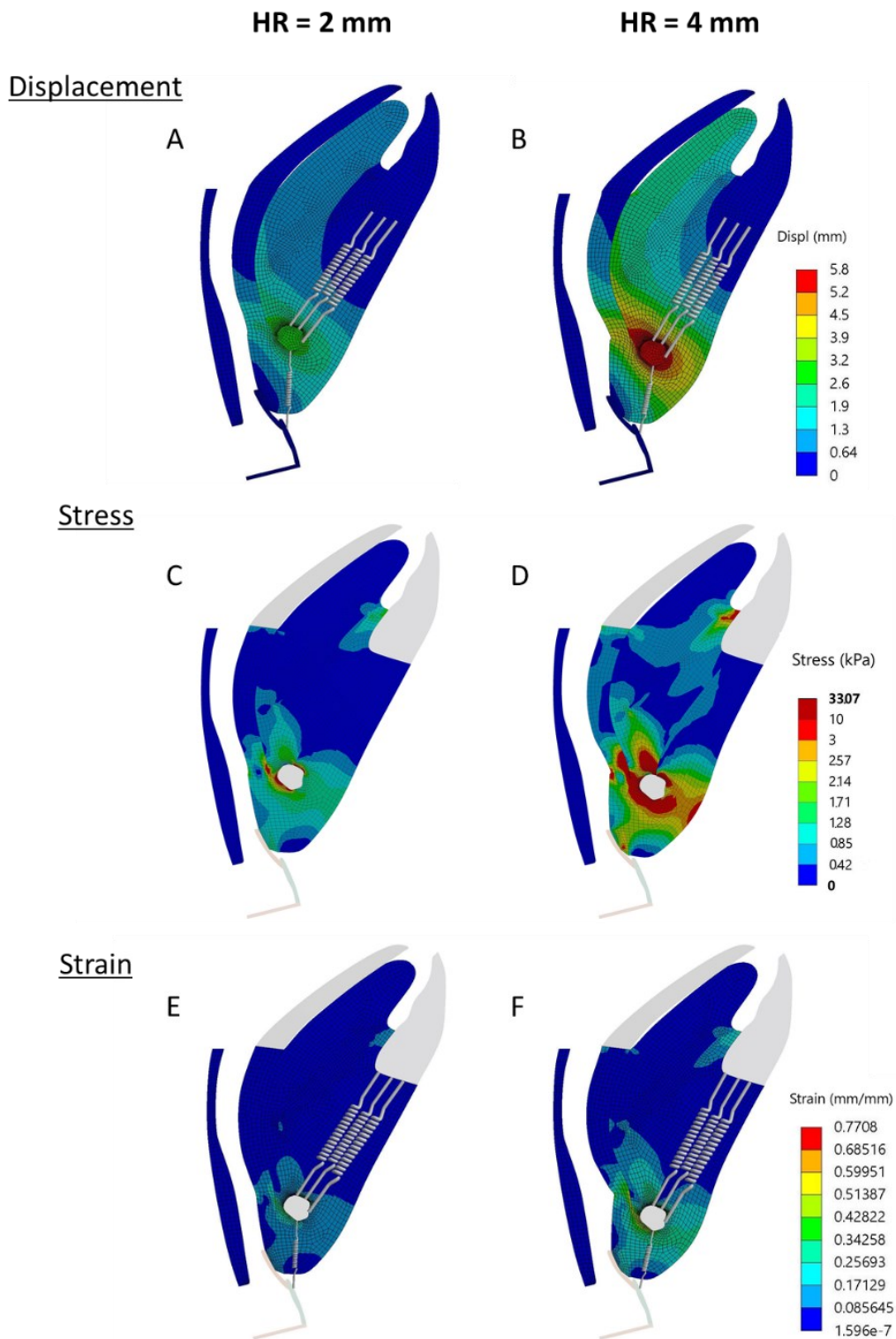


Figure 44: Tissue mechanics outcomes for **anterior-caudal surgical hyoid repositioning** simulations. Total displacement (A, B), stress (C, D) and strain (E, F) distributions are represented for 2mm (A, C, E) and 4mm (B, D, F) of surgical hyoid repositioning (HR) load. Note that only select spring-represented muscles (genioglossus, geniohyoid, mylohyoid and thyrohyoid) are shown in the figure and the rest are hidden to improve visibility of the simulation results.



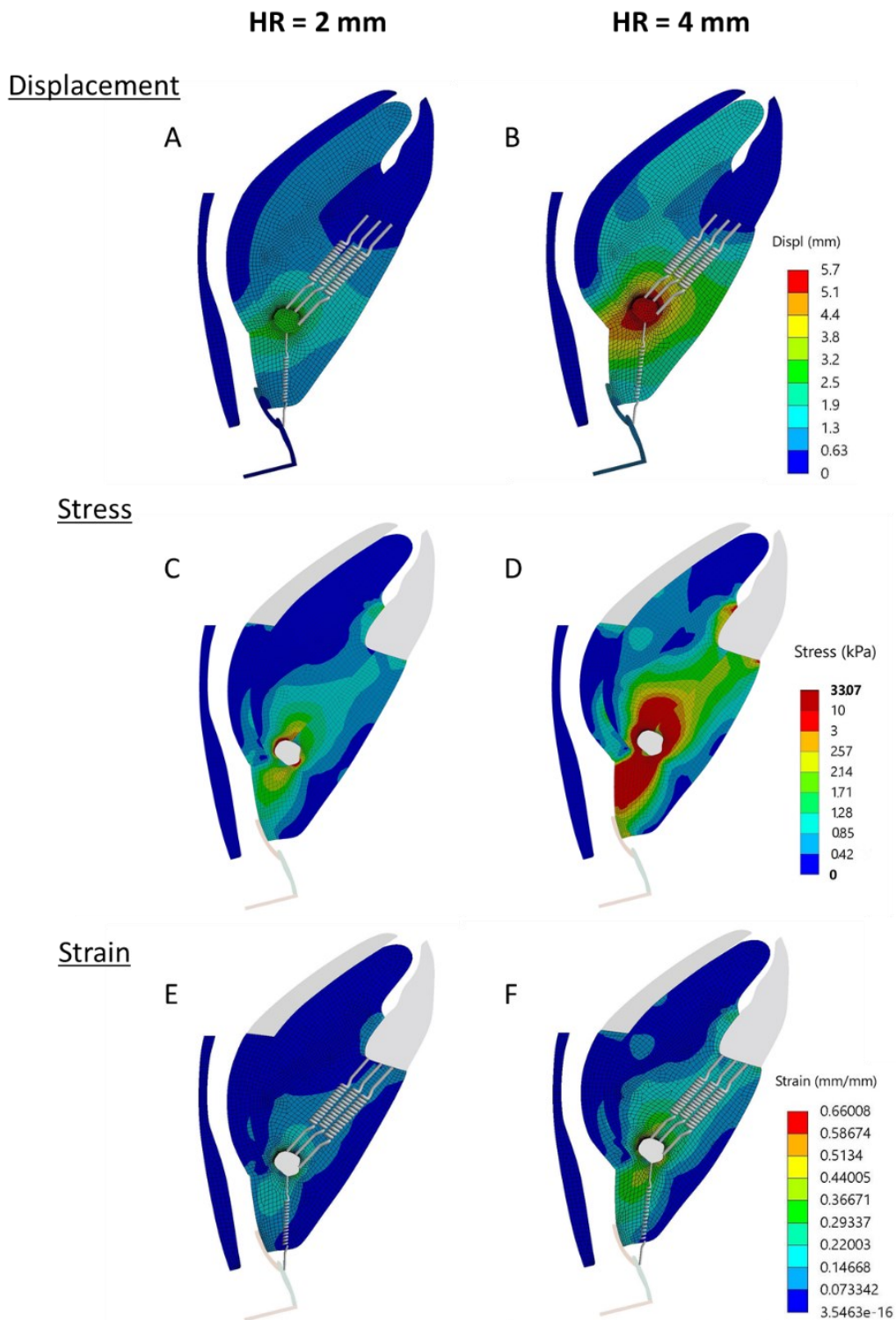


Figure 45: Tissue mechanics outcomes for **anterior-cranial surgical hyoid repositioning** simulations. Total displacement (A, B), stress (C, D) and strain (E, F) distributions are represented for 2mm (A, C, E) and 4mm (B, D, F) of surgical hyoid repositioning (HR) load. Note that only select spring-represented muscles (genioglossus, geniohyoid, mylohyoid and thyrohyoid) are shown in the figure and the rest are hidden to improve visibility of the simulation results.

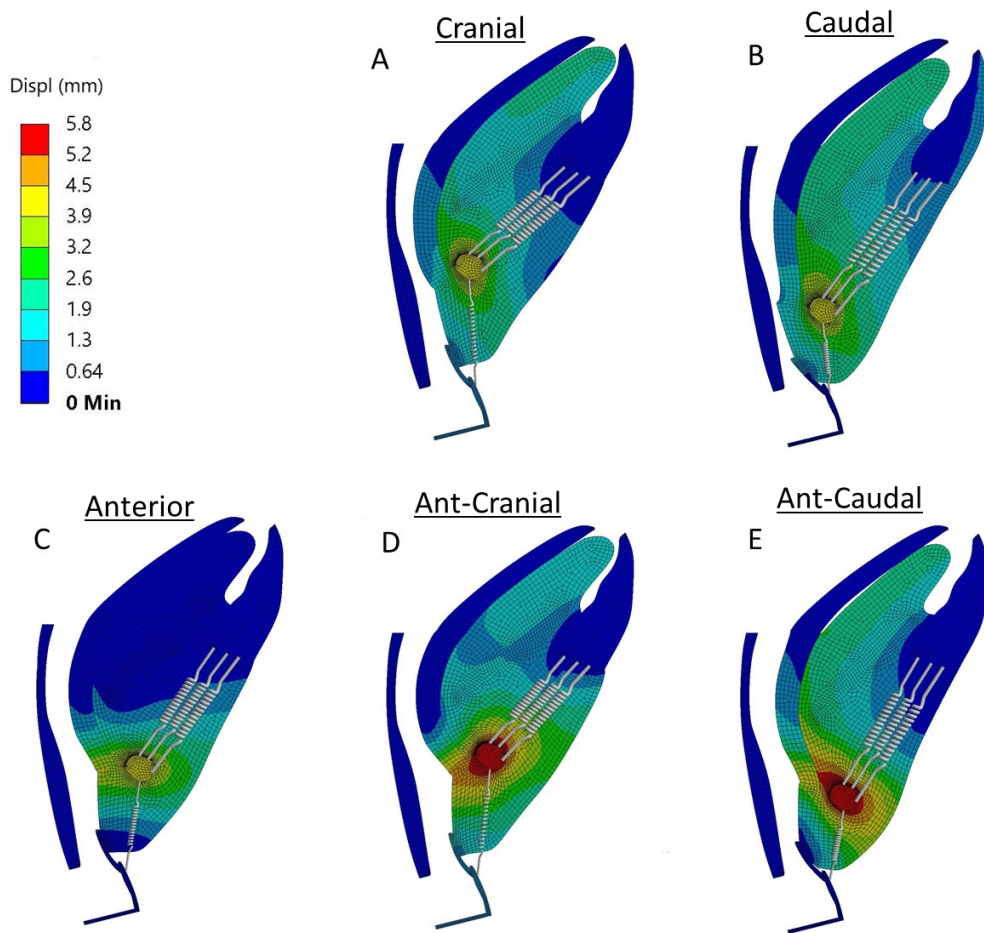


Figure 46: Total displacement of upper airway tissues vs. surgical hyoid repositioning load starting from the zero-baseline hyoid position. The resultant tissue displacement is represented as color-coded contours map shown on the deformed mesh for a selected surgical hyoid repositioning load of 4mm in the cranial (A), caudal (B) anterior (C), anterior-cranial (D) and anterior-caudal (E) directions. Note that only select spring-represented muscles (genioglossus, geniohyoid, mylohyoid and thyrohyoid) are shown in the figure and the rest are hidden to improve visibility of the simulation results.

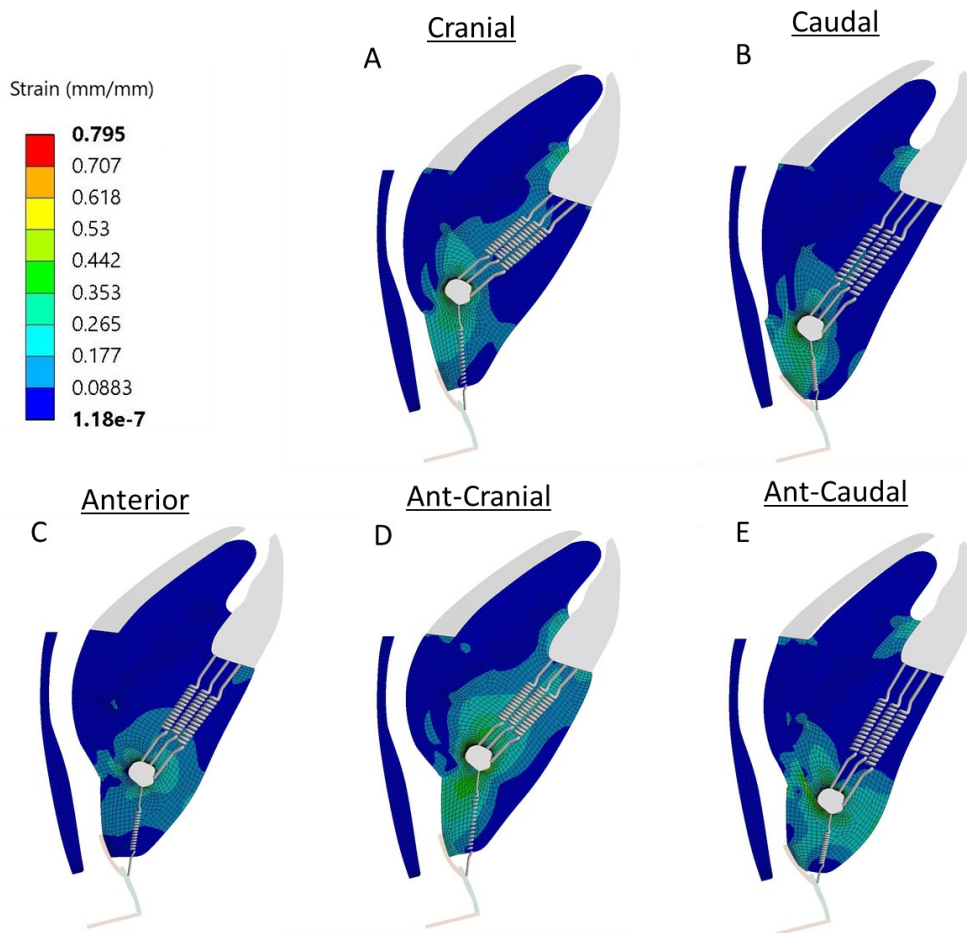


Figure 47: Equivalent (Von-Mises) strain distribution in the soft tissues vs. surgical hyoid repositioning load starting from the zero-baseline hyoid position. The strain is represented as color-coded contours map shown on the deformed mesh for a selected surgical hyoid repositioning load of 4mm in the cranial (A), caudal (B) anterior (C), anterior-cranial (D) and anterior-caudal (E) directions. Note that only select spring-represented muscles (genioglossus, geniohyoid, mylohyoid and thyrohyoid) are shown in the figure and the rest are hidden to improve visibility of the simulation results.

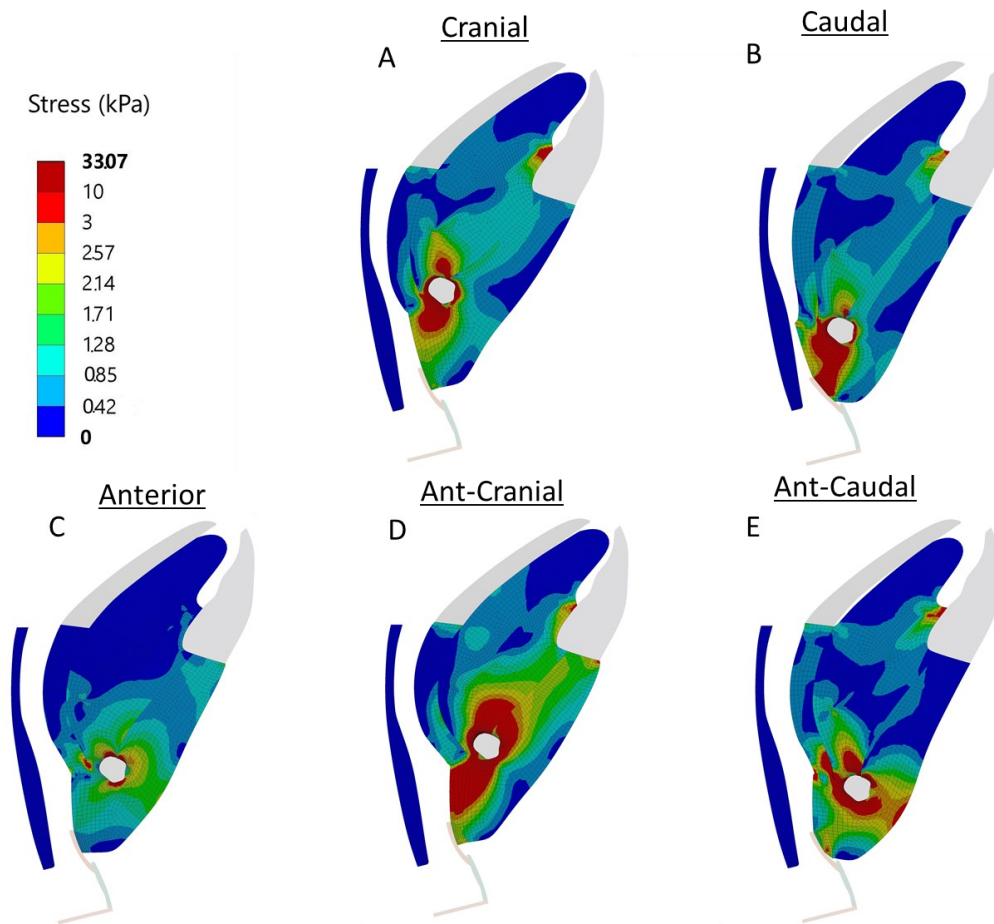


Figure 48: Equivalent (Von-Mises) stress distribution in the soft tissues vs. surgical hyoid repositioning load starting from the zero-baseline hyoid position. The stress is represented as color-coded contours map shown on the deformed mesh for a selected surgical hyoid repositioning load of 4mm in the cranial (A), caudal (B) anterior (C), anterior-cranial (D) and anterior-caudal (E) directions.

#### 4.4.4 Lumen Geometry Metrics

The percent changes in lumen geometry in response to the different increments and directions of surgical hyoid repositioning is represented in Figure 49. Anterior, anterior-caudal and anterior-cranial hyoid displacements of 4mm produced increases of 30 to 40% in the midsagittal cross-sectional area (CSA) of the airway lumen. The change in anteroposterior diameters (APD) indicates that the upper airway was mainly enlarged in region R2 (hyoid region) for these directions, with an increase in the APD

of region R2 of 140% for anterior-cranial, 100% for anterior and 85% for anterior-caudal hyoid repositioning simulations.

Cranial surgical hyoid repositioning led to a slight increase in the APD of region R2 and an equivalent decrease in the APD in region R1 (base of the tongue region) resulting in a negligible change in the lumen's CSA.

Finally, a relatively minor reduction in CSA (7%) was induced by a 4mm of caudal hyoid repositioning of 4mm accompanied predominantly by the narrowing of region R2.

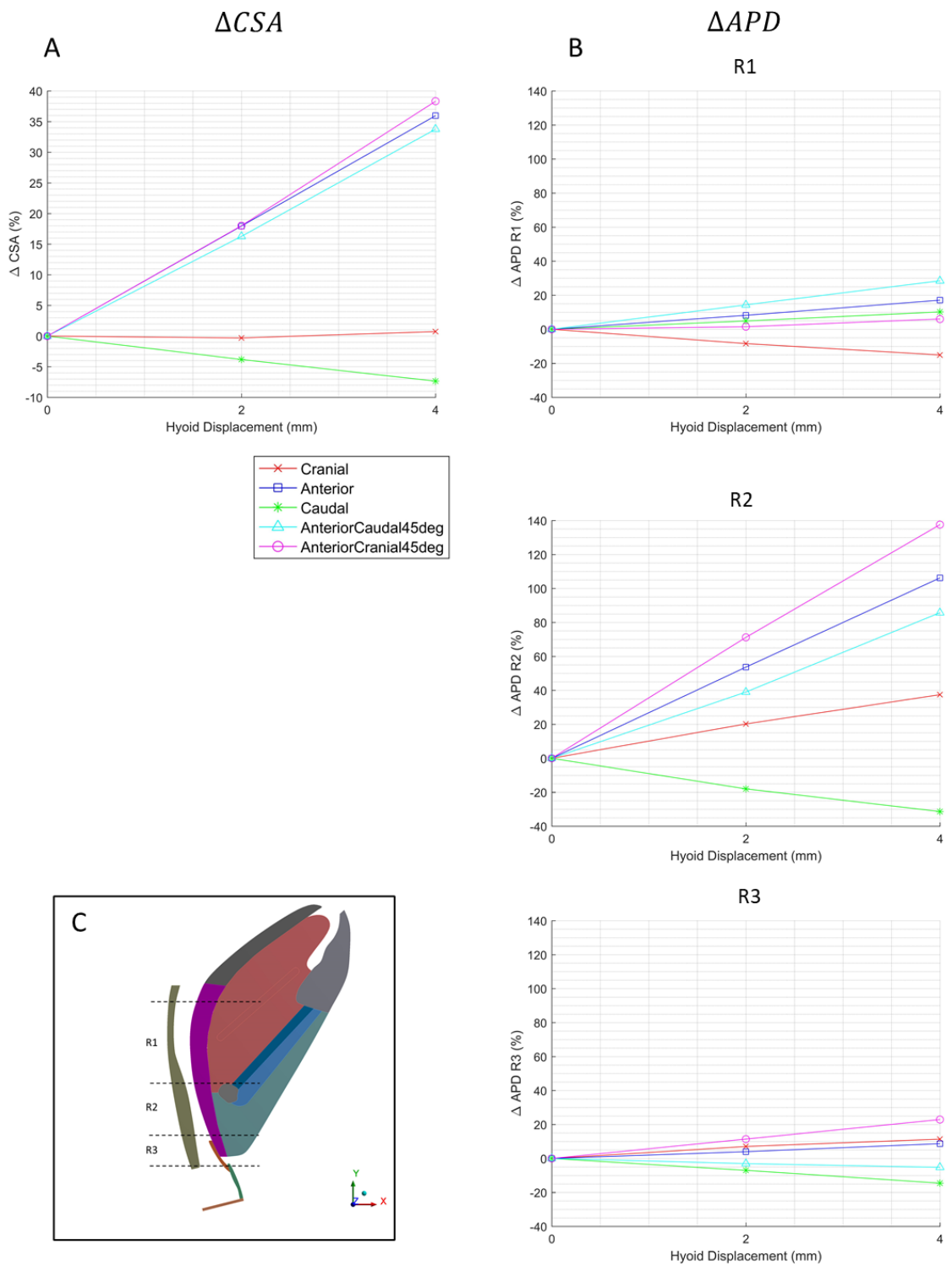


Figure 49: Upper airway lumen geometry changes in response to surgical hyoid repositioning from zero-baseline hyoid position. Percent change in upper airway lumen area (A) and anteroposterior diameters (B) with respect to the zero-baseline airway geometry for 2mm and 4mm of surgical hyoid repositioning in all directions.  $\Delta APD$  was represented as the average value calculated for each region (R1, R2 and R3). The undeformed model geometry with the region delimitations is shown for reference (C).



#### 4.4.5 Site of Collapse

The site at which the airway collapsed in response to intraluminal negative pressure simulation depended on the direction of surgical hyoid repositioning but not on the increment of hyoid displacement. When the hyoid is repositioned in the anterior, anterior-cranial and anterior-caudal direction, the site of collapse remained at the lower end of the tongue base region (region R1) at the boundary with the hyoid region (region R2) as it was the case for the collapse at the zero-baseline hyoid position (Section 4.2). The site of collapse was slightly shifted upwards, into the tongue base region, after applying cranial surgical hyoid repositioning and located respectively lower, at the middle of the hyoid region in the case of surgical hyoid repositioning in the caudal direction as illustrated in Figure 50.

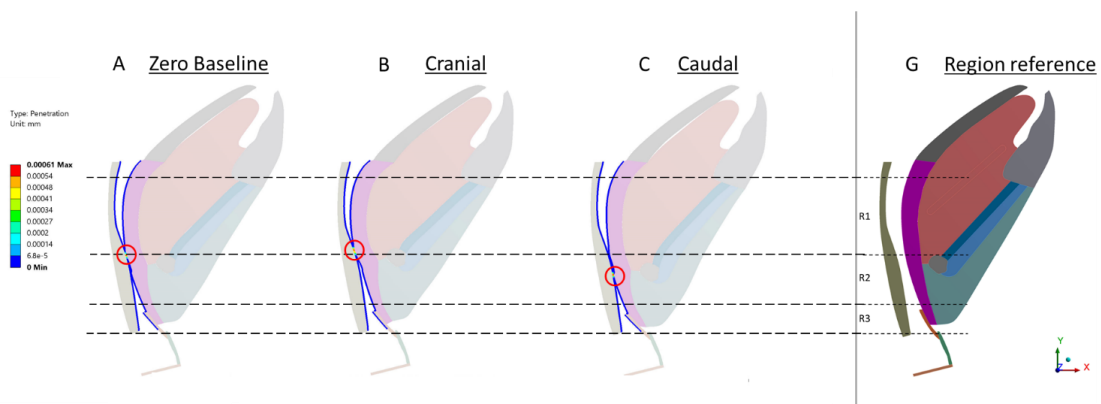


Figure 50: Contact penetration results showing sites of collapse after Pua simulations. Site of collapse at zero-baseline hyoid position (A), after cranial surgical repositioning by 2mm (B) and caudal surgical hyoid repositioning by 2mm (C) illustrated by airway wall contact penetration results. The sites of collapse are circled in red. The undeformed model geometry (G) is shown as a reference for extending the different region delimitations (R1, R2 and R3) to collapsed models.

## 4.5 Combined Influence of Baseline Hyoid Position and Surgical Hyoid Repositioning (Aim 3)

### 4.5.1 *Pclose*

#### 4.5.1.1 Patterns of Change in Pclose

Pclose results in this section are considered for shifts of hyoid baseline position in all directions but only by 2mm, approximate amount of change in hyoid position phenotype between healthy and OSA patients, and 4mm as discussed in Section 3.3.4. Figure 51 and Figure 52 illustrate the change in Pclose produced by all surgical hyoid repositioning simulations from the select hyoid baseline positions.

Overall, the model predicted the same patterns of change in Pclose as for the zero-baseline hyoid position when surgical hyoid repositioning loads were applied from different hyoid baseline positions. Anterior, ant-caudal and ant-cranial surgical repositioning directions still produced the largest decrease in Pclose for all hyoid baseline positions. Cranial surgical hyoid repositioning generally caused a small decrease in Pclose but led to an almost zero change in Pclose when applied from the caudal and anterior-caudal baseline positions. Moreover, a minor rise in Pclose is observed in response to caudal surgical hyoid repositioning except for the caudal and anterior-caudal baseline positions for which caudal hyoid repositioning induced a very small reduction in Pclose. Thus, the caudal and anterior-caudal baseline position simulations resulted in slightly different Pclose outputs as compared to the zero baseline hyoid position results.

As presented earlier in Section 4.3, shifting the hyoid baseline position led to an increase in Pclose with respect to the zero baseline Pclose ( $P_0$ ). This is illustrated in Figure 52 and Figure 52 by the vertical shift in the Pclose plots: each different baseline



position plot starts from its corresponding baseline  $P_{close}$  value (Table 8), which is higher than  $P_0$  in all cases. We also establish in Section 4.3 that the change in  $P_{close}$  increases linearly with the increment of hyoid baseline shift. This is represented here by a larger vertical shift in the  $P_{close}$  plots for a 4mm hyoid baseline position increment (Figure 52) as compared to the 2mm increment (Figure 51). Therefore, depending on the model's baseline hyoid position, the application of a certain increment of hyoid displacement load (surgical repositioning) in a particular direction decreased  $P_{close}$  back to a value equal to or less than  $P_0$ .

#### 4.5.1.2 Impact on Effectiveness of Surgical Hyoid Repositioning

The change in  $P_{close}$  produced by the same surgical hyoid repositioning simulation but from different hyoid baseline positions is presented in Figure 53 to examine the effect that the hyoid baseline position shift has on the effectiveness of surgical hyoid repositioning. Anterior-cranial and anterior-caudal surgical hyoid repositioning simulations with 2mm increment were examined since they represent the clinically performed hyoid suspension procedures (See Section 3.3.4). The 4mm increments of hyoid repositioning in these directions (not illustrated in Figure 53) showed similar results. Note that the change in  $P_{close}$  ( $\Delta P_{close}$ ) was calculated as the change from the baseline  $P_{close}$  of the respective baseline position here to only take into account the influence of hyoid repositioning alone on  $P_{close}$  and not the change in baseline position ( $P_{close}$  values for the different hyoid baseline positions as summarized in Table 8). The model predicted that the impact of hyoid baseline position change depends on the direction of the baseline shift.

When the hyoid baseline position is more caudal, the same surgical hyoid repositioning simulation (same direction and same increment) produces less change in  $P_{close}$  than the one produced from the zero-baseline position. More specifically, an anterior-cranial hyoid repositioning of 2mm decreased  $P_{close}$  by ~70% for the zero-baseline hyoid position. However, for a more caudally positioned hyoid bone by 2mm and 4mm, only a 56% and 43% decrease in  $P_{close}$  was produced by the same hyoid repositioning simulation (anterior-cranial with 2mm increment), respectively. Thus, the anterior-cranial surgical hyoid repositioning intervention produced less change in  $P_{close}$  meaning that it is less effective when the hyoid baseline position was more caudal. Similarly, anterior-caudal hyoid repositioning of 2mm led to a less important decrease in  $P_{close}$  by ~10% when the hyoid baseline position was shifted caudally by 4mm compared to the zero-baseline hyoid position.

On the contrary, shifting the hyoid baseline position in the anterior directions by 2mm and 4mm improved the decrease in  $P_{close}$  produced by anterior-cranial hyoid repositioning of 2mm reaching respectively 83% and 105% decrease in  $P_{close}$  as compared to only 67% decrease in  $P_{close}$  for the zero-baseline hyoid position. Similarly, the reduction in  $P_{close}$  in response to anterior-caudal hyoid repositioning of 2mm was improved when the hyoid baseline position was more anterior.

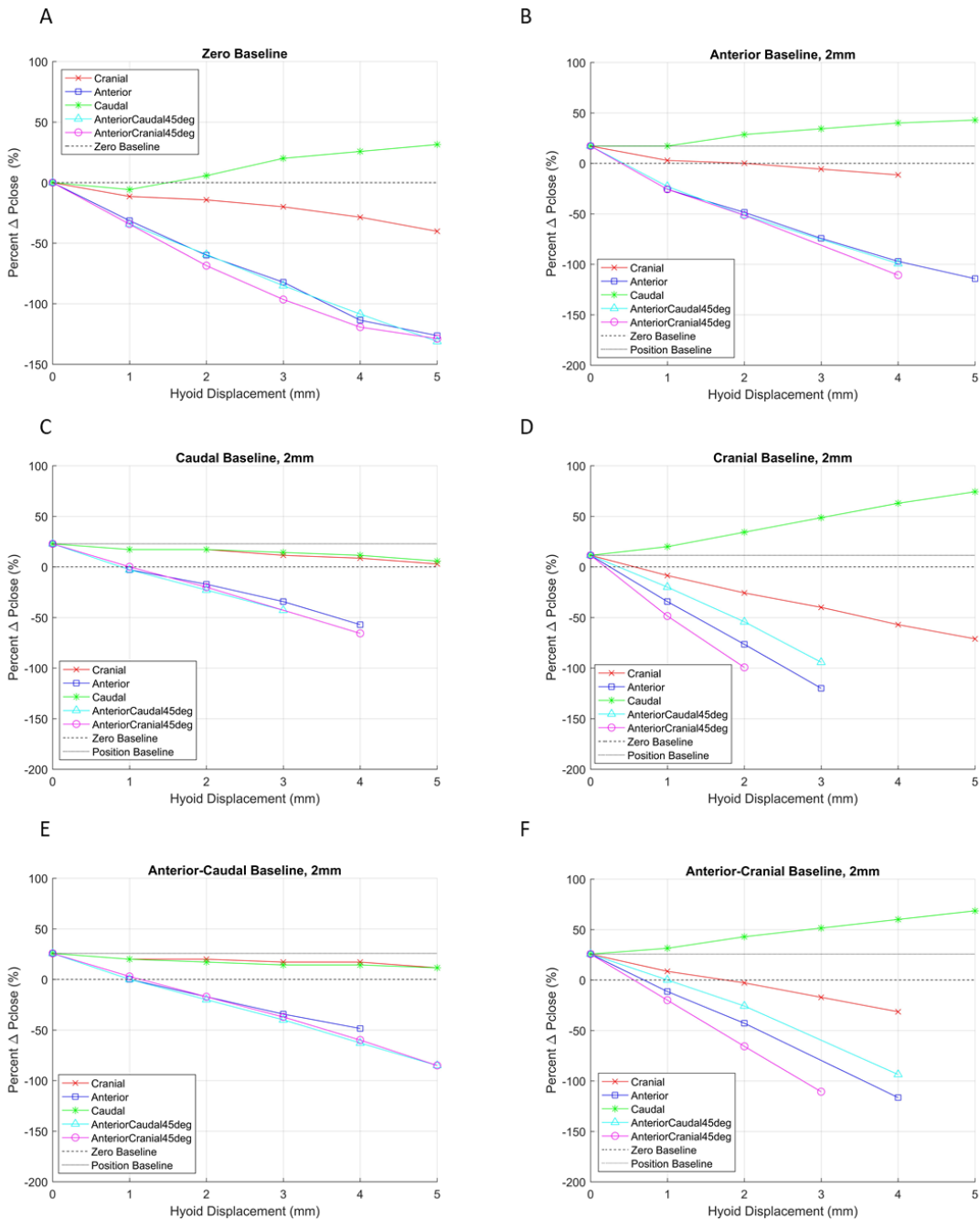


Figure 51: Change in  $P_{close}$  ( $\Delta P_{close}$  %, with respect to  $P_0$ ) produced by surgical hyoid repositioning simulations after a 2mm relocation of the baseline hyoid position. Results for the original zero-baseline hyoid position (A) and a baseline hyoid position shifted by 2mm in the anterior (B), caudal (C), cranial (D), anterior-caudal (E), and anterior-cranial (F) directions. Each plot includes the results for hyoid repositioning load simulations of 1 to 5mm increments in all 5 directions. The ‘Zero Baseline’ dashed line represents  $P_0$  and the ‘Current Baseline Position’ grey line denotes the change between  $P_0$  and the baseline  $P_{close}$  value of the corresponding hyoid baseline position (values found in Table 8). Note: The results of some hyoid displacement increments are missing either because the intraluminal negative pressure simulation did not produce airway closure for the applied pressure or the finite element solution failed to converge.

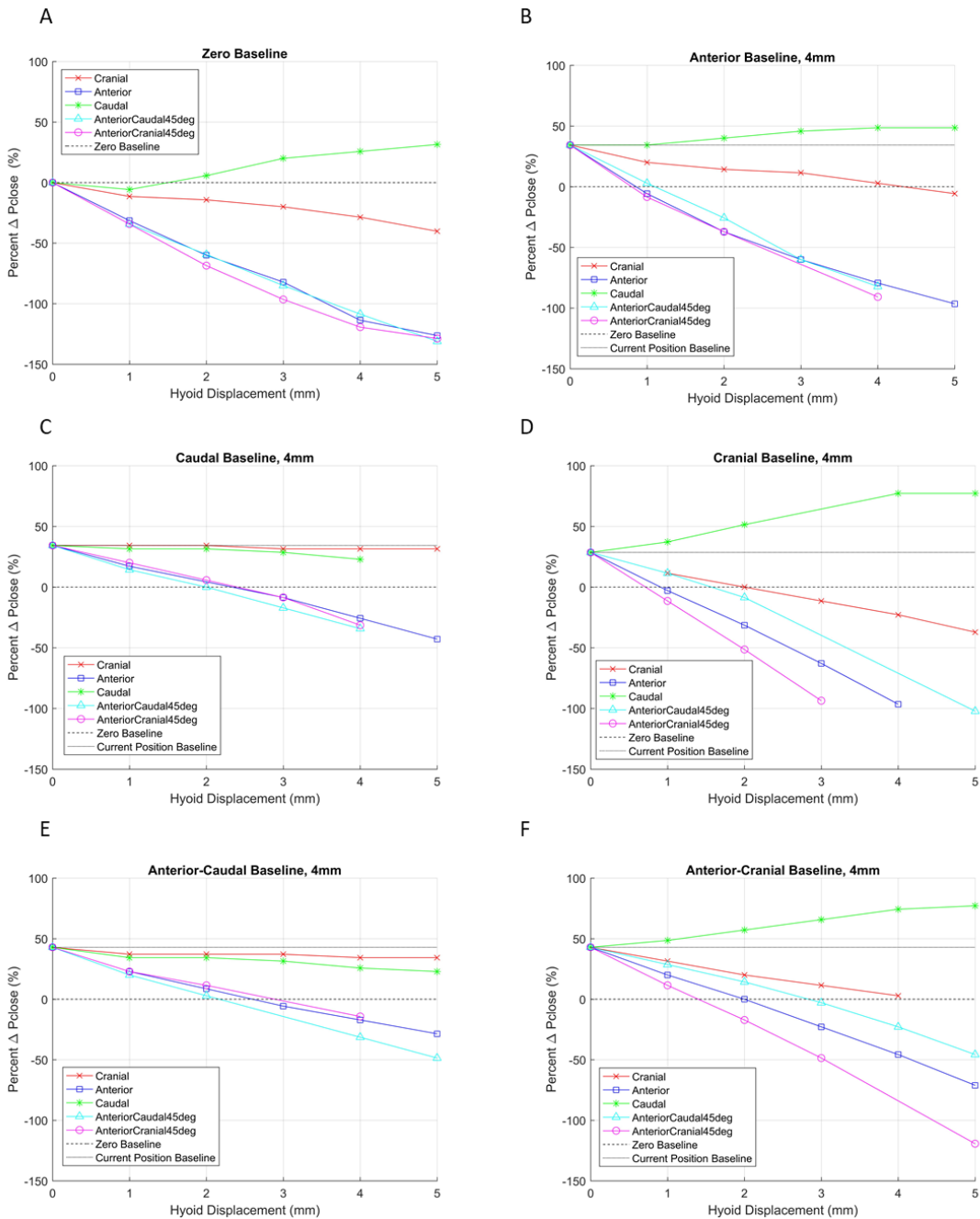


Figure 52: Change in  $P_{close}$  ( $\Delta P_{close}$  %, with respect to  $P_0$ ) produced by surgical hyoid repositioning simulations after a 4mm relocation of the baseline hyoid position. Results for the original zero-baseline hyoid position (A) and a baseline hyoid position shifted by 4mm in the anterior (B), caudal (C), cranial (D), anterior-caudal (E), and anterior-cranial (F) directions. Each plot includes the results for hyoid repositioning load simulation of 1 to 5mm increments in all 5 directions. The ‘Zero Baseline’ dashed line represents  $P_0$  and the ‘Current Baseline Position’ grey line denotes the change between  $P_0$  and the baseline  $P_{close}$  value of the corresponding hyoid baseline position (values found in Table 8). Note: The results of some hyoid displacement increments are missing either because the intraluminal negative pressure simulation did not produce airway closure for the applied pressure or the finite element solution failed to converge.

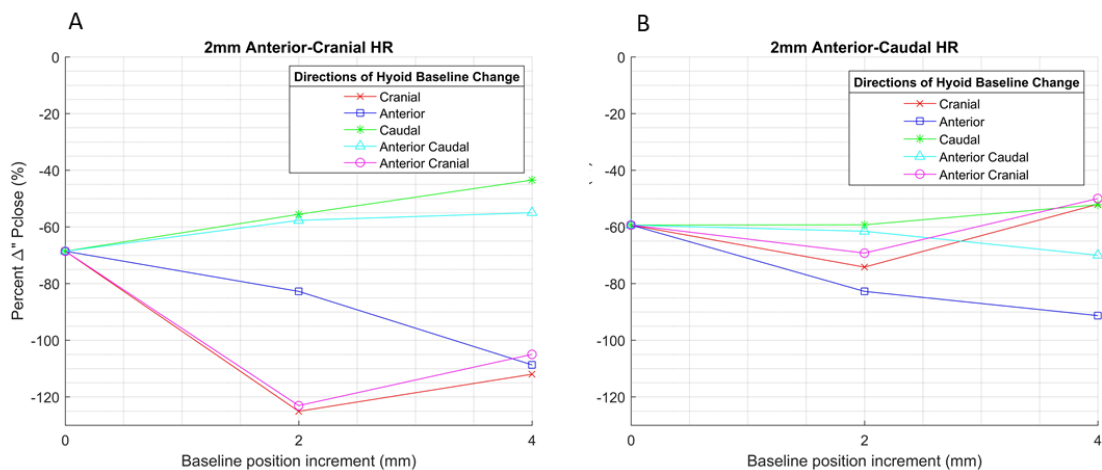


Figure 53: Plots showing the effect of the hyoid baseline position modification on the effectiveness of 2mm surgical hyoid repositioning (HR) in the (A) anterior-cranial and (B) anterior-caudal directions. Anterior-cranial and anterior-caudal surgical hyoid repositioning represent hyomandibular suspension and hyothyroidopexy surgical procedures, respectively. Each plot shows the change in Pclose produced when the hyoid baseline position was modified by 0, 2 and 4mm in the cranial, anterior, caudal, anterior-cranial and anterior-caudal directions. The change in Pclose is calculated for each different hyoid baseline position with respect to its current baseline position Pclose value (found in Table 8) to exclude the effect of the baseline position modification on Pclose.

#### 4.5.2 Tissue Displacement, Stress and Strain

Tissue displacement, stress and strain results are shown only for a shift in caudal hyoid baseline position, as is the case with OSA, and for anterior-cranial and anterior-caudal hyoid displacement loads, representing current clinical hyoid surgical treatments. This was discussed in Section 3.3.4.

The tissue displacement, stress and strain distributions resulting from the hyoid repositioning simulations are very similar for the models with a caudal hyoid baseline position and the zero baseline positions. Figure 54, Figure 55 and Figure 56 present the results for a caudal hyoid baseline position with 2mm baseline increment and Figure

57, Figure 58 and Figure 59 the results for the caudal hyoid position with 4mm increment. The results for the 4mm increment of caudal baseline position shift had relatively the same patterns as the 2mm increment but with increased magnitudes.

The resultant tissue displacement contours indicate that anterior-caudal and anterior-cranial surgical hyoid repositioning caused much larger soft tissue movements than cranial surgical hyoid repositioning. Similarly, the soft tissue stress and strain results are the lowest for the cranial surgical hyoid repositioning simulations.

Anterior-cranial surgical hyoid repositioning produced the largest amount of displacement in the soft palate, directly behind the hyoid bone. However, a larger portion of the soft palate was deformed and larger movements in the tongue were induced by anterior-caudal hyoid repositioning.

The strain resulting from anterior-cranial surgical hyoid repositioning were distributed over a larger portion of the soft tissues while the strain produced by anterior-caudal hyoid repositioning was more concentrated in the region around the hyoid bone. Moreover, larger strains were observed in the soft palate when an anterior-cranial hyoid repositioning load was applied (see Figure 55).

Finally, the stresses generated from the anterior-caudal hyoid repositioning were larger overall and were mainly located in the soft tissue mass below the hyoid bone and at the anterior edge of the soft palate where it is in contact with the tongue. Anterior-cranial hyoid repositioning led to higher stresses at the boundary between the tongue and the hyoid bone and produced larger stresses in the lower soft palate region behind the hyoid bone.

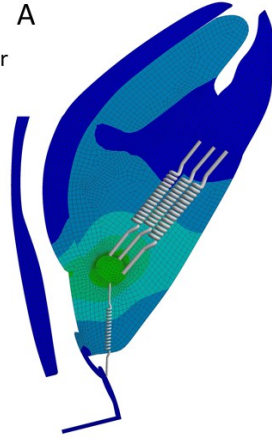
### Caudal Hyoid Baseline Position, 2mm

HR= 2mm

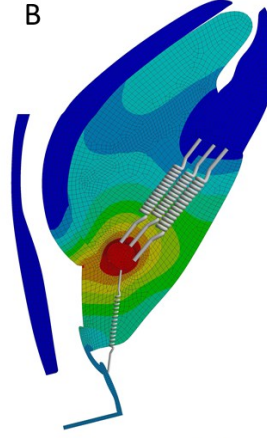
HR= 4mm

#### Ant-Cranial A

( Hyomandibular suspension )

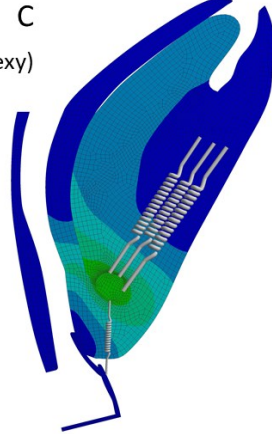


#### B



#### Ant-Caudal C

( Hyothyroidopexy )



#### D

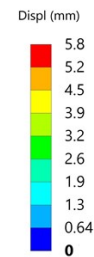
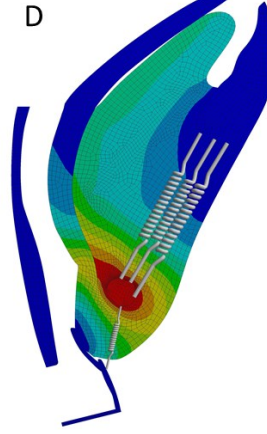


Figure 54: Total displacement of upper airway tissues as a result of surgical hyoid repositioning (HR) starting from a 2mm caudal hyoid baseline position. Displacement results are shown for anterior-cranial (A, B) and anterior-caudal (C, D) hyoid repositioning simulations. The tissue displacement is represented as a color-coded contours map shown on the deformed mesh for a hyoid repositioning increment of 2mm (A, C) and 4mm (B, D). Anterior-cranial and anterior-caudal surgical hyoid repositioning represent hyomandibular suspension and hyothyroidopexy surgical procedures, respectively. Note that only select spring-represented muscles (genioglossus, geniohyoid, mylohyoid and thyrohyoid) are shown in the figure and the rest are hidden to improve visibility of the simulation results.

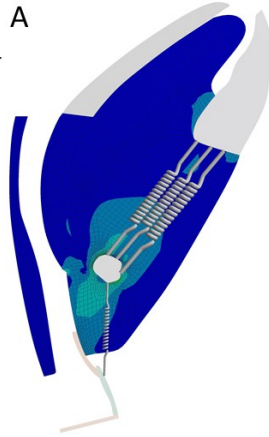
### Caudal Hyoid Baseline Position, 2mm

HR= 2mm

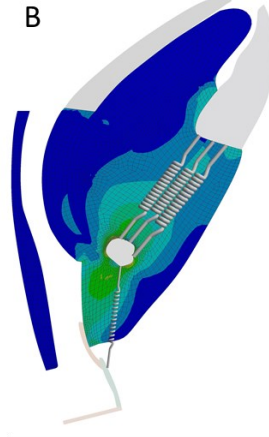
HR= 4mm

#### Ant-Cranial A

( Hyomandibular suspension )

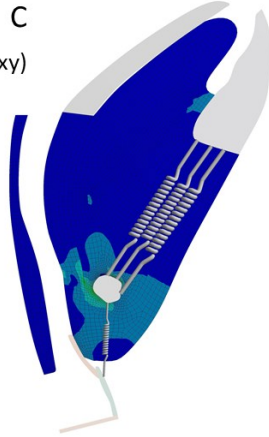


#### B

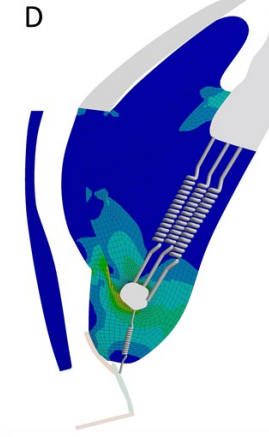


#### Ant-Caudal C

( Hyothyroidopexy )



#### D



Strain (mm/mm)

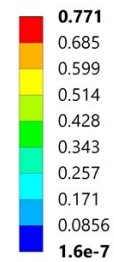


Figure 55: Equivalent (Von-Mises) strain distribution in the soft tissues as a result of surgical hyoid repositioning (HR) starting from a 2mm caudal hyoid baseline position. Strain results are shown for anterior-cranial (A, B) and anterior-caudal (C, D) hyoid repositioning simulations. The strain is represented as a color-coded contours map shown on the deformed mesh for a hyoid repositioning increment of 2mm (A, C) and 4mm (B, D). Anterior-cranial and anterior-caudal surgical hyoid repositioning represent hyomandibular suspension and hyothyroidopexy surgical procedures, respectively. Note that only select spring-represented muscles (genioglossus, geniohyoid, mylohyoid and thyrohyoid) are shown in the figure and the rest are hidden to improve visibility of the simulation results.

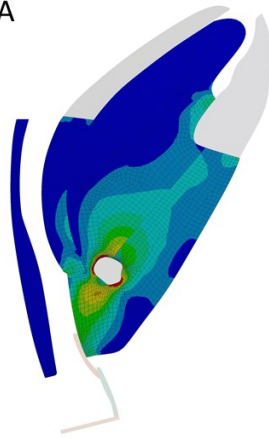


**Caudal Hyoid Baseline Position, 2mm**

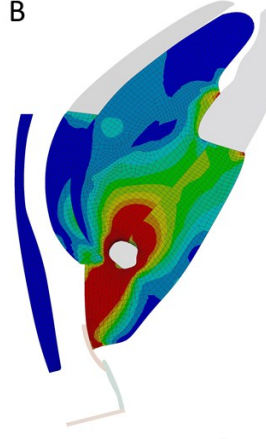
HR= 2mm

HR= 4mm

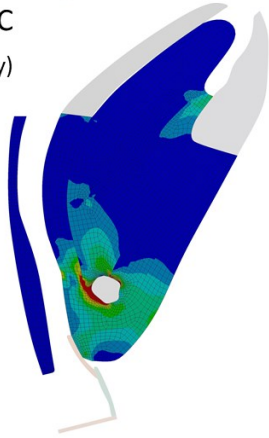
**Ant-Cranial** A  
( Hyomandibular  
suspension )



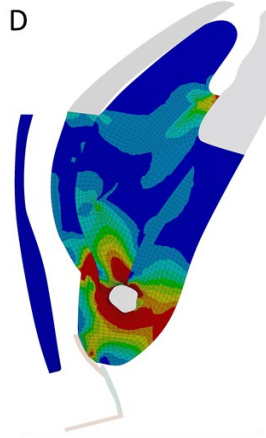
B



**Ant-Caudal** C  
( Hyothyroidopexy )



D



Stress (kPa)

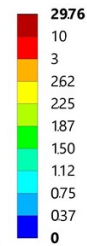


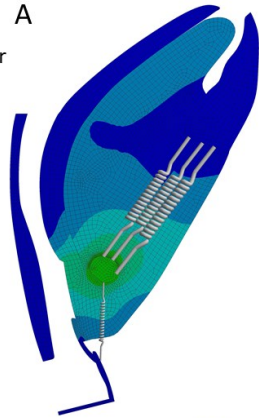
Figure 56: Equivalent (Von-Mises) stress distribution in the soft tissues as a result of surgical hyoid repositioning (HR) starting from a 2mm caudal hyoid baseline position. Stress results are shown for anterior-cranial (A, B) and anterior-caudal (C, D) hyoid repositioning simulations. The stress is represented as a color-coded contours map shown on the deformed mesh for a hyoid repositioning increment of 2mm (A, C) and 4mm (B, D). Anterior-cranial and anterior-caudal surgical hyoid repositioning represent hyomandibular suspension and hyothyroidopexy surgical procedures, respectively.

### Caudal Hyoid Baseline Position, 4 mm

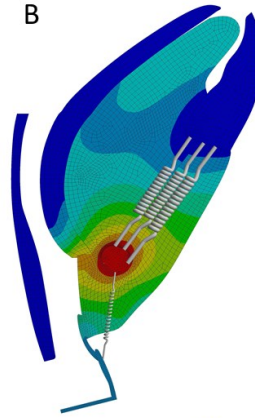
HR= 2mm

HR= 4mm

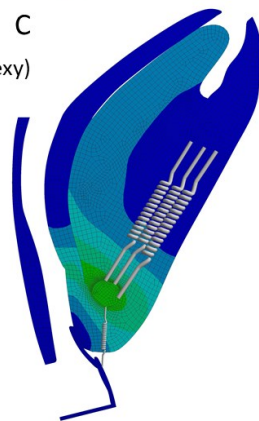
**Ant-Cranial** A  
( Hyomandibular  
suspension )



B



**Ant-Caudal** C  
( Hyothyroidopexy )



D

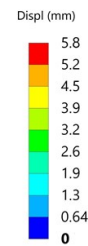
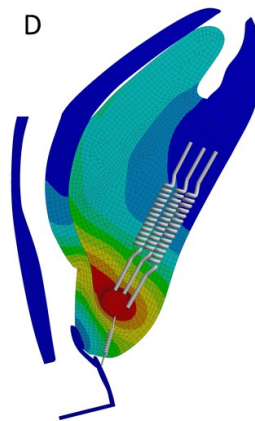


Figure 57: Total displacement of upper airway tissues as a result of surgical hyoid repositioning (HR) starting from a 4mm caudal hyoid baseline position. Displacement results are shown for anterior-cranial (A, B) and anterior-caudal (C, D) hyoid repositioning simulations. The tissue displacement is represented as a color-coded contours map shown on the deformed mesh for a hyoid repositioning increment of 2mm (A, C) and 4mm (B, D). Anterior-cranial and anterior-caudal surgical hyoid repositioning represent hyomandibular suspension and hyothyroidopexy surgical procedures, respectively. Note that only select spring-represented muscles (genioglossus, geniohyoid, mylohyoid and thyrohyoid) are shown in the figure and the rest are hidden to improve visibility of the simulation results.

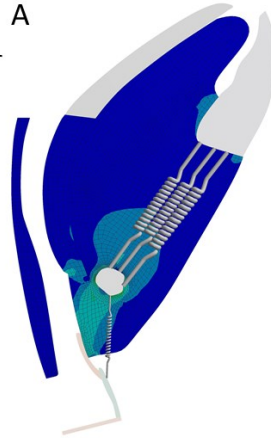
### Caudal Hyoid Baseline Position, 4 mm

HR= 2mm

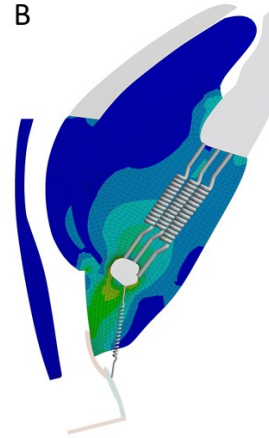
HR= 4mm

#### Ant-Cranial A

( Hyomandibular suspension )

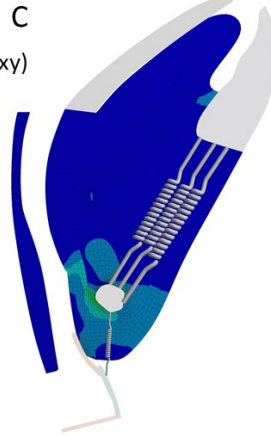


#### B

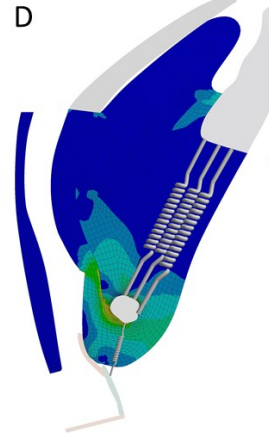


#### Ant-Caudal C

( Hyothyroidopexy )



#### D



Strain (mm/mm)

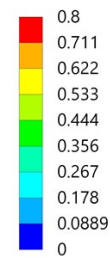


Figure 58: Equivalent (Von-Mises) strain distribution in the soft tissues as a result of surgical hyoid repositioning (HR) starting from a 4mm caudal hyoid baseline position. Strain results are shown for anterior-cranial (A, B) and anterior-caudal (C, D) hyoid repositioning simulations. The strain is represented as a color-coded contours map shown on the deformed mesh for a hyoid repositioning increment of 2mm (A, C) and 4mm (B, D). Anterior-cranial and anterior-caudal surgical hyoid repositioning represent hyomandibular suspension and hyothyroidopexy surgical procedures, respectively. Note that only select spring-represented muscles (genioglossus, geniohyoid, mylohyoid and thyrohyoid) are shown in the figure and the rest are hidden to improve visibility of the simulation results.

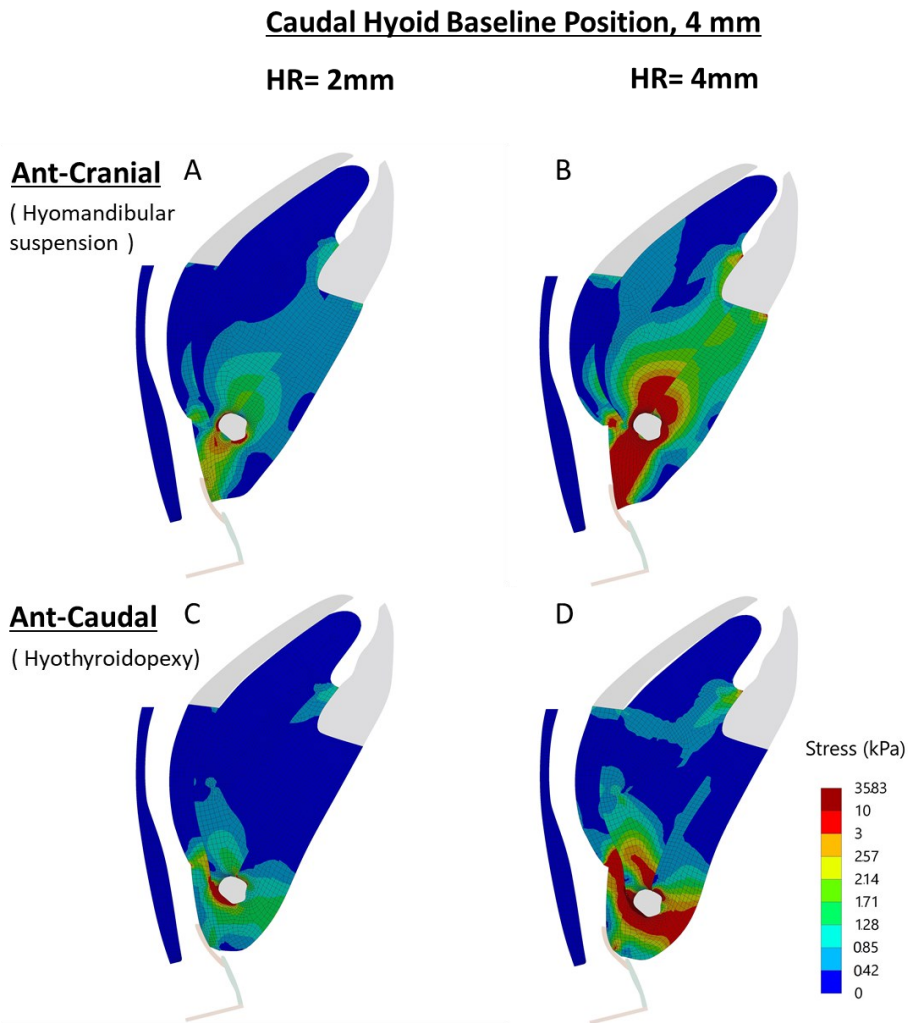


Figure 59: Equivalent (Von-Mises) stress distribution in the soft tissues as a result of surgical hyoid repositioning (HR) starting from a 4mm caudal hyoid baseline position. Stress results are shown for anterior-cranial (A, B) and anterior-caudal (C, D) hyoid repositioning simulations. The tissue displacement is represented as a color-coded contours map shown on the deformed mesh for a hyoid repositioning increment of 2mm (A, C) and 4mm (B, D). Anterior-cranial and anterior-caudal surgical hyoid repositioning represent hyomandibular suspension and hyothyroidopexy surgical procedures, respectively.

#### 4.5.3 Lumen Geometry Metrics

Figure 60 and Figure 61 present the change in upper airway lumen geometry metric in response to 2mm and 4mm anterior-cranial and anterior-caudal surgical hyoid repositioning from a caudal hyoid baseline position by 2mm (Figure 60) as well as 4mm

(Figure 61) to examine how different surgical hyoid repositioning procedures impact the upper airway geometry.

Cranial surgical hyoid repositioning caused a slight increase in the APD in region R2 and a decrease in R1 leading to a negligible change in the overall CSA. Anterior-cranial and anterior-caudal hyoid repositioning produced a significant increase in the lumen's CSA of about 35% with the lumen enlargement mainly occurring in region R2 for both repositioning directions. The increase in the APD dimension in region R2 is higher for anterior-cranial hyoid repositioning while it is higher in region R1 for the anterior-caudal direction.

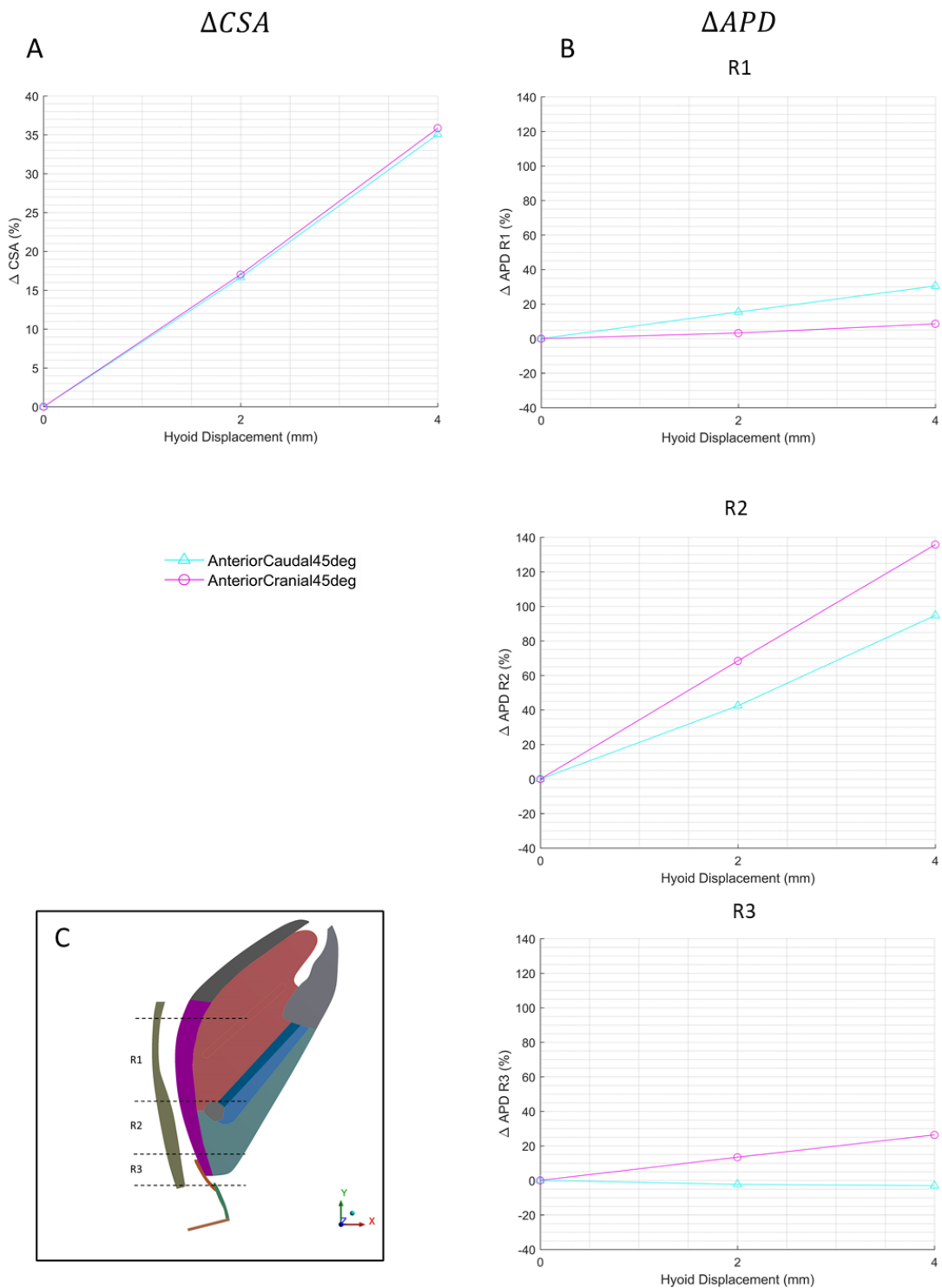


Figure 60: Upper airway lumen geometry changes in response to surgical hyoid repositioning from a 2mm caudal hyoid baseline position. Percent change in upper airway lumen area (A) and anteroposterior diameters (B) vs. surgical hyoid repositioning in the anterior-cranial and anterior-caudal directions for caudal baseline position of 2mm.  $\Delta APD$  was represented as the average value calculated for each region (R1, R2 and R3). The undeformed model geometry with the region delimitations is shown for reference (C).

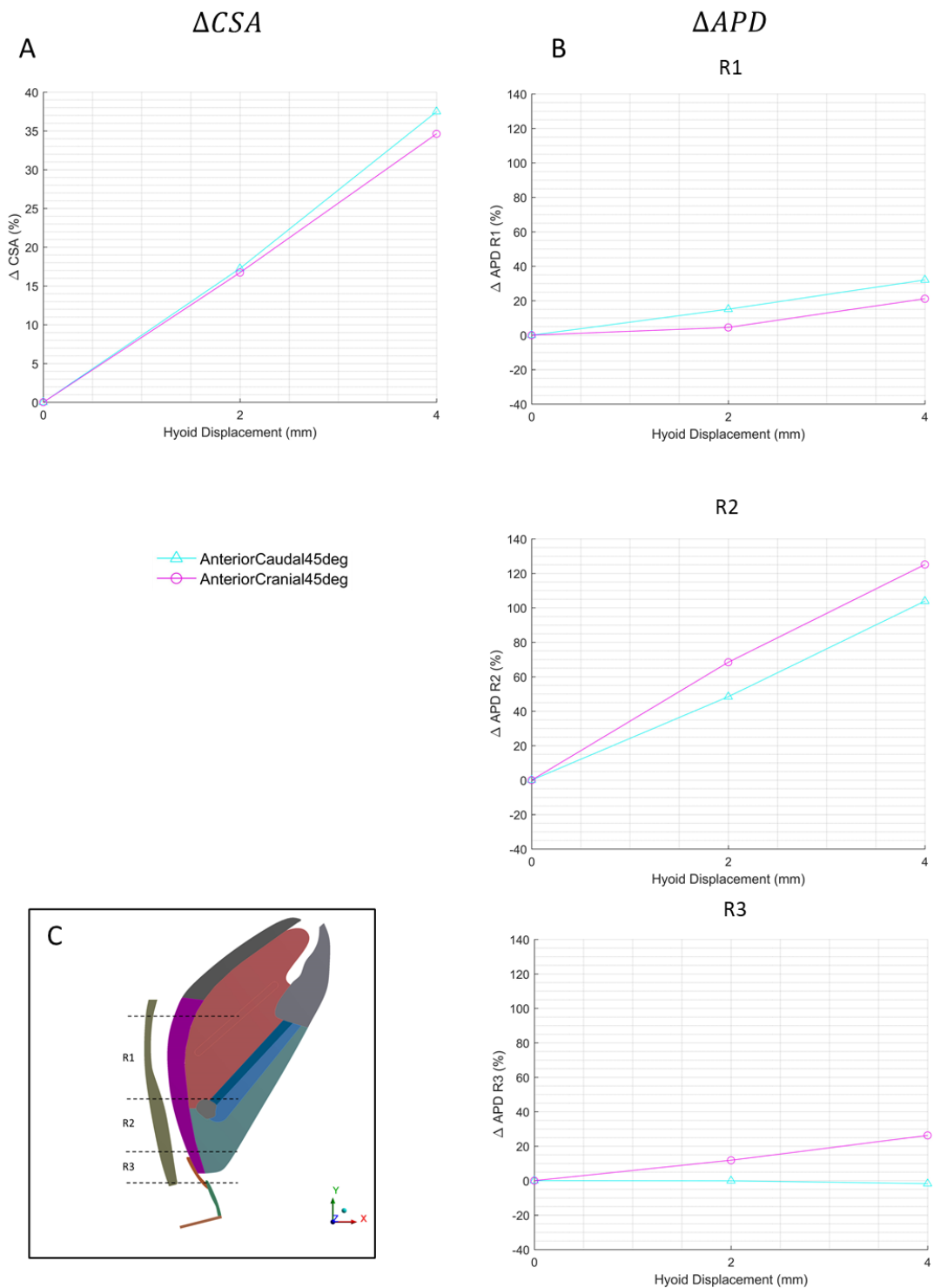


Figure 61: Upper airway lumen geometry changes in response to surgical hyoid repositioning from a 4mm caudal hyoid baseline position. Percent change in upper airway lumen area (A) and anteroposterior diameters (B) vs. surgical hyoid repositioning in the anterior-cranial and anterior-caudal directions for caudal baseline position of 4mm.  $\Delta APD$  was represented as the average value calculated for each region (R1, R2 and R3). The undeformed model geometry with the region delimitations is shown for reference (C).

## CHAPTER 5

### DISCUSSION AND CONCLUSION

#### 5.1 Strengths and Key Outcomes

This project introduces the first upper airway computational finite element model study that allows the thorough examination of the role of the hyoid bone in upper airway patency and tissue mechanics. The computational model is a mid-sagittal 2D representation of the passive rabbit upper airway that includes most upper airway structures (bony and soft tissues) and upper airway muscles (refer Chapter 2, Section 2.5).

Upper airway computational models have been previously developed, but none permit the direct study of hyoid bone position on upper airway mechanics. Particular strengths of this computational modeling study include:

- It uniquely permits the specific investigation of the effect of hyoid baseline position “phenotype” on upper airway outcomes, which cannot be studied in animal or human physiological models.
- The computational model is validated against physiological data and is capable of successfully predicting the percent change in  $P_{close}$  produced by surgical hyoid repositioning procedures.
- In addition to the collapsibility ( $P_{close}$ ), numerous outcomes can be easily observed and examined such as tissue displacement, stress and strain and the change in the airway lumen dimensions to allow a better understanding of the role of the hyoid bone in upper airway mechanics.

The key outcomes of this study are:



- Any change in the hyoid baseline “phenotypic” position, in both direction and magnitude with respect to the zero-baseline position, leads to an increase in upper airway collapsibility. This indicates that the zero-baseline hyoid position is the optimal phenotype in this model.
- Changes in upper airway collapsibility in response to surgical hyoid repositioning are dependent on the direction and magnitude of hyoid displacement applied, from any baseline hyoid position.
- Anterior, anterior-cranial and anterior-caudal surgical hyoid repositioning directions achieved the greatest decrease in upper airway collapsibility and most important enlargement of airway lumen in the hyoid bone region (R2), from any hyoid baseline position.
- Different distributions of tissue displacements, stress and strain are produced for different surgical hyoid repositioning directions. Anterior-cranial and anterior-caudal surgical hyoid repositioning procedures led to greatest magnitudes of tissue stress and strains increase.
- The effectiveness of surgical hyoid repositioning in decreasing upper airway collapsibility is dependent on the baseline “phenotypic” position of the hyoid bone as it varies with the direction as well as the magnitude of change in hyoid baseline position.
- When the hyoid bone is more caudally positioned (mimicking OSA) surgical hyoid repositioning procedures are less effective in decreasing upper airway collapsibility.
- For a caudally positioning hyoid phenotype (common in OSA patients), anterior-cranial surgical hyoid repositioning (hyo-mandibular suspension)

produces the most favorable outcomes in terms of airway lumen enlargement and tissue stiffening, particularly in the hyoid and epiglottal regions (regions R2 and R3)

## **5.2 Upper Airway Collapsibility and Site of Collapse at Baseline**

In this study, the baseline  $P_{close}$  value obtained from the rabbit upper airway computational model at baseline was  $-40.15 \text{ cmH}_2\text{O}$ . This is considerably higher than experimentally measured  $P_{close}$  values in anaesthetized rabbits usually between 3 and 4  $\text{cmH}_2\text{O}$  [63, 70, 97]. Kairaitis et al. [63] and Lam et al. [70] measured  $P_{close}$  in anaesthetized rabbits and obtained values of  $3.1 \pm 1.1$  (mean $\pm$ SD) and 3.8 (1.9-6.5) (mean (interquartile range))  $\text{cmH}_2\text{O}$ , respectively. Using the same method of  $P_{close}$  measurement, the rabbit study performed in the SUARG at AUB [97] found an average  $P_{close}$  value of  $-3.72 \pm 0.7 \text{ cmH}_2\text{O}$ . Moreover, a study by Isono et al. [59] determined a closing pressure in anaesthetized and healthy humans of  $-3.77 \pm 3.44 \text{ cmH}_2\text{O}$ . The  $P_{close}$  value for OSA patients varied between 0.9 and 2.78  $\text{cmH}_2\text{O}$  [59]. The potential reason for this discrepancy is that the model is stiffer than the actual upper airway and needs to be optimized in the future to collapse at physiological pressures.

Several existing computational models of the human upper airway have simulated airway narrowing and determined  $P_{close}$  [10, 71, 72, 79]. The  $P_{close}$  values obtained from these models are highly variable and were measured differently depending on the model (e.g. pressure when the distance between the airway walls is smaller than a certain threshold [71] or pressure when the luminal cross-sectional area of the upper airway is zero [72]). Fluid-structure interaction 3D models of the simplified healthy human upper airway predicted  $P_{close}$  to be approximately  $-4 \text{ cmH}_2\text{O}$  [79] [71],

while a  $P_{close}$  value of  $-0.51$  cmH<sub>2</sub>O was found for a 3D computational model of an OSA patient [10]. These outputs are comparable to the physiological  $P_{close}$  discussed above [59]. A more complex 3D upper airway computational model including the hyoid bone obtained higher  $P_{close}$  value of  $-13.97$  cmH<sub>2</sub>O. However, none of the existing upper airway computational models validated their  $P_{close}$  predictions against experimental data.

Despite the inaccurate absolute value of  $P_{close}$  found in this study, the percent change in  $P_{close}$  obtained from the model in response to surgical hyoid repositioning was found to successfully reproduce experimental results of the rabbit study performed at AUB [97]. Additionally, the current FE model truthfully predicted the site of collapse in the airway, which was found to be behind the hyoid bone, at the base of the tongue, i.e. at the boundary between regions R1 and R2. This corresponds to the human velopharyngeal airway region, considered to be the primary site of collapse in humans [59]. Other FE models of the healthy human upper airway have also predicted upper airway closure in the lower velopharynx region (tip of the soft palate) [71, 72].

### **5.3 Influence of Baseline Hyoid Position “Phenotype” on Upper Airway Collapsibility (Aim 1)**

In the current study, altering the hyoid baseline position in any direction and magnitude caused an increase in upper airway collapsibility. Hyoid baseline position is a phenotypic characteristic and cannot be altered in any physiological model (animal or human). Nevertheless, several epidemiological studies have focused on examining hyoid position of different individuals/population groups and relating it to upper airway function and patency. The hyoid bone was found to be located significantly more

inferiorly in patients with OSA compared to healthy individuals [30] [11]. The hyoid baseline position (hyoid to mentum distance) and severity of OSA (measured with AHI) were shown to be positively correlated ( $r=0.368$ ,  $P=0.005$ ) [16]. Hyoid position was also shown to be significantly and positively correlated with upper airway collapsibility, as measured by upper airway critical closing pressure ( $P_{crit}$ ), indicating that the more caudal the hyoid position, the higher the  $P_{crit}$  value. Overall, these studies indicate that a more caudal hyoid baseline position leads to an increase in upper airway collapsibility which is consistent with the results of this study.

However, many factors other than the hyoid baseline position are different between the healthy and the OSA individuals examined in these epidemiological studies such as age, BMI, tongue fat, neck circumference which makes it difficult to investigate the effect of changing the hyoid baseline position alone on upper airway collapse. On the contrary, in the current study, the differences between models compared only involved a change in the hyoid baseline position accompanied by a change in the tongue surface area and a modification of the passive upper airway muscle's length and angle to maintain an anatomically coherent airway structure. Thus, this study demonstrates that the anatomical changes strictly related to shifting the hyoid bone baseline position have a significant impact on upper airway collapsibility, independently of the other factors present in the clinical studies.

Moreover, the results of this study suggest that the zero-hyoid baseline position is the optimal and most favorable anatomical configuration of hyoid position, tongue area and passive muscle properties in order to minimize upper airway collapsibility. This was expected given that the zero-baseline hyoid position corresponds to the initial airway anatomy of the healthy rabbit. Modifying the baseline position of this crucial

bone might alter the balance of forces that maintain airway patency by increasing the area of unsupported tissues below, above or behind the hyoid bone, depending on the direction of hyoid baseline shift. Moreover, the change in the length and orientation of the muscles attached to the hyoid bone could potentially impact the passive muscle stretch that is produced during Pua simulation, reducing its ability to resist upper airway collapse.

## **5.4 Influence of Surgical Hyoid Repositioning for Zero-Baseline Hyoid Position (Aim 2)**

### **5.4.1 General Overview**

According to the outcomes of the current study, the effect of surgical hyoid repositioning from the zero-baseline hyoid position on upper airway collapsibility can be summarized as follows. Hyoid repositioning in an anterior-based direction (anterior, anterior-caudal or anterior-cranial) led to the most substantial reduction in  $P_{close}$ . Cranial hyoid repositioning caused a relatively minor improvement in  $P_{close}$  while caudal hyoid repositioning resulted a minor increase in  $P_{close}$ . Regardless of the direction of hyoid repositioning, a higher magnitude of hyoid displacement generates a larger change in airway collapsibility.

The tissue mechanics changes obtained from the FE model demonstrated that each direction of surgical hyoid repositioning resulted in correspondingly different tissue displacement, stress and strain distributions. Increasing the magnitude of hyoid displacement increased the magnitude of the displacement, stress and strain outcomes for each direction, while conserving the pattern of their distribution. Similarly, the changes

in airway lumen geometry depended on the direction of surgical hyoid repositioning and increased linearly with the increment of hyoid displacement.

The percent change in  $P_{close}$  obtained from the current FE model hyoid repositioning simulations was generally found to be in agreement (within the 95% confidence interval) with the corresponding anesthetized rabbit experimental results [97]. The current model was able to correctly predict the changes in  $P_{close}$  produced by repositioning the hyoid bone in five different directions and at all increments, except for select magnitudes of caudal and cranial displacement. The fact that the model was not able to predict these select  $P_{close}$  changes is potentially due to the very small changes in  $P_{close}$  (less than 10%) obtained experimentally for caudal and cranial surgical hyoid repositioning. It might also be the result of some model boundary condition simplifications as discussed in Sections 5.4.3 and 5.4.4.

## ***5.4.2 Anterior Hyoid Repositioning***

### **5.4.2.1 $P_{close}$**

The outcomes of this thesis showed a large and progressive decrease in upper airway collapsibility with anterior hyoid displacement, reaching up to a 130% decrease in  $P_{close}$  for a displacement magnitude of 5mm. Moreover, the current model predicted the percent changes in  $P_{close}$  for all magnitudes of anterior hyoid displacement (from 1 to 5mm) to be within the 95% confidence interval of the experimental results.

Previous studies have also illustrated the beneficial impact of anterior hyoid repositioning on the upper airway properties. A considerable reduction in upper airway resistance to airflow was commonly observed as a result of anterior hyoid advancement in dogs (5 to 8 mm displacement) [45], in rabbits (unspecified magnitude of

advancement) [14] as well as in human cadavers (1cm of advancement) [95]. The human cadaveric study by Rosenbluth et al. [95] also showed that anterior hyoid displacement produced a progressive increase in the critical airflow at which the airway collapsed reaching almost 4 folds for 1cm of hyoid advancement. These results indicate a significant improvement in airway collapsibility associated with anterior surgical hyoid repositioning, as is observed in this study.

#### 5.4.2.2 Upper Airway Geometry

Furthermore, in the current study, anterior hyoid displacement simulations resulted in an increase in airway lumen dimensions (midsagittal CSA and APD), particularly in the hyoid bone region. This increase in airway dimensions was primarily the result of anterior movement of the tongue and tissue mass, as well as the soft palate portion behind the hyoid.

The displacement of upper airway soft tissues in response to surgical hyoid repositioning has not been previously quantified experimentally. Some studies qualitatively observed the advancement of the tongue and widening of the velopharynx or hypopharynx in response to hyoid advancement [95] [45] [14], supporting results in this thesis.

#### 5.4.2.3 Tissue mechanics

Since the soft tissues in the current model are defined as hyperelastic materials, an increase in stress and strain indicates a stiffening of these tissues [1]. Thus, anterior hyoid displacement led to the stiffening of soft tissues in a small area around the hyoid bone and in the lower portion of the soft palate (anterior wall of the airway here).

No previous studies have measured the tissue stretch or pressure in response to anterior hyoid displacement. Nonetheless, tissue stiffening around the hyoid can be expected as anterior hyoid displacement would stretch the hyoid muscles which possibly leads to the stiffening of airway tissues. Compared to the other hyoid displacement directions, anterior hyoid displacement produced the least tissue stiffening in this study.

### ***5.4.3 Caudal Hyoid Repositioning***

#### **5.4.3.1 Pclose**

In this study, caudal hyoid displacement was found to progressively increase upper airway collapsibility as the magnitude of the caudal displacement is higher. Compared to the experimental study [97], the current FE model overestimated the changes in Pclose produced by caudal surgical hyoid repositioning with model outcomes slightly outside the 95% confidence interval of the experimental results for select magnitudes of caudal hyoid displacement.

Nonetheless, this slight difference in model vs. experimental outcomes could be attributed to the simplification of the model boundary condition definition at the intersection of the tongue, tissue mass and epiglottis with the soft palate. These boundaries are defined as “bonded” or “no separation” contacts in the current model, which is not representative of the actual upper airway physiological conditions and possibly causes an exaggerated deformation of the soft palate as a result of soft tissue displacements below the hyoid bone after caudal surgical hyoid repositioning. This might lead to the development of lumps in the soft palate part behind the hyoid bone, making this region more prone to collapse. Following caudal hyoid repositioning, the



site of collapse in the FE model was in fact lower than at zero-baseline, down to the infrahyoid region where the pharyngeal tissues were lumped. This may not occur in physiological circumstances. Moreover, the small sample size of the experimental study and the minor variation in experimental  $P_{close}$  results found for caudal hyoid repositioning could be another explanation to the model vs. experimental outcome discrepancy.

No other studies have examined the impact of caudal surgical hyoid repositioning directly. Caudal movement of the hyoid bone was consistently observed with caudal tracheal displacement (TD) [1, 2]. However, TD was shown to improve upper airway function and collapsibility [2, 63, 96], as opposed to the current model outcomes in response to caudal hyoid repositioning. As discussed in the next sections, the current study suggests that caudal tracheal displacement and caudal hyoid displacement applied alone do not impact upper airway patency in the same manner.

#### 5.4.3.2 Upper Airway Geometry

Caudal surgical hyoid repositioning was shown to reduce upper airway lumen dimensions (CSA and APD) in this study. In a rabbit upper airway experimental study [2], 9mm of TD produced caudal hyoid displacement of 2mm and was accompanied by an increase in the upper airway lumen size (including CSA and APD). These results are in opposition with the current model outcomes: 2mm of caudal hyoid repositioning in the current study led to a decrease by 18% in the APD in the hyoid bone region (R2) whereas the same magnitude of hyoid movement induced by TD in the experimental study [2] increased the APD by 20% in that same region.

### 5.4.3.3 Tissue Mechanics

In the current study, increased tissue stress and this tissue stiffening was observed in response to caudal surgical hyoid repositioning mainly in the tissues around the hyoid bone and in the epiglottic airway region (R3).

The improvement of airway function associated with TD and is suggested to be a result of stretching and stiffening pharyngeal soft tissues (both supra- and infra-hyoid muscles) and reducing upper airway tissue pressure through the caudal movement of the hyoid bone produced [2, 63, 96]. Although airway wall stiffening was also observed in this study, the greatest increase in predicted tissue stiffness in response to TD was in the tongue base region (R1) [1, 2], and not the epiglottic region (R3). This difference suggests that the increase in tissue stiffness produced by caudal hyoid repositioning alone is not enough to improve upper airway stability since the soft tissues below the hyoid are lumped and lead to the narrowing of the airway lumen.

Additional investigation of the tissue deformation in physiological experimental studies through imaging is needed to further understand the effect of caudal surgical hyoid repositioning on upper airway mechanics.

## ***5.4.4 Cranial Hyoid Repositioning***

### 5.4.4.1 Pclose

Cranial hyoid repositioning led to a slight and progressive decrease in upper airway collapsibility in this study. Apart from the rabbit experimental study conducted by the SUARG at AUB [97], no studies are previously investigated the influence of cranial hyoid repositioning procedures on the upper airway.

Compared to the experimental study [97], there is a general overestimation of the change in  $P_{close}$  obtained from the model. However, current FE model outcomes are still within the 95% confidence interval of the experimental results for all different magnitudes of cranial hyoid displacements, except for the 5mm magnitude. Similarly to caudal hyoid repositioning, this difference is potentially due to the simplified model boundary conditions and the small signal attained experimentally for this intervention that would require further investigation (e.g. greater rabbit numbers to remove potential noise).

#### 5.4.4.2 Upper Airway Geometry and Tissue Mechanics

The airway tissue displacement and mechanics and the lumen geometry outcomes from this study allow a better understanding of the mechanisms underlying cranial surgical hyoid repositioning.

The first observation is that cranial hyoid displacement led to the cranial displacement of tissues below the hyoid bone, which implies that the infrahyoid muscles are stretched leading to the enlargement of the airway lumen and the stiffening of its walls in the hyoid bone and epiglottis regions (regions R2 and R3). This is confirmed by the increase in lumen APD mainly in region R2 and the rise of soft tissue stress and strain around the hyoid bone and in the portion of soft palate inferior to the hyoid bone.

In the region above the hyoid bone, the soft tissues are compressed cranially by the hyoid displacement forming a protrusion at the base of the tongue, which forces the soft palate portion above the hyoid bone (in the tongue base region, R1) posteriorly. In fact the APD of the lumen in region R1 is decreased and the site of collapse is raised to

a point behind the soft palate protrusion. As previously mentioned, this posterior deformation of the soft palate may be exaggerated in the model due to the potentially unrealistic contact condition set with the tongue (“no separation contact”). However, anatomically the tongue and soft palate are closely connected through the palatoglossus muscle, which is partially mimicked through this contact.

Additionally, cranial hyoid displacement produced changes in the tongue tissue. The entire tongue was advanced anteriorly and its transverse fibers were stiffened as shown by the increase in the tissue stress in the tongue area between the hyoid and the mandible. This stiffening is likely related to the stretching of the genioglossus muscle and some suprahyoid muscles (geniohyoid and mylohyoid).

Overall, the cross-sectional area of the airway lumen is not changed after cranial hyoid repositioning. Further experimental studies evaluating tissue displacement, pressure, and lumen dimensions are needed to confirm the above observations.

#### ***5.4.5 Anterior-Cranial and Anterior-Caudal Hyoid Repositioning***

##### ***5.4.5.1 P<sub>close</sub>***

A considerable and progressive decrease in upper airway collapsibility was produced by anterior-cranial and anterior-caudal hyoid repositioning in this study. This was larger or equal to the  $P_{close}$  decrease in response to anterior hyoid displacement alone, which is in agreement with the observations from the rabbit experimental study [97]. The current model was able to predict experimental outcomes for the percent change in  $P_{close}$  values obtained from all five magnitudes of surgical hyoid repositioning in the anterior-cranial and anterior-caudal directions.

Rosenbluth et al. [95] also observed an improvement in airway patency and stability in human cadavers with anterior-cranial and anterior-caudal hyoid displacement (at a 30° angle from the antero-posterior direction). No other studies have investigated hyoid displacement in these directions. However, indirect anterior-cranial hyoid movement has commonly been observed with mandibular advancement procedures [3, 29, 40, 69], associated with the improvement of upper airway collapsibility [56, 82] which is consistent with the current results for anterior-cranial surgical hyoid repositioning.

#### 5.4.5.2 Upper Airway Geometry

Anterior-cranial and anterior-caudal surgical hyoid repositioning were accompanied by an enlargement of the airway lumen as shown in this study by the increase in midsagittal CSA between 30% and 40% for a hyoid displacement increment of 4mm. The APD was also generally increased in all airway regions with the highest enlargement in the hyoid bone region (R2) reaching up to a 140% increase in APD for anterior-cranial and 85% for anterior-caudal hyoid repositioning.

An anesthetized rabbit experimental study by Amatoury et al. [3] showed that mandibular advancement (MA) of 4.6mm led to a hyoid displacement of 2mm in the anterior-cranial direction at an angle of ~18° with respect to the antero-posterior axis (X-axis here). Although direct anterior-cranial hyoid repositioning in the current study was at a different angle (45°), the enlargement in upper airway lumen observed is comparable to the one produced by indirect hyoid displacement through MA. Anterior-Cranial surgical hyoid repositioning by 2mm led to an 18% increase in CSA in this

study and a 30% increase in CSA in the experimental MA study [3] with the largest widening in APD being at the hyoid bone region (R2) in both cases.

Anterior-caudal surgical hyoid repositioning produced a similar increase in overall lumen midsagittal cross-sectional area with the largest increase in APD also found in region R2. However, the anterior-caudal repositioning direction led to the enlargement of the airway in region R1 above the hyoid bone by ~30% while the enlargement of region R1 is minimal (2% increase) for the anterior-cranial direction. This is possibly due to the soft tissues squeezed above the hyoid bone after cranial hyoid displacement that might push the soft palate posteriorly into the airway lumen as discussed in Section 5.4.4.2. Moreover, anterior-caudal surgical hyoid repositioning led to a slight decrease in the APD of the epiglottic region (R3) probably due to the lump created in the soft palate by pushing together the soft tissues located below the hyoid bone.

#### 5.4.5.3 Tissue Mechanics

Anterior-cranial surgical hyoid repositioning produced the largest stress in tissues around the hyoid bone and specifically the airway wall in the region below the hyoid bone. These results suggest that anterior-cranial hyoid displacement stretches the tissues below the hyoid bone and infrahyoid muscles such as the sternohyoid and thyrohyoid leading to the enlargement of the airway lumen and the stiffening of the airway walls in that region (regions R2 and R3). Furthermore, the current stress and strain results show that anterior-cranial surgical hyoid repositioning led to the stiffening of a large portion of the tongue, mainly in its transverse fibers area between the hyoid and the mandible. In the experimental MA study [3], airway tissues were also largely

stretched and stiffened in all regions, non-uniformly. Nonetheless, the largest stress was found to be in the tongue base region (R1) as opposed to being in the hyoid bone and epiglottic regions (R2 and R3) in the current study. This difference is likely due to the fact that anterior-cranial hyoid displacement alone might not produce as much stretching of the suprahyoid hyoid muscles originating from the mandible (geniohyoid, mylohyoid and genioglossus) as when MA is applied.

Anterior-caudal hyoid displacement also led to an increase in stress in the tissues at the boundary of the hyoid bone. Stresses of lower magnitudes were uniformly distributed in the soft palate tissues along the entire airway length indicating a moderate soft palate stiffening in regions R1, R2 and R3. Although the tongue was pulled in an anterior-caudal direction with the hyoid bone displacement, the tissue stress distribution reveals that, apart from the region at the boundary with the soft palate, the tongue tissues were not stiffened by anterior-caudal hyoid displacement as was the case with anterior-cranial hyoid displacement.

The major difference between anterior-cranial and anterior-caudal surgical hyoid displacements is in the resulting tissue stiffening produced. The stresses produced by anterior-caudal hyoid repositioning were more concentrated around the hyoid bone leading to the stiffening of a smaller region of soft tissues (mainly tissue mass located below the hyoid bone). On the other hand, anterior-cranial hyoid repositioning generated larger stresses that indicate higher stiffening of the soft tissues particularly in soft palate in region R2 but also a wider spread of the stresses among the upper airway soft tissues. In fact, a large portion of the tongue tissue and the majority of the tissue mass is stiffened in response to anterior-cranial hyoid displacement. These observations

lead to the proposition that anterior-cranial hyoid repositioning might results in a better improvement of airway tissue mechanics.

Although the change in  $P_{close}$  produced and the overall lumen CSA changes are very similar, the outcomes of this study indicate that the ways in which anterior-cranial and anterior-caudal hyoid repositioning affect the upper airway lumen properties are different.

## **5.5 Combined Influence of Baseline Hyoid Position and Surgical Hyoid Repositioning (Aim 3)**

### ***5.5.1 Overall Impact of Different Hyoid Baseline Positions***

Irrespectively of the initial hyoid baseline position, the patterns of change in  $P_{close}$  produced by surgical hyoid repositioning in different directions (anterior, cranial, caudal anterior-cranial and anterior-caudal) were overall very similar to the patterns produced when the hyoid was in the zero-baseline position. Moreover, tissue displacement, stress and strain outcomes resulted in distributions matching the zero-baseline position model outcomes with same pattern but different magnitudes. The same applies to the change in upper airway lumen geometry produced. Therefore, the mechanisms through which the various directions and magnitudes of surgical hyoid repositioning impact the upper airway behavior and properties (discussed in Section 5.4) are generally analogous amongst the FE models with different hyoid baseline positions.

Nonetheless, due to the fact that a change in hyoid baseline position (regardless of the direction) leads to a progressive increase in upper airway collapsibility, the larger the magnitude shift of the hyoid baseline position (in any direction), the further away



the “position baseline”  $P_{close}$  is from the zero baseline  $P_{close}$  value ( $P_0$ ) and the higher the hyoid repositioning increment must be to reduce  $P_{close}$  back to the  $P_0$ . For example, in the case of a caudal baseline position shift by 4mm, a hyoid displacement load of 2mm in the anterior-caudal direction and ~2.5mm in the anterior or anterior-cranial directions reduced  $P_{close}$  back to  $P_0$ . When the hyoid was positioned inferiorly by 2mm only, a hyoid repositioning of 1mm in the anterior, anterior-caudal or anterior-cranial direction is enough to reduce  $P_{close}$  to the value of  $P_0$ .

As a matter of fact, the effectiveness of surgical hyoid repositioning procedures (i.e. anterior-cranial and anterior-caudal hyoid displacements) in decreasing  $P_{close}$  was impacted by changes in the hyoid baseline position. The variation in the effectiveness of the repositioning procedures was dependent on both the direction and increment of the hyoid baseline position change. However, there was no visible pattern in the variation of effectiveness with respect to baseline position increments (unlike linear variation of  $P_{close}$  with surgical hyoid repositioning increments). Depending on the direction of hyoid baseline position shift, an increase in the increment of the baseline change can lead to either an increase or a decrease in the effectiveness of the same hyoid repositioning procedure. For example, shifting the hyoid baseline position in the cranial by 2mm increased the effectiveness of surgical hyoid repositioning in the anterior-cranial and anterior-caudal directions; but a cranial hyoid baseline position shift by 4mm decreased the effectiveness of the same surgical hyoid repositioning interventions. These findings propose an explanation to the high variability and unpredictability of the surgical outcomes of hyoid repositioning procedures performed as an OSA treatment. A review of hypopharyngeal surgery studies by Kezirian et al. reported that the success rate of hyoid suspension surgeries varied from 17% to 78% [64].

### ***5.5.2 Impact of Caudal Hyoid Baseline Position***

Although general patterns of percent change in  $P_{close}$  for different hyoid baseline positions are similar to the zero-baseline hyoid position results, there is a noticeable difference in the change in  $P_{close}$  produced when the hyoid baseline position is caudal (as compared to when the hyoid is in the zero-baseline position). Caudal surgical hyoid repositioning was shown to cause a small but progressive increase in  $P_{close}$ ; but when performed for the caudal hyoid position phenotype, it led to a minor decrease in  $P_{close}$ . In other words, when the hyoid is phenotypically situated in a more caudal position (as is commonly the case in OSA patients), a forced caudal hyoid displacement is capable of slightly decreasing upper airway collapsibility in the same manner of cranial hyoid displacement. Nonetheless, both these hyoid displacement directions decrease  $P_{close}$  by less than 20% at maximum magnitude. The model suggests that adding an anterior component to the hyoid repositioning direction is necessary to obtain considerable improvement in upper airway collapsibility. It so happens that this is the case in the clinically available hyoid repositioning surgeries: hyomandibular suspension has an anterior-cranial vector and hyothyroidopexy an anterior-caudal vector [15].

Both anterior-cranial and anterior-caudal hyoid repositioning directions produced similar improvements in upper airway collapsibility and overall lumen enlargement in this study. However, there was a considerable difference in tissue displacements, stresses and strains induced by the two repositioning directions. Anterior-cranial surgical hyoid repositioning produced larger anterior displacements in the soft palate, particularly in the region behind the hyoid bone, and resulted in the advancement of the epiglottis which led to a larger increase in the lumen APD in the hyoid and epiglottic regions (R2 and R3) corresponding to the lower portion of the

velopharynx and the hypopharynx. Moreover, the base of the tongue was advanced with anterior-cranial hyoid displacement. A recent retrospective study by Van Tassel et al. [119] confirmed the increase in the airway size and anterior advancement of the tongue and epiglottis after hyomandibular suspension through endoscopic evaluation of the airway in awake and anesthetized patients. On the other hand, anterior-caudal hyoid displacement was found in the current study to pull the tongue downwards and did not displace of the epiglottis. A moderate increase in the airway behind the base of the tongue was observed after hyothyroidopexy procedure in a clinical study, but overall the airway anatomical changes in response to the procedure were not significant [111].

Moreover, the pattern of tissue and passive muscle stretching in response to anterior-cranial hyoid displacement produced a larger increase and wider distribution in the tissue stresses compared to anterior-caudal hyoid displacement. This indicates that anterior-cranial hyoid displacement resulted in an increase in the stiffness of the soft tissues (including the tongue, tissue mass and soft palate), particularly in the hyoid bone and epiglottal regions (R2 and R3). On the other hand, the stress and strain results in response to anterior-caudal hyoid repositioning showed that significant tissue stiffening only occurred in a small area around the hyoid bone and was not spread across the different soft tissues. No previous studies have examined airway tissue mechanics in response to surgical hyoid repositioning procedures in a caudal hyoid baseline position phenotype or in OSA patients directly.

## 5.6 Clinical Implications

In general, shifting the hyoid baseline position in the caudal direction in this study (mimicking the OSA condition) caused a decrease in the effectiveness of surgical hyoid repositioning simulations in reducing upper airway collapsibility. Although the correlation between hyoid baseline position and surgical success of hyoid suspension surgeries has not been previously demonstrated, several studies have shown that the success rate of hyoid suspension surgeries is reduced with increased OSA severity (AHI), reflecting a more inferior/caudal hyoid baseline position [83, 119, 122]. For instance, Vilaseca et al. [122] reported a surgical success rate for hyothyroidopexy procedure of 100% in their mild OSA group, 57% for moderate OSA and only 9% in the case of severe OSA.

The existing surgical hyoid repositioning procedures performed clinically in OSA patients are hyomandibular suspension and hyothyroidopexy [93], displacing the hyoid bone along an anterior-cranial or anterior-caudal vector, respectively (see Figure 6 in Section 2.3.2.2). This study shows that in the case of a caudally positioned hyoid phenotype (mimicking the OSA condition), anterior-cranial and anterior-caudal hyoid displacement leads to a considerable decrease in upper airway collapsibility (more than 50% reduction in  $P_{close}$  when increment of hyoid displacement is higher than 2mm) and an overall increase in airway lumen midsagittal cross-sectional area. These findings are consistent with the numerous studies that have demonstrated that hyoid suspension surgeries significantly decreased the AHI in most cases, although the surgical success rates were variable [64, 105]. Note that in clinical studies found in literature, surgical success of hyoid suspension procedures is defined as a 50% decrease in AHI and an AHI of less than 20 (indicating mild OSA severity).

Furthermore, the tissue mechanics outcomes for anterior-cranial and anterior-caudal surgical hyoid repositioning simulations from a caudal baseline position found in this study (discussed in Section 5.5.2) suggest that repositioning the hyoid bone in an anterior-cranial direction (hyo-mandibular suspension) in OSA patients will produce more favorable outcomes than the anterior-caudal hyoid displacement (hyothyroidopexy). Very few studies comparing hyo-mandibular suspension and hyothyroidopexy procedures have been undertaken. A small sample size study that included only women found that hyo-mandibular suspension produced larger reduction in the number of respiratory disturbances during sleep (apnea, hypopnea or respiratory event-related arousals) and higher improvement in the lowest oxygen saturation levels compared to hyothyroidopexy [77]. A more thorough comparison between the techniques was later performed in a systematic review including patients with all OSA severities [105], which suggested that hyothyroidopexy resulted in a larger reduction in AHI on average (50.7%) compared to hyomandibular suspension (38.3% reduction in AHI). However, the results for hyothyroidopexy were highly skewed and the surgical technique for hyomandibular suspension used in the studies was the older and more invasive technique initially proposed by Riley et al. [93] that required considerable myotomy of the hyoid muscles. A minimally invasive hyo-mandibular suspension technique was later introduced by Gillespie et al. [43] in which only minimal muscle cutting was made. This is expected to maximize the effect of hyoid displacement through muscle stretching and further stabilize the airway. Van Tassel et al. [119] revealed that this improved hyo-mandibular suspension technique combined with palatal surgery produced a 62% improvement in AHI with a 76.9% success rate among patients with moderate-to-severe OSA.

Apart from the more favorable improvement in airway geometry and tissue mechanics demonstrated in this study (Section 5.5.2), hyo-mandibular suspension (with the improved surgical technique) presents several advantages compared to the hyothyroidopexy procedure. In general, there is more room for hyoid displacement when suspending it to the mandible rather than the thyroid cartilage, i.e. larger displacement magnitude, specifically in the anterior direction. The anterior direction is thought to be the vector component that mainly contributes to the upper airway improvement with hyoid suspension procedures [97], and as demonstrated in the current study. Furthermore, hyo-mandibular suspension surgery does not restrict the mobility of the hyoid bone in the cranial direction that is naturally required for swallowing, which minimizes post-operative discomfort and complications. Nonetheless, clinical studies that evaluate the minimally invasive hyo-mandibular suspension procedure are limited and further investigation is needed to assess this surgery.

The results of this study also support the observation made by Ong et al. [83] and Gillespie et al. [43] that the main effect of hyo-mandibular suspension is the advancement of the tongue and enlargement of the retro-epiglottic airspace by pulling on the hyoepiglottic ligament. Ong et al. [83] showed in their study that none of the patients that had undergone the hyo-mandibular suspension presented epiglottal collapse post-treatment. Besides, the results of the current study suggest that in addition to airway enlargement and tongue advancement, hyo-mandibular suspension is expected to stiffen the tongue tissues and improve the tissue properties in the hypopharynx, increasing the airway stability in this region. Consequently, the current study supports that hypopharyngeal and epiglottal collapse may be a potential useful patient selection criterion for hyomandibular suspension surgery.

## **5.7 Limitations and Critique of Methods**

### ***5.7.1 Original Model Limitations***

Limitations related to the original model by Amatory et al. [1] are discussed in Chapter 2, Section 2.5.4.

The fact that the model includes only passive airway behavior and the translation from rabbit to human limitations will be briefly discussed again in this section in the context of the current study.

#### **5.7.1.1 Passive Airway Behavior**

The model reproduces the passive upper airway behavior in anesthetized and tracheostomized rabbits and did not include active muscle contraction or airflow. However, understanding the behavior of the passive and static airway is important in obtaining fundamental knowledge of the upper airway collapse occurring in sleep-related breathing disorders such as OSA since the muscle activity is actually reduced during sleep [74, 126]. Eastwood et al. [37] revealed a strong association between the critical closing pressure ( $P_{cirt}$ ) measured during anesthesia in the human upper airway and the severity of OSA during sleep. Furthermore, a recent study measured  $P_{crit}$  of the same patients during anesthesia as well as during sleep and found a direct relationship between both  $P_{crit}$  results. In this context, the current passive model has the advantage of allowing us to study the role of the hyoid bone in upper airway mechanics without the confounding effects of muscle activity or airflow. Active muscles contraction and fluid-structure interaction can be integrated to the model in future studies to investigate more complex upper airway interactions and behavior.

### 5.7.1.2 Rabbit to Human Translation

Despite the obvious anatomical difference between rabbit and human head and neck anatomy, the rabbit is an applicable model for upper airway studies since its upper airway is very similar to the human, particularly with regards to the hyoid bone anatomy that is of central importance in this thesis (discussed in detail in Section 2.5.4.1).

The fact that the rabbit model does not replicate the pathophysiological conditions of OSA should also be considered. The hyoid bone baseline position was lowered as a tentative to represent some aspects of common OSA airway characteristics. Nonetheless, the purpose of this study was not to replicate the OSA pathophysiological behavior of the airway but rather to understand the complex interactions of the normal upper airway structures and particularly examine the impact of the position and movement of the hyoid bone on upper airway mechanics.

### **5.7.2 Closing Pressure ( $P_{close}$ ) Result**

In this study,  $P_{close}$  was quantified as the pressure at which the opposing upper airway walls (soft palate/epiglottis anteriorly and constrictor body posteriorly) first come into contact. The proposed technique for determining  $P_{close}$  is sensitive to the analysis settings of the finite element simulation and causes a certain measurement error that is lowered when the number of substeps is increased. The number of substeps chosen here (80 substeps) leads to a  $P_{close}$  measurement uncertainty of  $\pm 0.58$  cmH<sub>2</sub>O (Refer to Section 3.3.1.2. in methods). Furthermore, given that the model is 2D, the lateral upper airway walls are not represented and what is considered as upper airway collapse here might only be an antero-posterior airway narrowing in a 3D airway.



Another limitation of the current  $P_{close}$  results is that the absolute  $P_{close}$  values obtained are approximately 10 times larger than the physiological  $P_{close}$  values as discussed in Section 5.2. The reason for this difference is that the upper airway model behavior is stiffer than the actual upper airway. Some model definitions such as the boundary conditions, contacts and even the material properties must be optimized in future work to allow the airway model to collapse at lower pressures.

Despite these limitations, the changes in  $P_{close}$  obtained from the model matched the majority of experimental results for the various directions and magnitudes of surgical hyoid repositioning procedures tested. Moreover, compared to existing upper airway computational modeling studies, the  $P_{close}$  measurement technique used in this study can be considered more realistic. It is able to determine the point at which the airway walls are in direct contact through the contact penetration results, without any tolerance, as opposed to what has been done in previous computational modeling studies where contact was assumed when the distance between the airway walls was lower than a certain threshold value [53, 71].

### ***5.7.3 Hyoid Position Phenotype Changes***

Human upper airway phenotypes with different hyoid baseline positions usually include many other differences in the airway anatomy such as facial skeletal patterns or tissue distribution [46, 49, 61, 78, 100]. In the current model, the different hyoid position phenotypes were obtained by shifting the location of the hyoid bone body. Apart from the structures that are in direct contact with the hyoid bone in the model (inferior tongue edges, tissue mass and hyoid muscle connections), no other changes to the airway were made. While this does not represent the different phenotypes

assessed in clinical studies, this is beneficial in examining the isolated impact of the hyoid baseline position on upper airway behavior without the other OSA confounding factors (BMI, neck circumference, fat pads in the neck region, age, etc.).

Despite not mimicking the OSA condition, the outcomes from the FE model are still consistent with the observations made in clinical studies. The caudal change in hyoid baseline position in this study was selected to represent the typical change in vertical hyoid position between normal and apneic individuals according to the study by Chi et al. [30]. In the latter, apneic patients were found to have a 6.2% (~8mm) more inferior hyoid position compared to healthy individuals (as measured from hyoid to nasion, vertically) [30]. In the current rabbit upper airway model, a 6.2% change in the caudal hyoid position corresponds to an ~2mm caudal shift, which was investigated along with an additional doubled shift (4mm) to further examine the impact on upper airway behavior. Furthermore, the increase in tongue volume that is usually associated with the inferior hyoid position in OSA patients [30, 41] was also inherently replicated in the current FE model. For instance, Genta et al. showed that a more inferior hyoid baseline position by 8mm was accompanied by an 8% increase in the tongue volume in humans (derived from the results in Table 1 of Genta et al. [41]). In the current model, a 5% increase in the tongue's surface area was produced by the corresponding caudal shift in the hyoid baseline position (2mm).

#### ***5.7.4 Replication of Hyoid Suspension Surgical Procedures***

Hyo-mandibular suspension and hyothyroidopexy surgical procedures are represented in this study by an anterior-cranial and anterior-caudal hyoid displacement at a 45° angle. No actual suspension to the mandible or thyroid cartilage were

performed, however the hyoid was fixed in its new position following displacement to generally mimic these surgeries. Nonetheless, it is difficult to precisely replicate hyoid surgical procedures. The general lack of guidance for the hyoid suspension surgical procedures in terms of the amount and angle of hyoid displacement makes it difficult to simulate the exact procedure in the model. These factors (magnitude and angle of repositioning) depend on patient-specific skeletal and craniofacial characteristics and thus vary from one patient to another, but even then, they are not actually quantified [43, 92, 93].

Considering the human upper airway anatomy, hyo-mandibular suspension will involve for all patients a combination of cranial and anterior hyoid displacement components and hyothyroidopexy a combination of caudal and anterior components [15]. The current model simulations can therefore provide an insight on the changes in upper airway collapsibility and tissue properties in response to a hyoid displacement in these directions. Nevertheless, the angle of hyoid displacement in the surgical procedures is expected to be smaller than  $45^\circ$  since in general the cranial and caudal displacement components are larger than the anterior. A preliminary examination of anterior-cranial and anterior-caudal hyoid displacement at a  $30^\circ$  angle from the +Y-axis showed that the patterns of  $P_{close}$  change and tissue displacement, stress and strain distributions were very similar to the  $45^\circ$  angle but the magnitude of the results was lower.

The increments of hyoid displacement selected to observe all model results in detail are comparable to the amount of displacement achieved surgically (See Section 3.6). Van Tassel et al. [119] indicated that the hyoid is generally advanced by 1 to 2 cm in hyo-mandibular suspension procedures which corresponds on average to 4mm of

hyoid displacement in the model (given that 8mm of hyoid position change in the human upper airway was previously found to correspond to a 2mm hyoid position change in the current model from Chi et al. [30]). This suggests that overall results of hyo-mandibular suspension and hyothyroidopexy in this study are a reasonable approximation to the common clinically observed changes in upper airway. Further investigation of different hyoid displacement angles is needed in future studies to represent the range of angles potentially used in hyoid suspension procedures and confirm the observations of this study.

Other differences between the surgical procedures and the model simulations include the fact that myotomy of the hyoid muscles is not considered in the model. This may lead to differences in airway behavior between the model and physiological circumstance where more invasive action is undertaken with the older suspension procedures. In the most recent improvement of the hyoid suspension surgical techniques [43], the hyoid muscles remain almost completely undisrupted as is the case in the model simulations.

#### ***5.7.5 Computational Limitations***

Due to the non-linearity typically present when modeling biological structures and the large tissue deformation produced by the intraluminal negative pressure load, select simulation solutions failed to converge. Further optimization of the model properties will be needed to improve solution convergence, such as refining the mesh in the areas of highest tissue displacement or adjusting the sub-step number in the analysis settings for Pua load application. The large number of variations in the model geometry and loading conditions in this study made it challenging to achieve convergence in all

cases. However, the current model solution converged for the majority of simulations performed.

Furthermore, the computational time could potentially be improved if the results of a multitude of simulations are required instantly. With the automation process developed in this study, the time required to run the simulations and save the results for all surgical hyoid repositioning scenarios (5 directions and 5 increments each) is approximately 5 hours. All surgical hyoid repositioning simulations were repeated from 11 different hyoid baseline positions (baseline shift in all directions by increments of 2 and 4mm), totaling up to a duration of ~55 hours to complete all simulations in this study. Nonetheless, this computational time is relatively short compared to other finite element modeling studies in which a single simulation can take up to 72 hours to solve [71].

## **5.8 Conclusion and Future Studies**

A computational finite element model of a rabbit passive upper airway was redeveloped and enhanced and allowed the comprehensive study of the influence of the hyoid position (phenotypic and surgically repositioned) on upper airway patency and tissue mechanics. The FE model successfully predicted changes in upper airway collapsibility in response to various directions and magnitudes of surgical hyoid repositioning interventions. The model was also able to predict upper airway geometry, tissue displacement, stress and strain changes with surgical hyoid repositioning interventions which were qualitatively in agreement with literature.

Moreover, the influence of the hyoid ‘phenotypic’ baseline position on upper airway collapsibility directly but also on the effectiveness of surgical hyoid

repositioning procedures to reduce airway collapsibility were quantified. As a matter of fact, the original baseline position of the healthy rabbit airway is the optimal. Any change in the baseline hyoid position considerably increases upper airway collapsibility and impacts surgical hyoid repositioning procedures outcomes as well.

Thus, the outcomes of this study can help lead to a better understanding of the role of the hyoid bone in upper airway collapse as occurs in OSA pathophysiology and provide initial insight for the improvement of OSA treatments by guiding hyoid repositioning surgeries.

Future work should include simulations of surgical hyoid repositioning procedures in different angles to better replicate the clinical hyoid suspension procedures and assess the impact of changing the angle of hyoid displacement on their effectiveness. Combining the current simulations with other OSA related loads such as mandibular advancement and tracheal displacement would also be a great addition to assess the impact of hyoid position and/or movement on the effectiveness of such loads.

Furthermore, future work should focus on improving the model itself by current primarily optimizing the model definitions to allow airway collapse at physiological pressures. Incorporating airflow and active muscle contraction is also a future step in the model development to better reproduce the in-vivo conditions.

## REFERENCES

- [1] J. Amatory, S. Cheng, K. Kairaitis, J. R. Wheatley, T. C. Amis, and L. E. Bilston, "Development and validation of a computational finite element model of the rabbit upper airway: simulations of mandibular advancement and tracheal displacement," (in eng), *Journal of applied physiology (Bethesda, Md. : 1985)*, vol. 120, no. 7, pp. 743-57, 2016.
- [2] J. Amatory, K. Kairaitis, J. R. Wheatley, L. E. Bilston, and T. C. Amis, "Peripharyngeal tissue deformation and stress distributions in response to caudal tracheal displacement: pivotal influence of the hyoid bone?," (in eng), *Journal of applied physiology (Bethesda, Md. : 1985)*, vol. 116, no. 7, pp. 746-56, 2014.
- [3] J. Amatory, K. Kairaitis, J. R. Wheatley, L. E. Bilston, and T. C. Amis, "Peripharyngeal tissue deformation, stress distributions, and hyoid bone movement in response to mandibular advancement," vol. 118, no. 3, pp. 282-291, 2015.
- [4] P. Anderson *et al.*, "Chapter 20 - FRANK: A Hybrid 3D Biomechanical Model of the Head and Neck," Elsevier Inc, 2017, pp. 413-447.
- [5] P. Anderson, S. Fels, I. Stavness, J. W. G. Pearson, and B. Gick, "Intravelar and Extravelar Portions of Soft Palate Muscles in Velic Constrictions: A Three-Dimensional Modeling Study," *Journal of speech, language, and hearing research*, vol. 62, no. 4, pp. 802-814, 2019.
- [6] I. Ayappa and D. M. Rapoport, "The upper airway in sleep: physiology of the pharynx," (in eng), *Sleep medicine reviews*, vol. 7, no. 1, pp. 9-33, 2003.
- [7] M. S. Badr and J. A. Rowley, "Upper Airway Mechanics," in *Wiley Encyclopedia of Biomedical Engineering*.
- [8] O. Bafkar *et al.*, "Impact of sleeping position, gravitational force & effective tissue stiffness on obstructive sleep apnoea," *Journal of biomechanics*, vol. 104, pp. 109715-109715, 2020.
- [9] A. Baisch, J. T. Maurer, and K. Hormann, "The effect of hyoid suspension in a multilevel surgery concept for obstructive sleep apnea," (in eng), *Otolaryngology--head and neck surgery : official journal of American Academy of Otolaryngology-Head and Neck Surgery*, vol. 134, no. 5, pp. 856-61, 2006.
- [10] T. J. Barber, M. Y. Zhao, K. Sutherland, G. Rosengarten, and P. A. Cistulli, "Using Two-Way Fluid-Structure Interaction to Study the Collapse of the Upper Airway of OSA Patients," *Applied mechanics and materials*, vol. 553, pp. 275-280, 2014.

- [11] J. E. Barrera, C. Y. Pau, V. I. Forest, A. B. Holbrook, and G. R. Popelka, "Anatomic measures of upper airway structures in obstructive sleep apnea," (in eng), *World J Otorhinolaryngol Head Neck Surg*, vol. 3, no. 2, pp. 85-91, 2017.
- [12] A. J. Bates *et al.*, "Assessing the relationship between movement and airflow in the upper airway using computational fluid dynamics with motion determined from magnetic resonance imaging," *Clinical biomechanics (Bristol)*, vol. 66, pp. 88-96, 2019.
- [13] M. Bayat *et al.*, "Cephalometric risk factors of obstructive sleep apnea," *CRANIO®*, vol. 35, no. 5, pp. 321-326, 2017.
- [14] G. F. Benderro, J. Gamble, M. A. Schiefer, J. Z. Baskin, Y. Hernandez, and K. P. Strohl, "Hypoglossal nerve stimulation in a pre-clinical anesthetized rabbit model relevant to OSA," *Respiratory Physiology & Neurobiology*, vol. 250, pp. 31-38, 2018.
- [15] L. B. L. M. D. Benoist, J. P. M. D. P. van Maanen, and N. M. D. P. de Vries, "Hyoid suspension: hyothyroid and hyomandibular options," *Operative techniques in otolaryngology--head and neck surgery*, vol. 26, no. 4, pp. 178-182, 2015.
- [16] S. Bilici, O. Yigit, O. O. Celebi, A. G. Yasak, and A. H. Yardimci, "Relations Between Hyoid-Related Cephalometric Measurements and Severity of Obstructive Sleep Apnea," (in eng), *J Craniofac Surg*, vol. 29, no. 5, pp. 1276-1281, 2018.
- [17] L. E. Bilston and S. C. Gandevia, "Biomechanical properties of the human upper airway and their effect on its behavior during breathing and in obstructive sleep apnea," (in eng), *Journal of applied physiology (Bethesda, Md. : 1985)*, vol. 116, no. 3, pp. 314-24, 2014.
- [18] M. Böl, R. Iyer, J. Dittmann, M. Garcés-Schröder, and A. Dietzel, "Investigating the passive mechanical behaviour of skeletal muscle fibres: Micromechanical experiments and Bayesian hierarchical modelling," *Acta Biomaterialia*, vol. 92, pp. 277-289, 2019.
- [19] M. T. Bowden, E. J. Kezirian, D. Utley, and R. L. Goode, "Outcomes of Hyoid Suspension for the Treatment of Obstructive Sleep Apnea," *Archives of Otolaryngology-Head & Neck Surgery*, vol. 131, no. 5, pp. 440-445, 2005.
- [20] M. J. Brennick, S. Pickup, L. Dougherty, J. R. Cater, and S. T. Kuna, "Pharyngeal airway wall mechanics using tagged magnetic resonance imaging during medial hypoglossal nerve stimulation in rats," (in eng), *J Physiol*, vol. 561, no. Pt 2, pp. 597-610, 2004.
- [21] E. C. Brown, S. Cheng, D. K. McKenzie, J. E. Butler, S. C. Gandevia, and L. E. Bilston, "Tongue and lateral upper airway movement with mandibular advancement," (in eng), *Sleep*, vol. 36, no. 3, pp. 397-404, 2013.



- [22] J. E. Butler and S. C. Gandevia, "The output from human inspiratory motoneurone pools," (in eng), *J Physiol*, vol. 586, no. 5, pp. 1257-1264, 2008.
- [23] S. M. Caples *et al.*, "Surgical modifications of the upper airway for obstructive sleep apnea in adults: a systematic review and meta-analysis," (in eng), *Sleep*, vol. 33, no. 10, pp. 1396-407, 2010.
- [24] J. C. Carberry, J. Amatory, and D. J. Eckert, "Personalized Management Approach for OSA," (in eng), *Chest*, vol. 153, no. 3, pp. 744-755, 2018.
- [25] J. C. Carberry, A. S. Jordan, D. P. White, A. Wellman, and D. J. Eckert, "Upper Airway Collapsibility (Pcrit) and Pharyngeal Dilator Muscle Activity are Sleep Stage Dependent," (in eng), *Sleep*, vol. 39, no. 3, pp. 511-21, 2016.
- [26] N. B. Carrigy *et al.*, "Simulation of muscle and adipose tissue deformation in the passive human pharynx," *Computer methods in biomechanics and biomedical engineering*, vol. 19, no. 7, pp. 780-788, 2016.
- [27] B. Carvalho, J. Hsia, and R. Capasso, "Surgical therapy of obstructive sleep apnea: a review," (in eng), *Neurotherapeutics*, vol. 9, no. 4, pp. 710-716, 2012.
- [28] A. S. Chan, R. W. Lee, and P. A. Cistulli, "Non-positive airway pressure modalities: mandibular advancement devices/positional therapy," (in eng), *Proceedings of the American Thoracic Society*, vol. 5, no. 2, pp. 179-84, 2008.
- [29] A. S. L. Chan *et al.*, "The effect of mandibular advancement on upper airway structure in obstructive sleep apnoea," vol. 65, no. 8, pp. 726-732, 2010.
- [30] L. Chi *et al.*, "Identification of craniofacial risk factors for obstructive sleep apnoea using three-dimensional MRI," vol. 38, no. 2, pp. 348-358, 2011.
- [31] L. Chi *et al.*, "Identification of craniofacial risk factors for obstructive sleep apnoea using three-dimensional MRI," *The European respiratory journal*, vol. 38, no. 2, pp. 348-358, 2011.
- [32] T. M. Davidson, "The Great Leap Forward: the anatomic basis for the acquisition of speech and obstructive sleep apnea," (in eng), *Sleep Med*, vol. 4, no. 3, pp. 185-94, 2003.
- [33] R. J. Davies, N. J. Ali, and J. R. Stradling, "Neck circumference and other clinical features in the diagnosis of the obstructive sleep apnoea syndrome," (in eng), *Thorax*, vol. 47, no. 2, pp. 101-5, 1992.
- [34] J. A. Dempsey, S. C. Veasey, B. J. Morgan, and C. P. O'Donnell, "Pathophysiology of Sleep Apnea," *Physiological Reviews*, vol. 90, no. 1, pp. 47-112, 2010.
- [35] C. den Herder, H. van Tinteren, and N. de Vries, "Hyoidthyroidpexia: a surgical treatment for sleep apnea syndrome," (in eng), *The Laryngoscope*, vol. 115, no. 4, pp. 740-745, 2005.

- [36] S. S. Dhaliwal, S. M. Hesabgar, S. M. H. Haddad, H. Ladak, A. Samani, and B. W. Rotenberg, "Constructing a patient-specific computer model of the upper airway in sleep apnea patients," *The Laryngoscope*, vol. 128, no. 1, pp. 277-282, 2018.
- [37] P. R. Eastwood, I. Szollosi, P. R. Platt, and D. R. Hillman, "Comparison of upper airway collapse during general anaesthesia and sleep," *The Lancet (British edition)*, vol. 359, no. 9313, pp. 1207-1209, 2002.
- [38] D. J. Eckert, Y. L. Lo, J. P. Saboisky, A. S. Jordan, D. P. White, and A. Malhotra, "Sensorimotor function of the upper-airway muscles and respiratory sensory processing in untreated obstructive sleep apnea," *Journal of Applied Physiology*, vol. 111, no. 6, pp. 1644-1653, 2011.
- [39] B. A. Edwards and D. P. White, "Control of the pharyngeal musculature during wakefulness and sleep: implications in normal controls and sleep apnea," (in eng), *Head & neck*, vol. 33 Suppl 1, pp. S37-45, 2011.
- [40] A. Gale, P. V. Kilpelainen, and M. T. Laine-Alava, "Hyoid bone position after surgical mandibular advancement," (in eng), *Eur J Orthod*, vol. 23, no. 6, pp. 695-701, 2001.
- [41] P. R. Genta *et al.*, "Upper Airway Collapsibility is Associated with Obesity and Hyoid Position," *Sleep*, vol. 37, no. 10, pp. 1673-1678, 2014.
- [42] J. M. Gerard, J. Ohayon, V. Luboz, P. Perrier, and Y. Payan, "Non-linear elastic properties of the lingual and facial tissues assessed by indentation technique. Application to the biomechanics of speech production," (in eng), *Medical engineering & physics*, vol. 27, no. 10, pp. 884-92, 2005.
- [43] M. B. Gillespie, C. M. Ayers, S. A. Nguyen, and M. R. Abidin, "Outcomes of Hyoid Myotomy and Suspension Using a Mandibular Screw Suspension System," *Otolaryngology--head and neck surgery*, vol. 144, no. 2, pp. 225-229, 2011.
- [44] Y. H. Goh, V. Abdullah, and S. W. Kim, "Genioglossus Advancement and Hyoid Surgery," (in eng), *Sleep medicine clinics*, vol. 14, no. 1, pp. 73-81, 2019.
- [45] W. B. V. d. Graaff, S. B. Gottfried, J. Mitra, E. v. Lunteren, N. S. Cherniack, and K. P. Strohl, "Respiratory function of hyoid muscles and hyoid arch," vol. 57, no. 1, pp. 197-204, 1984.
- [46] S. Gündüz Arslan, N. Dildeş, and J. Devecioglu Kama, "Cephalometric Investigation of First Cervical Vertebrae Morphology and Hyoid Position in Young Adults with Different Sagittal Skeletal Patterns," *TheScientificWorld*, vol. 2014, pp. 159784-8, 2014.
- [47] J. G. Ha *et al.*, "The dimension of hyoid bone is independently associated with the severity of obstructive sleep apnea," (in eng), *PloS one*, vol. 8, no. 12, pp. e81590-e81590, 2013.

- [48] A. G. Hannam, I. Stavness, J. E. Lloyd, and S. Fels, "A dynamic model of jaw and hyoid biomechanics during chewing," *Journal of biomechanics*, vol. 41, no. 5, pp. 1069-1076, 2007.
- [49] N. B. Haralabakis, N. M. Toutountzakis, and S. C. Yiagtzis, "The hyoid bone position in adult individuals with open bite and normal occlusion," *European journal of orthodontics*, vol. 15, no. 4, pp. 265-271, 1993.
- [50] T. Hashimoto *et al.*, "Development of a Musculoskeletal Model of Hyolaryngeal Elements for Understanding Pharyngeal Swallowing Mechanics," *Applied sciences*, vol. 10, no. 18, p. 6276, 2020.
- [51] R. C. Heinzer *et al.*, "Lung Volume and Continuous Positive Airway Pressure Requirements in Obstructive Sleep Apnea," *American journal of respiratory and critical care medicine*, vol. 172, no. 1, pp. 114-117, 2005.
- [52] R. C. Heinzer *et al.*, "Effect of increased lung volume on sleep disordered breathing in patients with sleep apnoea," *Thorax*, vol. 61, no. 5, pp. 435-439, 2006.
- [53] M. Henrik Strand Moxness, F. Wülker, B. Helge Skallerud, and S. Nordgård, "Simulation of the upper airways in patients with obstructive sleep apnea and nasal obstruction: A novel finite element method: Novel FE Method for OSA and Nasal Obstruction," *Laryngoscope investigative otolaryngology*, vol. 3, no. 2, pp. 82-93, 2018.
- [54] N. Hermant, P. Perrier, and Y. Payan, "Human tongue biomechanical modeling," Academic Press, 2017, pp. 395-411.
- [55] Y. Huang, A. Malhotra, and D. P. White, "Computational simulation of human upper airway collapse using a pressure-/state-dependent model of genioglossal muscle contraction under laminar flow conditions," (in eng), *Journal of applied physiology (Bethesda, Md. : 1985)*, vol. 99, no. 3, pp. 1138-1148, 2005.
- [56] Y. Huang, D. P. White, and A. Malhotra, "The impact of anatomic manipulations on pharyngeal collapse: results from a computational model of the normal human upper airway," (in eng), *Chest*, vol. 128, no. 3, pp. 1324-1330, 2005.
- [57] S. Isono, "Obesity and obstructive sleep apnoea: mechanisms for increased collapsibility of the passive pharyngeal airway," (in eng), *Respirology*, vol. 17, no. 1, pp. 32-42, 2012.
- [58] S. Isono, "Physiology and Dynamics of the Pharyngeal Airway," vol. 1, ed, 2013, pp. 533-544.
- [59] S. Isono, J. E. Remmers, A. Tanaka, Y. Sho, J. Sato, and T. Nishino, "Anatomy of pharynx in patients with obstructive sleep apnea and in normal subjects," *Journal of Applied Physiology*, vol. 82, no. 4, pp. 1319-1326, 1997.

- [60] A. R. Jacobsen *et al.*, "Determinants for adherence to continuous positive airway pressure therapy in obstructive sleep apnea," (in eng), *PloS one*, vol. 12, no. 12, p. e0189614, 2017.
- [61] A. K. Jena and R. Duggal, "Hyoid bone position in subjects with different vertical jaw dysplasias," *The Angle orthodontist*, vol. 81, no. 1, pp. 81-85, 2011.
- [62] K. Kairaitis, "Is the pharynx a muscular hydrostat?," *Medical Hypotheses*, vol. 74, no. 3, pp. 590-595, 2010.
- [63] K. Kairaitis, K. Byth, R. Parikh, R. Stavrinou, J. R. Wheatley, and T. C. Amis, "Tracheal Traction Effects on Upper Airway Patency in Rabbits: The Role of Tissue Pressure," *Sleep*, vol. 30, no. 2, pp. 179-186, 2007.
- [64] E. J. Kezirian and A. N. Goldberg, "Hypopharyngeal Surgery in Obstructive Sleep Apnea: An Evidence-Based Medicine Review," *Archives of Otolaryngology-Head & Neck Surgery*, vol. 132, no. 2, pp. 206-213, 2006.
- [65] S.-H. Kim, S.-K. Chung, and Y. Na, "Numerical investigation of flow-induced deformation along the human respiratory upper airway," *Journal of Mechanical Science and Technology*, vol. 29, no. 12, pp. 5267-5272, 2015.
- [66] Y. Kim and G. H. McCullough, "Maximum hyoid displacement in normal swallowing," (in eng), *Dysphagia*, vol. 23, no. 3, pp. 274-9, 2008.
- [67] J. P. Kirkness *et al.*, "Decreased surface tension of upper airway mucosal lining liquid increases upper airway patency in anaesthetised rabbits," (in eng), *J Physiol*, vol. 547, no. Pt 2, pp. 603-11, 2003.
- [68] A. Kohno *et al.*, "Displacement of the hyoid bone by muscle paralysis and lung volume increase: the effects of obesity and obstructive sleep apnea," (in eng), *Sleep*, vol. 42, no. 1, 2019.
- [69] S. T. Kuna, L. C. Woodson, D. R. Solanki, O. Esch, D. E. Frantz, and M. Mathru, "Effect of progressive mandibular advancement on pharyngeal airway size in anesthetized adults," *Anesthesiology*, vol. 109, no. 4, pp. 605-612, 2008.
- [70] J. C. M. Lam, K. Kairaitis, M. Verma, J. R. Wheatley, and T. C. Amis, "Saliva production and surface tension: influences on patency of the passive upper airway," (in eng), *J Physiol*, vol. 586, no. 22, pp. 5537-5547, 2008.
- [71] T. B. Le, M. G. Moghaddam, B. T. Woodson, and G. J. M. Garcia, "Airflow limitation in a collapsible model of the human pharynx: physical mechanisms studied with fluid-structure interaction simulations and experiments," *Physiological Reports* vol. 7, no. 10, pp. e14099-n/a, 2019.
- [72] H. Liu, M. H. S. Moxness, V. E. Prot, and B. H. Skallerud, "Palatal implant surgery effectiveness in treatment of obstructive sleep apnea: A numerical method with 3D patient-specific geometries," *Journal of Biomechanics*, vol. 66, pp. 86-94, 2018.

- [73] Y. Liu, J. Mitchell, Y. Chen, W. Yim, W. Chu, and R. C. Wang, "Study of the upper airway of obstructive sleep apnea patient using fluid structure interaction," *Respiratory Physiology & Neurobiology*, vol. 249, pp. 54-61, 2018.
- [74] A. Malhotra and D. P. White, "Obstructive sleep apnoea," *The Lancet*, vol. 360, no. 9328, pp. 237-245, 2002.
- [75] E. N. Marieb, *Human anatomy & physiology*, Sixth Edition ed. (no. Book, Whole). United States: Pearson Education, Inc., Benjamin Cummings, 2004.
- [76] K. Matsuo and J. B. Palmer, "Kinematic linkage of the tongue, jaw, and hyoid during eating and speech," (in eng), *Archives of oral biology*, vol. 55, no. 4, pp. 325-31, 2010.
- [77] S. A. M. D. F. A. Mickelson, "Hyoid advancement to the mandible (hyo-mandibular advancement)," *Operative techniques in otolaryngology--head and neck surgery*, vol. 23, no. 1, pp. 56-59, 2012.
- [78] S. Mortazavi *et al.*, "Hyoid bone position in different facial skeletal patterns," *Journal of clinical and experimental dentistry*, vol. 10, no. 4, pp. e346-e351, 2018.
- [79] J. S. Na, H.-D. Jung, H.-J. Cho, Y. J. Choi, and J. S. Lee, "Computational analysis of airflow dynamics for predicting collapsible sites in the upper airways: a preliminary study," *Journal of applied physiology (Bethesda, Md. : 1985)*, vol. 126, no. 2, pp. 330-340, 2019.
- [80] B. C. Neelapu *et al.*, "Craniofacial and upper airway morphology in adult obstructive sleep apnea patients: A systematic review and meta-analysis of cephalometric studies," *Sleep medicine reviews*, vol. 31, pp. 79-90, 2016.
- [81] C. Neruntarat, "Hyoid myotomy with suspension under local anesthesia for obstructive sleep apnea syndrome," *European Archives of Oto-Rhino-Laryngology*, vol. 260, no. 5, pp. 286-290, 2003.
- [82] A. T. Ng, H. Gotsopoulos, J. Qian, and P. A. Cistulli, "Effect of Oral Appliance Therapy on Upper Airway Collapsibility in Obstructive Sleep Apnea," *American journal of respiratory and critical care medicine*, vol. 168, no. 2, pp. 238-241, 2003.
- [83] A. A. Ong, J. Buttram, S. A. Nguyen, D. Platter, M. R. Abidin, and M. B. Gillespie, "Hyoid myotomy and suspension without simultaneous palate or tongue base surgery for obstructive sleep apnea," (in eng), *World J Otorhinolaryngol Head Neck Surg*, vol. 3, no. 2, pp. 110-114, 2017.
- [84] P. E. Peppard, T. Young, J. H. Barnett, M. Palta, E. W. Hagen, and K. M. Hla, "Increased prevalence of sleep-disordered breathing in adults," (in eng), *American journal of epidemiology*, vol. 177, no. 9, pp. 1006-14, 2013.

- [85] P. E. Peppard, T. Young, M. Palta, and J. Skatrud, "Prospective study of the association between sleep-disordered breathing and hypertension," (in eng), *The New England journal of medicine*, vol. 342, no. 19, pp. 1378-84, 2000.
- [86] L. V. Pham and A. R. Schwartz, "The pathogenesis of obstructive sleep apnea," (in eng), *J Thorac Dis*, vol. 7, no. 8, pp. 1358-72, 2015.
- [87] J. Pirnar, L. Dolenc-Grošelj, I. Fajdiga, and I. Žun, "Computational fluid-structure interaction simulation of airflow in the human upper airway," *Journal of Biomechanics*, vol. 48, no. 13, pp. 3685-3691, 2015.
- [88] A. Pugachev *et al.*, "Application of patient-specific simulation workflow for obstructive sleep apnea diagnosis and treatment with a mandibular advancement device," *International journal for numerical methods in biomedical engineering*, vol. 36, no. 8, pp. e3350-n/a, 2020.
- [89] B. E. Rapp, "Chapter 32 - Finite Element Method," in *Microfluidics: Modelling, Mechanics and Mathematics*, B. E. Rapp Ed. Oxford: Elsevier, 2017, pp. 655-678.
- [90] P. V. Rathod, S. Vidhyadharan, and S. Iyer, "Anatomy of Swallowing." Singapore: Springer Singapore, 2018, pp. 3-26.
- [91] W. Richard, D. Kox, C. den Herder, M. Laman, H. van Tinteren, and N. de Vries, "The role of sleep position in obstructive sleep apnea syndrome," *European archives of oto-rhino-laryngology*, vol. 263, no. 10, pp. 946-950, 2006.
- [92] R. Riley, C. Guilleminault, N. Powell, and S. Derman, "Mandibular osteotomy and hyoid bone advancement for obstructive sleep apnea: a case report," *Sleep (New York, N.Y.)*, vol. 7, no. 1, pp. 79-82, 1984.
- [93] R. W. Riley, N. B. Powell, and C. Guilleminault, "Obstructive sleep apnea and the hyoid: a revised surgical procedure," (in eng), *Otolaryngology--head and neck surgery : official journal of American Academy of Otolaryngology-Head and Neck Surgery*, vol. 111, no. 6, pp. 717-21, 1994.
- [94] J. L. Roberts, W. R. Reed, and B. T. Thach, "Pharyngeal airway-stabilizing function of sternohyoid and sternothyroid muscles in the rabbit," *Journal of Applied Physiology*, vol. 57, no. 6, pp. 1790-1795, 1984.
- [95] K. H. Rosenbluth, D. A. Kwiat, M. R. Harrison, and E. J. Kezirian, "Hyoid Bone Advancement for Improving Airway Patency: Cadaver Study of a Magnet-Based System," vol. 146, no. 3, pp. 491-496, 2012.
- [96] J. A. Rowley, S. Permutt, S. Willey, P. L. Smith, and A. R. Schwartz, "Effect of tracheal and tongue displacement on upper airway airflow dynamics," *Journal of Applied Physiology*, vol. 80, no. 6, pp. 2171-2178, 1996.

- [97] C. Samaha, "Role of hyoid bone position in maintaining upper airway patency," American University of Beirut, 2020.
- [98] F. Sériès, "Upper airway muscles awake and asleep," *Sleep medicine reviews*, vol. 6, no. 3, pp. 229-242, 2002.
- [99] E. Sforza, W. Bacon, T. Weiss, A. Thibault, C. Petiau, and J. Krieger, "Upper airway collapsibility and cephalometric variables in patients with obstructive sleep apnea," (in eng), *American journal of respiratory and critical care medicine*, vol. 161, no. 2 Pt 1, pp. 347-52, 2000.
- [100] C.-M. Sheng, L.-H. Lin, Y. Su, and H.-H. Tsai, "Developmental Changes in Pharyngeal Airway Depth and Hyoid Bone Position from Childhood to Young Adulthood," *The Angle orthodontist*, vol. 79, no. 3, pp. 484-490, 2009.
- [101] Y. Shirazawa *et al.*, "Relationship between pharyngeal airway depth and ventilation condition in mandibular setback surgery: A computational fluid dynamics study," *Orthodontics & craniofacial research*, vol. 23, no. 3, pp. 313-322, 2020.
- [102] M. A. Skinner, C. J. Robertson, R. N. Kingshott, D. R. Jones, and D. R. Taylor, "The Efficacy of a Mandibular Advancement Splint in Relation to Cephalometric Variables," *Sleep and Breathing*, vol. 6, no. 3, pp. 115-124, 2002.
- [103] P. L. Smith, R. A. Wise, A. R. Gold, A. R. Schwartz, and S. Permutt, "Upper airway pressure-flow relationships in obstructive sleep apnea," (in eng), *Journal of applied physiology (Bethesda, Md. : 1985)*, vol. 64, no. 2, pp. 789-95, 1988.
- [104] B. Song *et al.*, "Computational fluid dynamics simulation of changes in the morphology and airflow dynamics of the upper airways in OSAHS patients after treatment with oral appliances," *PloS one*, vol. 14, no. 11, p. e0219642, 2019.
- [105] S. A. Song *et al.*, "Hyoid surgery alone for obstructive sleep apnea: A systematic review and meta-analysis," (in eng), *The Laryngoscope*, vol. 126, no. 7, pp. 1702-8, 2016.
- [106] M. M. D. M. P. H. Sowho, J. M. P. Amatoury, J. P. P. Kirkness, and S. P. M. D. P. Patil, "Sleep and Respiratory Physiology in Adults," *Clinics in Chest Medicine*, vol. 35, no. 3, pp. 469-481, 2014.
- [107] P. D. Srodon, M. E. Miquel, and M. J. Birch, "Finite Element Analysis Animated Simulation of Velopharyngeal Closure," *The Cleft Palate-Craniofacial Journal*, vol. 49, no. 1, pp. 44-50, 2012.
- [108] I. Stavness, J. E. Lloyd, Y. Payan, and S. Fels, "Coupled hard-soft tissue simulation with contact and constraints applied to jaw-tongue-hyoid dynamics," *International journal for numerical methods in biomedical engineering*, vol. 27, no. 3, pp. 367-390, 2011.

- [109] K. P. Strohl, J. P. Butler, and A. Malhotra, "Mechanical properties of the upper airway," *Comprehensive Physiology* vol. 2, no. 3, pp. 1853-1872, 2012.
- [110] P. J. Strollo *et al.*, "Upper-Airway Stimulation for Obstructive Sleep Apnea," *The New England journal of medicine*, vol. 370, no. 2, pp. 139-149, 2014.
- [111] B. A. Stuck *et al.*, "Anatomic Changes After Hyoid Suspension for Obstructive Sleep Apnea: An MRI Study," *Otolaryngology--head and neck surgery*, vol. 133, no. 3, pp. 397-402, 2005.
- [112] X. Sun, C. Yu, Y. Wang, and Y. Liu, "Numerical simulation of soft palate movement and airflow in human upper airway by fluid-structure interaction method," *Acta mechanica Sinica*, vol. 23, no. 4, pp. 359-367, 2007.
- [113] J. Tong *et al.*, "Respiratory-related displacement of the trachea in obstructive sleep apnea," (in eng), *Journal of applied physiology (Bethesda, Md. : 1985)*, vol. 127, no. 5, pp. 1307-1316, 2019.
- [114] J. Tu, K. Inthavong, and G. Ahmadi, "The Human Respiratory System," in *Fluid Particle Dynamics in the Human Respiratory System – A Computational Approach*, 2013, pp. 19-44.
- [115] J. Tu, K. Inthavong, and G. Ahmadi, "The Human Respiratory System," 2013, pp. 19-44.
- [116] M. Urabe, T. Hashimoto, T. Kikuchi, Y. Michiwaki, and T. Koike, "Estimation of Muscle Activity Change under Different Bolus Conditions using Musculoskeletal Model of Swallowing," *Conference proceedings (IEEE Engineering in Medicine and Biology Society. Conf.)*, vol. 2019, p. 5314, 2019.
- [117] W. B. Van de Graaff, "Thoracic influence on upper airway patency," (in eng), *Journal of applied physiology (Bethesda, Md. : 1985)*, vol. 65, no. 5, pp. 2124-31, 1988.
- [118] E. van Lunteren and K. P. Strohl, "The Muscles of the Upper Airways," *Clinics in Chest Medicine*, vol. 7, no. 2, pp. 171-188, 1986.
- [119] J. Van Tassel, E. Chio, D. Silverman, R. S. Nord, D. Platter, and M. R. Abidin, "Hyoid Suspension With UPPP for the Treatment of Obstructive Sleep Apnea," *Ear, nose, & throat journal*, pp. 1455613211001132-1455613211001132, 2021.
- [120] S. C. Veasey and I. M. Rosen, "Obstructive Sleep Apnea in Adults," (in English), *The New England journal of medicine*, vol. 380, no. 15, pp. 1442-1449, 2019.
- [121] B. B. Vieira *et al.*, "Cephalometric evaluation of facial pattern and hyoid bone position in children with obstructive sleep apnea syndrome," (in eng), *Int J Pediatr Otorhinolaryngol*, vol. 75, no. 3, pp. 383-6, 2011.



- [122] I. Vilaseca, A. Morelló, J. M. Montserrat, J. Santamaría, and A. Iranzo, "Usefulness of Uvulopalatopharyngoplasty With Genioglossus and Hyoid Advancement in the Treatment of Obstructive Sleep Apnea," *Archives of Otolaryngology–Head & Neck Surgery*, vol. 128, no. 4, pp. 435-440, 2002.
- [123] K. L. Ward *et al.*, "Excessive daytime sleepiness increases the risk of motor vehicle crash in obstructive sleep apnea," (in eng), *Journal of clinical sleep medicine : JCSM : official publication of the American Academy of Sleep Medicine*, vol. 9, no. 10, pp. 1013-21, 2013.
- [124] B. B. Wheatley, G. M. Odegard, K. R. Kaufman, and T. L. Haut Donahue, "Modeling Skeletal Muscle Stress and Intramuscular Pressure: A Whole Muscle Active–Passive Approach," *Journal of biomechanical engineering*, vol. 140, no. 8, pp. 0810061-0810068, 2018.
- [125] A. T. Whittle, I. Marshall, I. L. Mortimore, P. K. Wraith, R. J. Sellar, and N. J. Douglas, "Neck soft tissue and fat distribution: comparison between normal men and women by magnetic resonance imaging," (in eng), *Thorax*, vol. 54, no. 4, pp. 323-328, 1999.
- [126] V. Wilkinson *et al.*, "Discharge Patterns of Human Genioglossus Motor Units During Sleep Onset," *Sleep (New York, N.Y.)*, vol. 31, no. 4, pp. 525-533, 2008.
- [127] B. D. Wingerd, *Rabbit dissection manual*. Baltimore: Johns Hopkins University Press (in English), 1985.
- [128] B. T. Woodson *et al.*, "Upper Airway Stimulation for Obstructive Sleep Apnea: 5-Year Outcomes," (in eng), *Otolaryngology--head and neck surgery : official journal of American Academy of Otolaryngology-Head and Neck Surgery*, vol. 159, no. 1, pp. 194-202, 2018.
- [129] X. Xu, J. Wu, W. Weng, and M. Fu, "Investigation of inhalation and exhalation flow pattern in a realistic human upper airway model by PIV experiments and CFD simulations," *Biomechanics and modeling in mechanobiology*, vol. 19, no. 5, pp. 1679-1695, 2020.
- [130] H. Yamada, *Strength of biological materials* (no. Book, Whole). United States, 1970.
- [131] S. H. Yeom, J. S. Na, H.-D. Jung, H.-J. Cho, Y. J. Choi, and J. S. Lee, "Computational analysis of airflow dynamics for predicting collapsible sites in the upper airways: machine learning approach," vol. 127, no. 4, pp. 959-973, 2019.
- [132] M. Younes, "Role of Arousals in the Pathogenesis of Obstructive Sleep Apnea," *American journal of respiratory and critical care medicine*, vol. 169, no. 5, pp. 623-633, 2004.

- [133] T. Young *et al.*, "Sleep disordered breathing and mortality: eighteen-year follow-up of the Wisconsin sleep cohort," (in eng), *Sleep*, vol. 31, no. 8, pp. 1071-8, 2008.
- [134] T. Young, J. Skatrud, and P. E. Peppard, "Risk factors for obstructive sleep apnea in adults," (in eng), *Jama*, vol. 291, no. 16, pp. 2013-6, 2004.
- [135] S. Zaghi *et al.*, "Maxillomandibular Advancement for Treatment of Obstructive Sleep Apnea: A Meta-analysis," *JAMA Otolaryngology–Head & Neck Surgery*, vol. 142, no. 1, pp. 58-66, 2016.
- [136] M. Zhao, T. Barber, P. A. Cistulli, K. Sutherland, and G. Rosengarten, "Simulation of upper airway occlusion without and with mandibular advancement in obstructive sleep apnea using fluid-structure interaction," *Journal of biomechanics*, vol. 46, no. 15, pp. 2586-2592, 2013.
- [137] T. Zhao *et al.*, "Effects of Maxillary Skeletal Expansion on Upper Airway Airflow: A Computational Fluid Dynamics Analysis," *The Journal of craniofacial surgery*, vol. 31, no. 1, pp. e6-e10, 2020.
- [138] Z. Zheng *et al.*, "Computational fluid dynamics simulation of the upper airway response to large incisor retraction in adult class I bimaxillary protrusion patients," *Scientific reports*, vol. 7, no. 1, p. 45706, 2017.

